UNIVERSITY OF ADELAIDE LIBRARY
4-12-96

A COMPUTATIONAL FLUID DYNAMIC STUDY OF BLOOD FLOW THROUGH STENOSED ARTERIES

by

Keng Cheng Ang, B.Sc (Hons.)(Ma.Sc.)

Thesis submitted for the degree of
Doctor of Philosophy
in the Department of Applied Mathematics,
The University of Adelaide

August 1996

CONTENTS

Summary iv

Signed Statement vi

Acknowledgements vii

List of Publications viii

CHAPTER 1 INTRODUCTION

1.1 General Introduction 1

1.2 Some Early Studies in Blood Flow Problems 4

1.3 Current State of Affairs 5

1.4 Outline of Approach in the Present Study 12

CHAPTER 2 THE HUMAN CIRCULATORY SYSTEM

2.1 Introduction 14

2.2 Brief Description of the Human Circulatory System 15

2.3 Arterial Vessels 19

2.4 Arterial Diseases 21

2.4.1 Arteriosclerosis 24

2.4.2 Risk Factors 25

2.4.3 Pathogenesis of Atherosclerosis 27

2.5 Hemodynamics and Atherogenesis 29

CHAPTER 3 CFD TECHNIQUES AND APPLICATIONS IN BLOOD FLOW STUDIES

3.1 Introduction 32

3.2 Fluid Dynamics of Blood Flow 33

3.3 Computational Fluid Dynamics 37

3.4 Basic Principles of CFD 39

3.5 Commercial CFD Codes 40

3.5.1 FIDAP : A Brief Description 44

3.5.2 PHOENICS : A Brief Description 45

CHAPTER 4 MODEL I : AXISYMMETRIC TRIPLE STENOSES

4.1 Introduction 47
4.2 Geometrical Description of Model 48
4.3 Governing Equations 53
4.4 Formulation of the problem in FIDAP 54
4.5 Results and Discussion 59
4.6 Conclusion 67

CHAPTER 5 MODEL II : SINGLE STENOSIS IN THREE DIMENSIONS

5.1 Introduction 69
5.2 Geometrical Description of Model 70
5.3 Formulation of the problem in PHOENICS 76
5.4 Results and Discussion 79
5.4.1 Pressure Drop 81
5.4.2 Velocity Field 86
5.4.3 Wall Shear Stress 90
5.5 Conclusion 97

CHAPTER 6 MODEL III : CURVED ARTERY MODEL IN THREE DIMENSIONS

6.1 Introduction 99
6.2 Description of the Model 100
6.3 Formulation of the problem in PHOENICS 106
6.4 Results and Discussion 110
6.4.1 Pressure Drop 110
6.4.2 Velocity Field 115
6.4.3 Wall Shear Stress 135
6.5 Conclusion 149

CHAPTER 7 CONCLUSION

7.1 A Brief Summary 151
7.2 Clinical Significance of Present Study 152
7.3 Recommendations for Future Study 154

Appendix A : File System in FIDAP 156

Appendix B : File System in PHOENICS 158

Appendix C : Sample FIDAP input file 161

Appendix D : Sample PHOENICS input file 165

Appendix E : Mathematical Modelling of Triple Arterial Stenoses 174

Bibliography 180

Summary

Computational fluid dynamic (CFD) techniques are applied to study the flow characteristics of steady flow through arteries with stenoses. Effects of stenoses on characteristics such as pressure drops, flow velocities and shearing stresses on the arterial walls are examined and their significance on the progression of arterial diseases is discussed.

Three models are constructed, each introducing an improvement upon the previous. The first model developed is for steady laminar flow through an axisymmetric vessel with three stenoses in series. Although fairly simple, this model demonstrates the potential effectiveness and usefulness of such techniques. This model is also an extension of previously published work.

The second model improves on the first by considering a stenosis which is not symmetrical about the axis. As stenoses and arteries are, in general, not symmetrical, this model provides a method of studying a more realistic situation. The model is solved for various degrees of stenosis at Reynolds number ranging from 100 to 1000. Flow characteristics such as pressure drops, velocity profiles and shearing stresses on the walls are computed and compared with published results.

The third model incorporates curvature into the geometry and is thus an extension of and improvement over the second model. In this curved artery model, we investigate the effects of curvature on the flow of blood by considering three separate cases, namely, artery without stenoses, artery with stenosis on inner wall of curvature and artery with stenoses on both the inner and outer wall of the curvature. The model is solved for a number of different degrees of stenoses at Reynolds number ranging from 100 to 1200. Results of pressure drops and wall shearing stresses are computed and compared with published results. Secondary flow motion leading to a significant increase of secondary wall shear stress is also investigated.

Through the use of computational fluid dynamic techniques, this research has provided valuable data for the pressure drops and shearing stress distributions for an artery suffering from stenosis. In particular, the second and third models described flows through arterial stenoses in three dimensions in a more realistic way, thus providing researchers in this area new insights into blood flow models. In addition, the long term application of this research is seen as a means of assisting cardiologists in understanding the progression of arterial diseases.

Signed Statement

This work contains no material which has been accepted for the award of any other degree or diploma in any university or other tertiary institution and, to the best of my knowledge and belief, contains no material previously published or written by another person, except where due reference has been made in the text.

I give consent to this copy of my thesis, when deposited in the University Library, being available for loan and photocopying.

K C Ang
23 August 1996

Acknowledgements

I wish to express my sincerest appreciation to my supervisor, Dr. J. Mazumdar, for his continued guidance and support during the course of this research. His constructive comments and sound suggestions have been most crucial and valuable. Without his constant encouragement, this research would not have been possible.

I am also thankful to Staff Cardiologists in the Department of Cardiology of the Wakefield Hospital, Adelaide, for their invaluable assistance in providing information on the practices of cardiological surgery in Australia. In particular, I would like to thank Mr. D. Alderson of the Angiography Department (Wakefield Hospital) for making available angiograms of coronary arteries used in this study. Special thanks also go to Dr. I. Hamilton Craig for many valuable discussions during the preparation of research materials of the thesis.

In addition, I am thankful to Dr. P. Gill and Dr. M. Tuebner of the Department of Applied Mathematics for their support and encouragement.

This thesis was supported financially with an Australian Overseas Postgraduate Research Scholarship and a University of Adelaide Scholarship, for which I am grateful.

The thesis was typeset using LaTeX 2_ε on a SUN Sparcstation in the Department of Applied Mathematics, University of Adelaide. Graphs were plotted using gnuplot (Version 3.5) and figures were drawn using xfig (Version 3.1).

List of Publications

1. Ang, K.C. and Mazumdar, J.N., 1994, Effects of relative severity and geometrical shapes of multiply stenosed arteries on flow of blood. In *Conference Abstracts of the World Congress on Medical Physics and Biomedical Engineering*, Rio de Janeiro, Brazil, Vol. 39a, pp. 221.

2. Ang, K.C. and Mazumdar, J.N., 1994, Effects of relative severity and geometrical shapes of multiply stenosed arteries on flow of blood. In *Conference Abstracts of the Conference of Engineering and Physical Sciences in Medicine*, Perth, Australia, pp. 43.

3. Ang, K.C. and Mazumdar, J.N., 1994, Modelling of blood flow through stenosed arteries using C.F.D. In *Conference Proceedings for the* 8^{th} *International Conference of Biomedical Engineering*, Singapore, pp. 228-230.

4. Ang, K.C. and Mazumdar, J.N., 1995, Mathematical modelling of triple arterial stenoses. *Australasian Physical & Engineering Sciences in Medicine*, Vol. 18, pp. 89-94.

5. Ang, K.C. and Mazumdar, J.N., 1996, Mathematical modelling of three dimensional flow through an asymmetric arterial stenosis. *Mathematical and Computer Modelling*, (to appear).

6. Ang, K.C., Mazumdar, J.N. and Hamilton Craig, I., 1996, A computational model for blood flow through highly curved arteries with asymmetric stenoses. *Journal of the Australian Mathematical Society, Series B*, (under review).

UNIVERSITY OF ADELAIDE LIBRARY

CHAPTER 1

INTRODUCTION

1.1 General Introduction

Occlusive arterial disease is one of the chief causes of death in most of the western world. A narrowing or stenosis in an artery would almost invariably interfere with the proper flow of blood in the vessel, producing regions of high fluid stress, elevated wall shear stress and recirculation of flow. These flow conditions may eventually cause serious pathological problems such as endothelial damage, haemolysis, thrombosis and other injury within the artery. Thus, it is not surprising that the study of blood flow through stenosed arteries has been the subject of numerous studies in the past few decades.

However, despite the vast amount of studies carried out in this area, the causes of arterial stenoses remain largely unknown. Many studies employing epidemiological techniques have been performed to determine the factors associated with arterial diseases. Factors such as age, sex, cigarette smoking, hypertension and high cholesterol level have been identified as risk factors. However, such studies have only been able to demonstrate the association between these factors and arterial diseases. They do not tell us anything about the causes of the diseases.

In recent years, researchers have turned to hemodynamics[1], the study of the fluid

[1] also spelt "haemodynamics"

dynamics of blood flow, in an attempt to understand its significance in the genesis and proliferation of arterial diseases. Such studies, which may be experimental or mathematical, usually consist of a model of blood flow through a tube, partially occluded or otherwise. Measurements of flow characteristics such as pressure, shear stress and flow velocity are made and analysed in these models.

Many *in vitro* experimental studies have provided much information. Flow visualisation techniques used in some of these experiments may give interesting qualitative information such as regions of recirculation and flow separation. However, to obtain quantitative information, some of these models may involve the use of some form of probing device (for example, a pressure probe) in the vessel to make various measurements. These physical measurements are limited in application as it is not feasible to insert probes in the entire flow domain. Moreover, the introduction of probes may sometimes alter the natural conditions of the flow considerably, giving rise to inaccurate results at times. The use of laser Doppler anemometer or ultra sound techniques to measure the velocity of flow is also limited in that measurements may only be made at specific points in the flow domain. Furthermore, it is almost impossible to measure shearing stresses experimentally.

Mathematical modelling provides a more economical and non-invasive method of studying blood flow through arteries. However, due to the complexity of the highly non-linear and coupled governing equations of the model, exact analytic solutions for the flow models have yet to be obtained. Early researchers in this field tend to simplify the equations in an attempt to find analytical solutions to the problem and in the process, assumptions and simplifications in the models are usually made.

With the advent of high speed digital computers in recent years, more researchers have turned to numerical methods of modelling blood flow. More recently, Computational Fluid Dynamic (CFD) computer codes have also been used successfully to study such problems.

In modelling blood flow, whether experimentally or mathematically, the main objective is to obtain qualitative or quantitative information about certain flow characteristics of blood through a vessel by means of a realistic simulation. The flow characteristics of interest are usually pressure drops, velocities of flow and shearing stresses on the vessel walls.

Pressure drops across the length of the vessel is related to the flow resistance in the vessel. Hence, information on how pressure drops are affected by certain physiological conditions simulated in the model will translate into information on how the flow of blood may be impeded.

The velocity, or average velocity, of the flow is related to the volume flow rate. This quantity will determine how much blood is supplied to the important organs. Also, abnormalities in the vessels may lead to abnormalities in the velocity profile and vice versa. It is thus of considerable interest to examine in a model how flow velocities may be influenced by different conditions in the model.

Shearing stresses on the arterial walls are difficult to measure in an experimental set-up. Very often, they are estimated in experiments or determined in a mathematical or numerical model. The amount of shearing stress experienced by the arterial walls may have a direct bearing on the formation or rupture of plaques in the walls, thus leading to various pathological problems.

Modelling studies thus form an integral part of the continuing research in the area of blood flow. Information on the flow characteristics serves to provide important insight into how the dynamics of blood flow can be related to arterial diseases. This will in turn assist cardiologists in their understanding of the pathogenesis and progression of these diseases.

1.2 Some Early Studies in Blood Flow Problems

Over the past few decades, numerous experimental studies have been carried out to model the flow of blood in arteries. These experiments, which may be *in vivo* or *in vitro*, would normally be performed to measure certain important flow characteristics such as pressure drops and blood flow velocities.

Some of the early experiments carried out to study the nature of blood flow in arteries were performed by investigators such as Mann *et al* (1938) and Shipley and Gregg (1944). These experimental studies had mainly concentrated on the estimation of the reduction in blood flow due to a reduction in the lumen of a vessel effected by an external compression. Shipley and Gregg found that blood flow through a vessel was reduced significantly only when the cross sectional area of the lumen was reduced by 50 to 70 percent. Although there were some doubts over the methods of measurement in these early experiments, a foundation for future experimental investigations was established as a result of these studies.

Further work was subsequently carried out by researchers such as May *et al* (1963), Fiddian *et al* (1964), Rodbard (1966) and Kindt and Youmans (1969) to study the dynamics of blood flow through stenotic arteries experimentally. By increasing the constriction on the iliac arteries of animals, May *et al* (1963) found that a consistent reduction in blood flow was observed only after the degree of stenosis reached 80 percent. Their experiments also found that a fourfold increase in the length of the stenotic segment (from 1 to 4 *cm*) caused an average flow reduction of 24.8 percent.

Fiddian *et al* (1964) performed experiments on dogs to investigate the effects of stenosis diameter, stenotic length, viscosity of fluid and peripheral resistance on the flow of blood. In addition to confirming Shipley and Gregg's findings, their experiments also revealed that the length of a stenosis has a disproportionately

small effect on the total flow of blood.

Fourteen dogs were used in an experiment carried out by Kindt and Youmans (1969) to study the effect of stricture length on critical arterial stenosis. Clamps of the same width but different lengths were constructed and used to partially occlude the blood flow in a vessel. Their study reported that at 80 percent stenosis, it required an eightfold increase in the stenotic length to reduce the flow by half.

Most of these early experiments were designed to measure or estimate the pressure drop across a stenosed artery as pressure drops are related to the resistance to flow. The basic conclusion that can be drawn from these studies is that in general, it requires a fairly severe reduction (about 70 to 80 percent) in the cross sectional area of the lumen to cause a significant reduction in the blood flow in the vessel.

Another important flow characteristic is the shearing stresses on the arterial wall. Unfortunately, measuring the wall shear stress is a very difficult task. Fry (1968) carried out a notable experiment to study the acute vascular endothelial changes associated with increase in flow velocity, and developed an indirect method for estimating shearing stresses. Fry performed *in vivo* studies on the thoracic arteries of anaesthetised mongrel dogs to determine typical limiting wall shear stress values at which endothelial failure will occur. His study indicated that exposure to averaged wall shear stress in excess of about 380 $dynes/cm^2$ for periods as short as one hour could result in a marked deterioration of the endothelial surface.

1.3 Current State of Affairs

Although experimental studies, such as those discussed in the preceding section, have provided some useful information, they are usually invasive and quite expensive to carry out. Also, it may not be possible to repeat some of the experiments performed on animals under the same or similar conditions. Furthermore, experi-

mental measurements are unable to provide a complete picture of the flow patterns present in the vessels studied (Reul, 1984). Hence, researchers have turned to using mathematical models to study such blood flow problems since the mathematical modelling approach is less invasive and relatively more economical.

Mathematical modelling of blood flow in arteries is usually based on the Navier-Stokes equations for fluid flow and the continuity equation. These equations are statements of the conservation of momentum and the conservation of mass respectively. Together, they form a set of coupled, non-linear partial differential equations. To date, there is no known analytical or closed-form solutions to the complete equations.

The introduction of a constriction in the blood vessel further complicates the mathematical model. However, some investigators have managed to overcome some of these difficulties, usually by making certain assumptions in the model, thus simplifying the equations. Alternatively, some form of approximation may be used to obtain a solution. Such assumptions or approximations are usually necessary to make the mathematical problem more tractable.

Young (1968) was probably one of the earliest researchers to carry out such a mathematical study of the behaviour of blood flow in a stenosed artery. Using the Navier-Stokes equations and assuming an axially symmetric flow for a Newtonian fluid in a rigid tube with mild stenosis and neglecting radial velocity components, he was able to obtain approximate solutions for the model through an integral method.

Subsequently, Forrester and Young (1970a, 1970b) improved the model by assuming that the radial dependence of the axial velocity can be expressed as a fourth order polynomial with constant coefficients. This procedure is similar to the Karman-Pohlhausen method (Schlichting 1968) commonly used in the study of laminar boundary layers. Although closed-form solutions were obtained, the method

was only able to model very mild stenosis for a fairly limited range of Reynolds numbers.

Based on the Forrester and Young study, Morgan and Young (1974) extended the model by using both the integral-momentum and integral-energy equations and obtained an approximate solution which is valid for both mild and severe constrictions . They have retained the assumption of a fourth-order polynomial velocity profile and obtained approximations for shearing stresses on the vessel walls for low Reynolds numbers. Chakravarty and Chowdhurry (1988) developed an analytical approach to study the response of blood flow in a stenosed artery by using a power series approximation.

Numerous other approximate analytical solutions have also been attempted. For example, Padmanabhan (1980) obtained solutions for a mild stenosis model at very low Reynolds numbers with negligible viscous terms. His method of solution involved the use of modified Bessel functions. Chow and Soda (1972) expressed the governing equations in a stream-function vorticity form and obtained approximate solutions for flow through a mild stenosis using a perturbation method.

Besides these analytical methods, much work has resulted from the use of numerical schemes to find approximate solutions to the equations. The main advantage of a numerical method of solution is that some of the assumptions used in analytical methods need not be made. For instance, in most numerical models, the velocity profile need only be specified at the boundaries (the inlet and outlet and at the walls of the tube) and no assumption on the radial components of velocity need to be made.

Lee and Fung (1970) obtained numerical solutions to the Navier-Stokes equations for flow through a constricted tube by using a Taylor-series approximation and ignoring higher order terms. The geometry of the constriction was defined by a

Gaussian normal distribution curve and solutions were sought for very low Reynolds numbers (0 to 25). Calculations were not extended to higher Reynolds numbers due to instabilities in the numerical procedures. Subsequently, Lee (1994) carried out some numerical studies at moderate Reynolds numbers ranging from 5 to 200.

The finite difference technique has also been successfully employed by investigators such as Deshpande *et al* (1976), Chakravarty and Datta (1989) and Huang *et al* (1993) to carry out studies on blood flow through stenosed arteries. Deshpande *et al* obtained results for an axisymmetric model which compared well with results from the experiments carried out by Young and Tsai (1973).

Chakravarty and Datta incorporated non-Newtonian characteristics (in the form of a Herschel-Bulkley model) into their model of flow through an anisotropic viscoelastic cylindrical tube. The resulting governing equations were solved using a finite difference scheme based on the central difference formula and the Thomas algorithm for solving a tridiagonal system of equations.

Huang *et al* solved a two-dimensional, incompressible flow model using the SIMPLE algorithm to solve the resulting algebraic equations after casting the problem in a finite difference formulation. Their scheme allows the model to include Reynolds numbers of up to 1000.

Besides the finite difference method, the other numerical scheme commonly used in the study of fluid flow is the finite element method. Rooz *et al* (1982) studied the effects of a pulsatile flow in a straight flexible tube with a partial obstruction using the finite element formulation. However, in their model, the governing equations used were the continuity equation, a one-dimensional momentum equation and an equation of state relating the tube cross sectional area to pressure. They had assumed that the relationship between the tube cross sectional area and the pressure can be expressed as a quadratic equation. Although the model forms an interest-

ing mathematical study, it is fairly limited in terms of application to a physiologic situation because of the assumptions made.

Recently, Rathish Kumar and Naidu (1996) proposed an ingenious numerical method for a mathematical modelling of a non-linear pulsatile flow in a stenosed artery using the finite element method.

Nakamura and Sawada (1988) also used the finite element method and developed a model for the flow of an non-Newtonian fluid (biviscosity model) through an axisymmetric stenosis. Their results show that non-Newtonian effects weaken the distortion of flow patterns, pressure distribution and shear stress at the arterial walls.

More recently, Tandon *et al* (1993) employed the finite element scheme to model the flow of a Casson fluid through a narrow artery with axisymmetric identical double stenoses. Their study concluded that the non-Newtonian nature of blood helps in reducing the magnitude of the peak wall shear stress at the throat of the stenosis and the length of the reduced flow region downstream of the stenosis.

The application of the finite element method would usually involve the solution of a large system of algebraic equations. With the advent of high speed digital computers, this task has since been made more manageable. Therefore, it is not surprising that in recent years, the use of this technique in modelling blood flow has been exploited by many other researchers such as Luo and Kuang (1992), Ma *et al* (1992), Tu *et al* (1992) and Perktold *et al* (1994).

While studies utilising such numerical schemes have produced much satisfactory results, most of the models have assumed an axisymmetric stenosis in a straight rigid tube. The solutions of the governing equations are usually solved in two dimensions and the shapes of the stenoses are determined by a formula which normally stipulates a symmetry about the axis of the tube. Although the use of numerical techniques

has allowed more features (such as non-Newtonian nature of blood, elastic nature of tube and so on) to be incorporated into the model compared to the analytical approach, it would be desirable to construct models which are not constrained by the condition of axisymmetry. Also, there has not been much work done in the three dimensional modelling of blood flow in vessels with asymmetric stenoses.

In recent years, the use of CFD computer codes has provided researchers with yet another useful tool to carry out investigations in this area. Johnston and Kilpatrick (1991a) used the CFD code, FIDAP, to study the effects of paired stenoses on the pressure drops across the stenoses. Besides obtaining conclusions on the effects of relative severity of stenoses on pressure drops, their study demonstrated the usefulness and efficiency of packages such as FIDAP in blood flow modelling. The flexibility in the use of such CFD codes was also demonstrated in their study on flow through an irregular stenosis (Johnston and Kilpatrick 1991b). More recently, Sidik and Mazumdar (1994) employed another code, PHOENICS, to construct and study a model of turbulent blood flow through an arterial bifurcation.

Dvinsky and Ojha (1994) developed and used a computer code, HEMO, on a workstation to simulate a three-dimensional flow through an asymmetric stenosis. However, the main objective of their study was to evaluate the code and as such, they have not considered certain important aspects, such as shearing stresses on the vessel walls, in their modelling study.

From the preceding discussion, it is clear that there are basically three approaches to the theoretical study of blood flow problems : analytic solution approach, numerical schemes and methods involving the use of CFD codes.

Because of the difficulties in solving the governing equations, in the analytic approach to solving blood flow problems, many assumptions had to be made, thus rendering the model less realistic. The application of numerical schemes has allowed

more features to be included and made fewer assumptions. However, problems of instabilities may arise at high Reynolds number. Also, most numerical schemes require the vessel boundaries and the stenoses to be specified in the form of an equation and this usually leads to an axisymmetry constraint.

The use of CFD codes is a promising alternative if the problem can be properly defined and cast into the program's problem formulation. With such powerful tools, it would be possible carry out studies of blood flow through asymmetric stenoses in three dimensions. As we can see from the general survey of the literature presented in this section, studies of blood flow in three dimensions with an asymmetry in the constriction have so far been very limited.

Moreover, most mathematical models of blood flow through stenosis have assumed flow in a straight tube. Blood vessels are seldom straight conduits and stenoses on bends or curves are not uncommon. Thus, it would be highly desirable to construct models of curved arteries with stenoses. To date, there has been very little work done in such modelling studies.

The present study is motivated by the need for geometrically realistic models in three dimensions as information from a three dimensional simulation may be helpful in enhancing our understanding of the arterial disease patterns. In this thesis, the application of CFD techniques in the construction of three dimensional models to elucidate the complex flow patterns associated with flow through stenosed arteries will be examined. The primary aim of the present study is to obtain quantitative solutions from these models as the solutions may provide some insight into how the dynamics of blood flow can be related to some of the pathological problems found in human arteries.

1.4 Outline of Approach in the Present Study

To achieve the aim stated above, the present study has been organised in the manner described below :

In Chapter 2, a brief description of the human circulatory system is first presented to provide the background required for the discussion in this thesis. The morphological structure of blood vessels, in particular, arterial vessels, and their associated pathological problems are discussed briefly. The risk factors for the arterial disease, atherosclerosis, are discussed and a widely accepted hypothesis for the genesis of atherosclerosis is described.

Chapter 3 examines how the basic physics and laws of fluid dynamics may be applied to flow through blood vessels. The application of CFD techniques in the solution of such problems is discussed. The use of commercial CFD codes will be justified and a brief description of the packages, FIDAP and PHOENICS, is given.

In the next three chapters, three models are constructed, each introducing subsequent improvement over the previous. In Chapter 4, an axisymmetric model is constructed to demonstrate the usefulness of CFD codes in blood flow modelling studies. Although the model is not in three dimensions and is fairly simple, it serves to demonstrate the potential effectiveness of using CFD codes in simulating blood flow. This first model uses the FIDAP code.

Chapter 5 describes the formulation of a three dimensional model using another commercial CFD code, PHOENICS. A geometrical description of the model and the formulation of the problem in PHOENICS are presented. The intrinsic difficulties in the description of results in three dimensional modelling are made apparent in this chapter. We also look at an important flow characteristic, namely, the wall shear stress, and how it can be estimated in our models.

In Chapter 6, we extend the study in Chapter 5 to a curved artery model in three dimensions. The formulation of the model is discussed in detail. Secondary flow phenomena are particularly important in this model and these are also examined in some detail. Arteries are generally not straight tubes, and the curved artery model described in this chapter hence represents a generalisation of models that can be constructed using CFD codes.

The concluding chapter, Chapter 7, summarises the work done and discusses the clinical significance of the present study. Suggestions for future work in this area are also presented.

CHAPTER 2

THE HUMAN CIRCULATORY SYSTEM

2.1 Introduction

As we have seen in the discussion in Chapter 1, numerous studies have been carried out in the past few decades in the area of modelling of blood flow in arteries. Information from these studies may provide some insight into vascular disorders and the disease process. Before considering these modelling studies, it would be expedient to first describe the human circulatory system to provide the background required for the discussion to follow.

In this chapter, a brief description of the human circulatory system is first presented. Arterial vessels are then described in some detail since our main interest is on arteries. This is followed by a discussion on arterial disorders and the risk factors that have been identified to be associated with the disease. A widely accepted hypothesis for the genesis of arterial disease will be discussed. Many researchers believe that this hypothesis may be supported by certain theories in hemodynamics. Some of these proposed theories will be discussed at the end of this chapter.

2.2 Brief Description of the Human Circulatory System

The circulation of blood in the human body is divided into two major systems known as the pulmonary circulation and the systemic circulation, arranged in series as shown in Figure 2.1. The two systems of circulation are very similar. Each consists of a pump, a network of distributing vessels and arteries, a diffusing system and a collection system.

The pulmonary circulation begins at the right ventricle of the heart and transports blood only to the lungs, where gas exchange can occur. As the lungs are in close proximity to the heart, the pulmonary circulation functions as a low-pressure system. The systemic circulation initiates at the left ventricle and is responsible for supplying blood to all the other organs and tissues of the body. The systemic circulation functions as a high-pressure system as it needs to transport blood to distant parts of the body.

The pumping action of the heart is a two-phase process. During its relaxation phase (diastole) the heart is filled with blood. It then expels some of the blood during the contraction phase (systole) and delivers blood to both the pulmonary and systemic circulation. Blood is returned to the right heart from the systemic circulation as deoxygenated blood, which is then pumped into the lungs where gas exchange takes place. It is then returned to the left heart from the lungs as oxygenated blood, which is subsequently pumped into the systemic circulation.

Blood pumped from the heart is carried by the arteries under pressure to the tissues and various organs of the body via smaller vessels called arterioles and capillaries. Arterioles have a narrower lumen (the space enclosed by the arterial wall) and are a major site of resistance to blood flow. The capillaries form a network with a very large total cross-sectional area through which blood flows slowly, providing ideal conditions for exchange between blood and interstitial fluid.

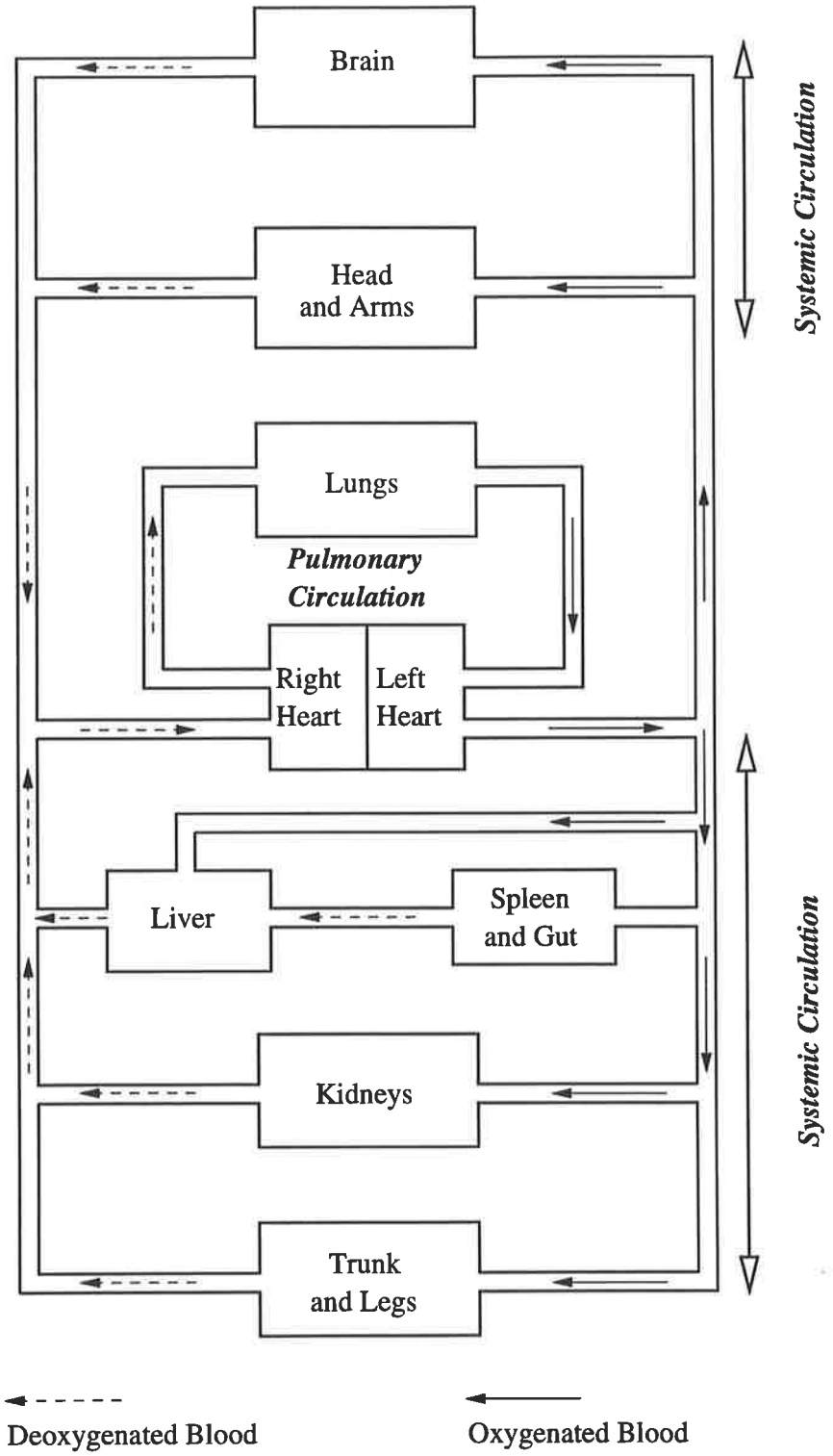

Figure 2.1: Schematic representation of the human circulatory system, showing the pulmonary circulation and the systemic circulation

Blood is returned to the heart through a collection system made up of a primary set of collecting tubules, the venules and veins. Systemic veins have a relatively large capacity and in the resting supine position, veins hold four times as much blood as do the arteries. However, the mean velocities of flow in the arteries are generally higher than that in the veins. The relationships between percentage of blood volume, cross-sectional area and mean velocity of blood flow in the vessels of the systemic circuit are summarised in Figure 2.2.

In the present study, the focus is on flow in the arteries of the systemic circulation and in particular, the coronary circulation. In the next section, we shall describe in some detail the general structure of arterial vessels.

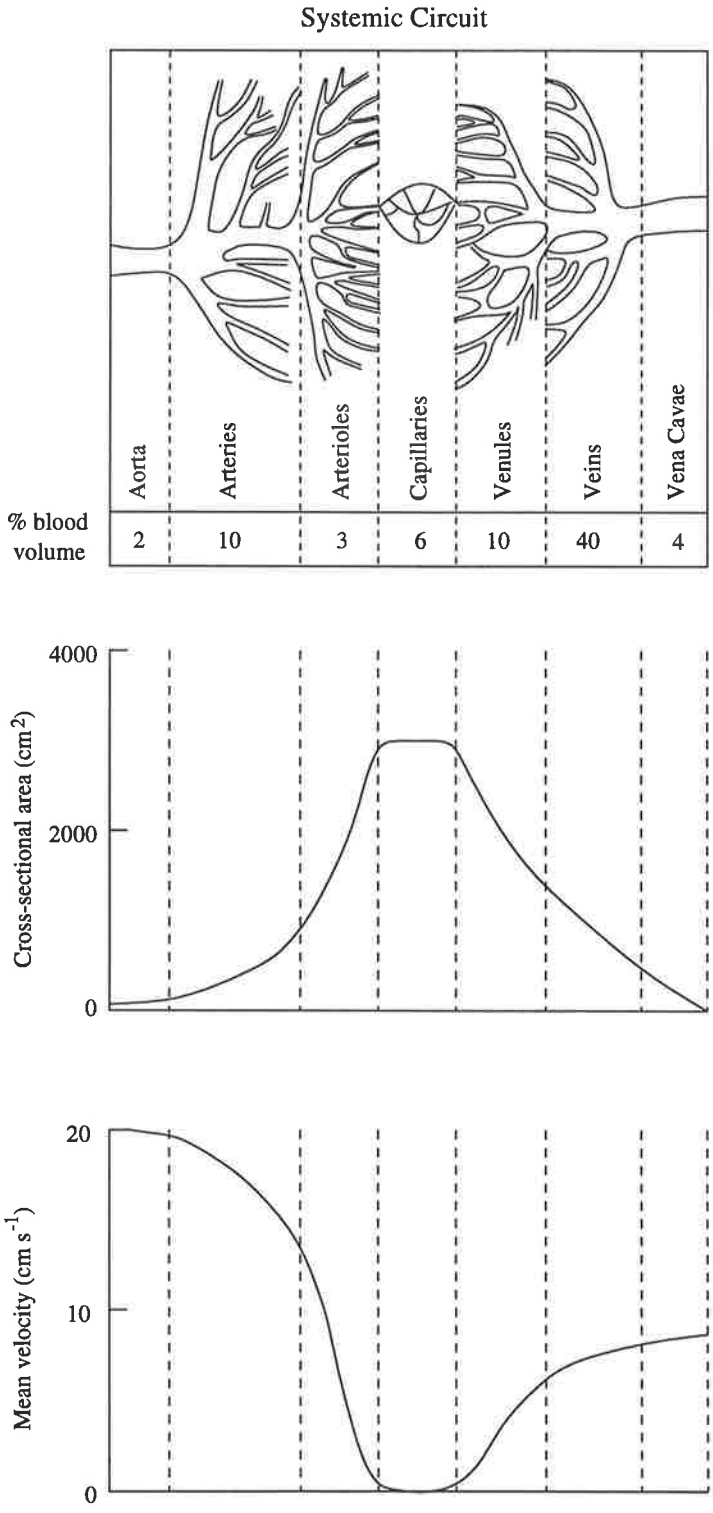

Figure 2.2: Relationships between % blood volume, cross-sectional area and mean velocity in the systemic circuit in the supine position. Adapted from Bray, J.J. *et al* (1989).

2.3 Arterial Vessels

The basic morphologic structure of the wall of an artery is shown in cross section in Figure 2.3. The wall of an artery consists of three main layers, *tunica intima*, *tunica media* and *tunica adventitia*, interspersed with elastic fibres and connective tissues. The innermost part of the arterial wall is lined with a layer of endothelial cells forming the *endothelium*. Between the main layers are elastic membranes whose thickness varies from artery to artery.

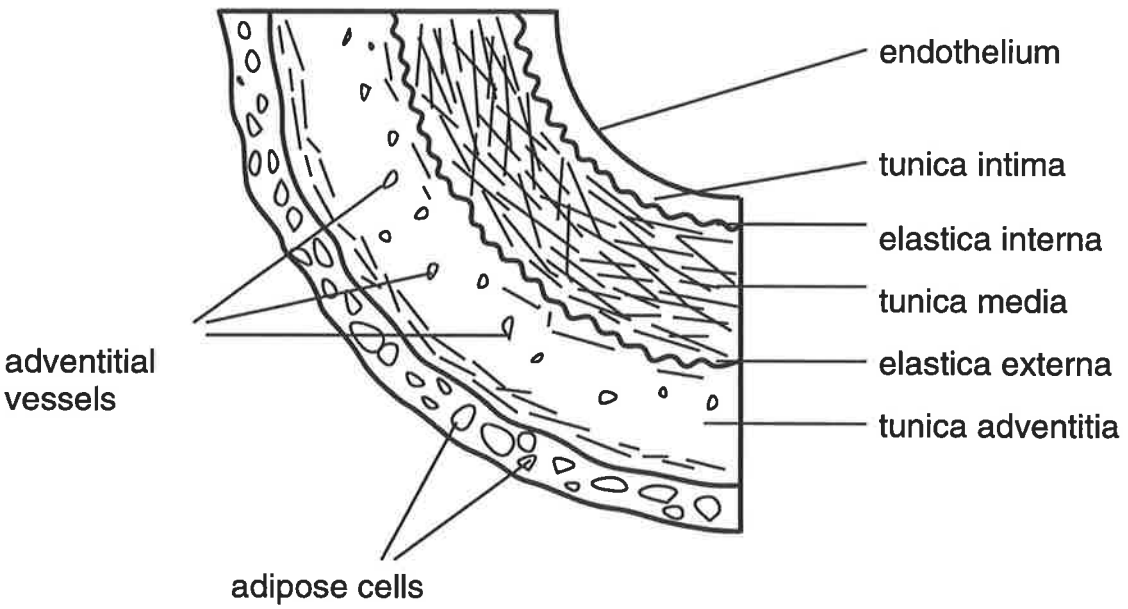

Figure 2.3: Cross-section of a typical artery to illustrate the several layers of tissue in the walls of an artery. Adapted from Jensen (1980).

Depending on the composition of the constituents, the relative diameter and distance from the heart, arteries may be classified as elastic arteries, muscular arteries or arterioles. Different classes of arteries bear different physical properties and generally have varying effects on the blood flow.

The largest arteries are predominantly elastic, even though their walls also contain smooth muscle. Elastic arteries are large and have thick walls with prominent series of elastic membranes within their walls. However, relative to the internal diameter, the walls of large arteries are thin as they have a much larger lumen. Elastic arteries are highly distensible and this particular characteristic, to a certain extent, helps in dampening the pulsations as blood is being pumped from the heart at high pressures. However, through disease or ageing, the arteries may become less elastic, making them distend less easily and recoil less forcibly. Thus as one ages, it is expected that one's arteries lose both their compliance and their elastance.

The most numerous arterial structure in the human body is the muscular arteries and these form the major distributing system of the systemic circuit. The walls of muscular arteries contain a thick layer of smooth muscle fibres, together with collagenous tissues. These arterial components are continuous with surrounding loose connective tissues, and thus their movements permit the vessels to change their diameter readily. Longitudinally, these arteries are under a state of tension and this property is evident from the fact that the vessels retract when severed (Fung 1981).

Arterioles are the smallest arteries with diameter ranging from about 20 μm to 200 μm. They are the components of the vascular system where the greatest resistance is sited. Of all vessels, the arterioles have the thickest walls relative to the size of their lumen. Internal elastic membranes are absent in arterioles but loose connective tissues are found in their walls. The smooth muscles in arterioles are arranged in a tight spiral such that its contraction decreases diameter and raises the resistance to blood flow. Because of the high resistance in arterioles, there is a steep fall in pressure as blood flows through them from arteries into capillaries. The more they constrict, the steeper the pressure drop. The characteristics of various types of blood vessels are shown in Table 2.1.

Table 2.1: Characteristics of various types of blood vessels in humans

	Lumen Diameter (mm)	Wall Thickness (mm)	Mean pressure (mm Hg)
Aorta	25	2	100
Artery	4	1	75-95
Arteriole	0.03	0.02	35-70
Capillary	0.005	0.001	15-35
Venule	0.02	0.002	10-15
Vein	5	0.5	10 or
Vena Cava	30	1.5	less

An important component of the arterial wall is the endothelium, the innermost layer of cells that comes into contact with the flowing blood. It has two major tasks. It has to prevent the adhesion of various species to the vessel wall, and at the same time selectively allow substances such as water, electrolytes and sugars to pass from the blood to the tissues. The endothelium is a single layer of cells, aligned in the direction of the flowing blood. There is also evidence to suggest that the endothelial cells will respond to changes in the flow pattern (Fry 1968). It is thus not surprising that the endothelium has received much attention in this area of research.

As can be seen from the above discussion, arterial vessels are by no means inert tubes. The presence of muscle tissues and elastic fibres in the walls of arteries and the nature of the living endothelium suggest that besides serving their main function as conduits in the circulatory system, arteries are capable of responding to the influences and dynamics of blood flow.

2.4 Arterial Diseases

Cardiovascular diseases (i.e. diseases of the heart and blood vessels) are responsible for more morbidity and mortality than any other human disease, particularly in Western societies. In Australia, for instance, cardiovascular disease claims a life

every ten minutes. Although the death rate [1] from cardiovascular diseases continues to fall in recent years, it remains the number one killer in Australia. Table 2.2 shows the total Australian deaths and their causes in 1993.

Table 2.2: Total Australian Deaths, 1993 : All Ages

Cause of Death	Males		Females		Total	
	No.	%	No.	%	No.	%
Cardiovascular Disease :						
Coronary Heart Disease	16,335	25.1	13,424	23.8	29,759	24.5
Stroke	4,818	7.4	7,319	13.0	12,137	10.0
Other Cardiovascular Disease	5,216	8.0	6,124	10.8	11,340	9.3
All Cardiovascular Disease	26,369	40.5	26,867	47.5	53,236	43.8
Cancer	18,479	28.4	14,212	25.1	32,691	26.9
Traffic Accidents	1,384	2.1	572	1.0	1,956	1.6
AIDS	689	1.1	29	0.1	718	0.6
All Other	18,164	27.9	14,829	26.2	32,993	27.1
All Causes	65,085		56,509		121,594	

Source : *The Annual Report, National Heart Foundation of Australia, 1994.*

It is evident that cardiovascular diseases are the main cause of death and of these, coronary heart disease (i.e. disease of the coronary arteries) alone is responsible for about a quarter of all deaths. Coronary arteries are arteries arising from the proximal ascending aorta immediately above the attached margins of the aortic valve and they supply blood to the heart muscles. Figure 2.4 shows the coronary arteries surrounding the heart. It is important to note that in general, the coronary arteries curve and bend around the heart and some of the branches can be extremely tortuous.

[1] "Death Rate" is defined as the number of deaths among a fixed number of the population

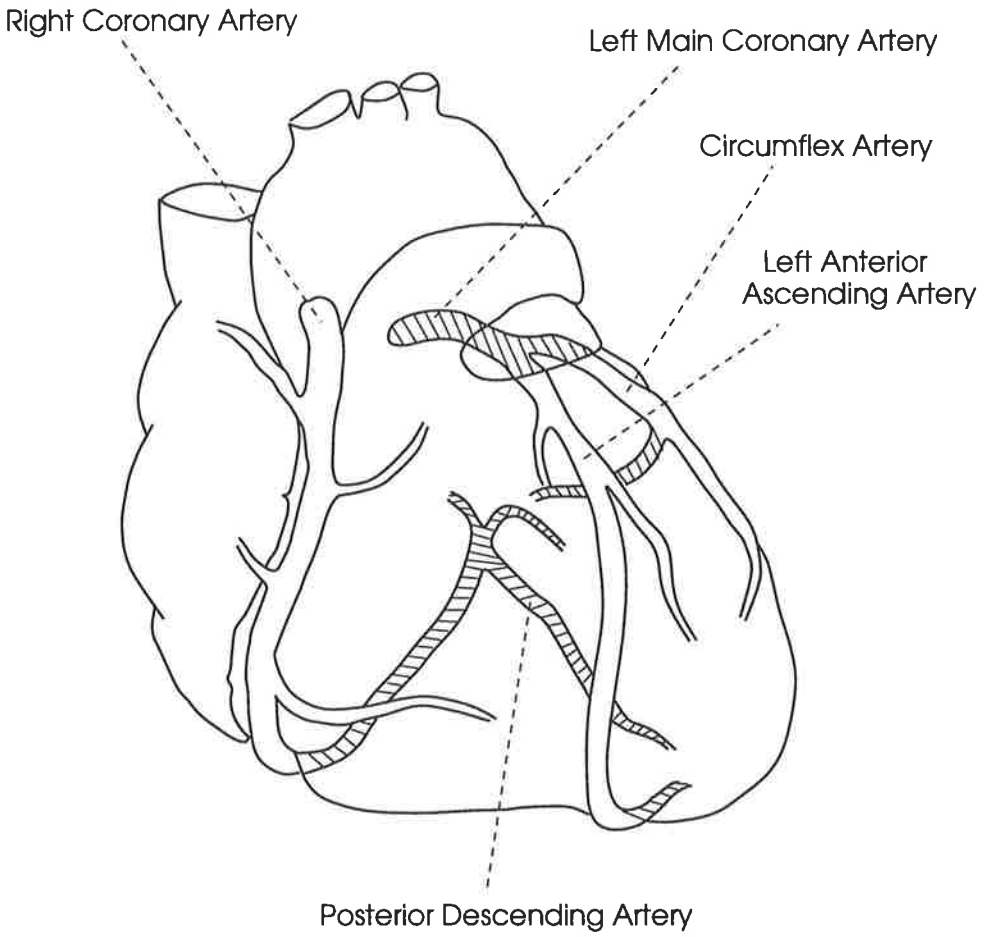

Figure 2.4: Schematic diagram of the heart in antero-posterior projection, showing the major coronary arteries. The proximal portion of the left coronary artery is shaded, as are the posterior portions of the right coronary and circumflex arteries.

2.4.1 Arteriosclerosis

Arterial disorders occur chiefly in three forms : (1) narrowing of vessels (2) damaging of endothelial lining, thus promoting intravascular thrombosis and (3) weakening of vessel walls leading to possible rupture of the walls. The generic term for vascular diseases associated with thickening and inelasticity of arteries is *arteriosclerosis.* There are three patterns of arteriosclerosis, namely, *atherosclerosis, Mönckeberg's medial calcific sclerosis* and *arteriolosclerosis.*

The first of these patterns, atherosclerosis, is the dominant form of arteriosclerosis. Characterised by the formation of intimal fibrofatty plaques, atherosclerosis is a disease of large- and medium-size arteries. The presence of these plaques or lesions inside the vessel causes a reduction in the lumen and supply of blood to the organs served by these arteries is subsequently reduced.

Although atherosclerosis can theoretically occur in any artery, the major targets are the aorta and the coronary and cerebral arteries. Stenosis of the coronary arteries, or coronary atherosclerosis, can result in a severe reduction of blood supply to the heart, inducing ischemia of the heart. Ischemia is a condition suffered by an organ or part of the body when its blood supply becomes deficient. When the arterial lesions are complicated by thrombosis (i.e. clotting inside a living blood vessel), myocardial infarction, more commonly known as "heart attack", may occur. Severe cases of myocardial infarction can be fatal.

Treatment for coronary stenosis is usually either balloon angioplasty or a surgical bypass. In balloon angioplasty, a catheter with a balloon at the tip is introduced into the diseased vessel and inflated at the location where the vessel is stenosed, thus pushing the blockage back into the wall. However, it is possible for patients who have undergone balloon angioplasty to experience regrowth of the stenosis, either at the original location of at a different site. More severe cases of coronary atherosclerosis

may require a bypass operation, in which part of a blood vessel taken from another part of the body is grafted to the diseased artery.

2.4.2 Risk Factors

The concept of risk factors for atherosclerosis has emerged from studies of ischemic heart disease in human populations. One notable study was conducted in Framingham, Massachusetts, where 5,127 individuals have been followed biennially for the development of initial attacks of coronary heart disease since 1949 (Kannel *et al* 1961). The Framingham study reveals a number of factors which are now recognised as risk factors. Any factor associated with doubling in the incidence of ischemia heart disease has been defined as a "risk factor". This section reports some of the findings from the Framingham study on risk factors of atherosclerosis.

Age and Sex

It has long been recognised that the severity of coronary atherosclerosis increases with age (Strong and McGill 1962). Although early lesions of atherosclerosis appear in childhood, the Framingham study found that clinically significant attack of the disease rarely occur before age 40.

Other factors being equal, males are much more prone to atherosclerosis than females. Between ages 35 and 55 years, white women have one fifth the mortality from ischemic heart disease of white males. However, the immunity of women to coronary heart diseases is only relative to men, since even in women, it is still a common disease and a leading cause of death.

Blood Cholesterol Level

It has been found that levels of serum cholesterol are directly correlated with the incidence of ischemic heart disease. A variety of lipids and their lipoproteins have been implicated in the initiation of atherosclerosis (Kannel *et al* 1964). How-

ever, there is still uncertainty over which lipid or lipoprotein is most basic to the atherosclerotic process. Nonetheless, the Framingham study found that each of the major lipids and lipoproteins encountered in blood is related to the incidence of ischemic heart disease.

Hypertension

An increase in blood pressure is consistently associated with a risk of myocardial infarction. All grades and types of high blood pressure, or hypertension, are contributors to coronary heart disease at all ages in both sexes. In the Framingham study, men aged 45 to 62 whose blood pressure exceeded 160/95 mm Hg had a more than fivefold greater risk of ischemic heart disease than those with blood pressures of 140/90 mm Hg or lower (Kannel *et al* 1967a). Control of hypertension has resulted in a significant decrease in the incidence of myocardial infarction and stroke. However, it is still unclear how elevated blood pressure accelerates the process of atherosclerosis.

Cigarette Smoking

Atherosclerosis of the coronary arteries and the aorta is more severe and common among cigarette smokers than among non-smokers. The risk is related to daily consumption, and the effect appears to be transient and reversible. It appears that giving up the smoking habit lowers the risk dramatically (Kannel *et al* 1968).

Diabetes

The incidence of myocardial infarction is twice as high in diabetics as in non-diabetics. Diabetics have a higher risk of occlusive vascular disease in many other organs as well, including the brain and lower extremities.

There exist other factors whose impact on the initiation of atherosclerosis is less clearly defined. For instance, the Framingham study found that being more than

30% overweight increases the mortality rate from ischemic heart disease (Kannel *et al* 1967b). Also, it appears that physical activity reduces the risk of sudden death from ischemic heart disease. However, the mechanism by which these factors accelerate the disease process is unclear.

Although the above factors have been identified and accepted to a certain extent as major risk factors, atherosclerosis may still develop in the absence of any of these factors. Those who live the "prudent life" and have no genetic predisposition are not immune to the disease. While knowledge of such risk factors may be useful in lowering the risk of the disease, it does not explain the cause of atherosclerosis.

2.4.3 Pathogenesis of Atherosclerosis

Because of the importance of atherosclerosis, much research has been carried out to discover its cause and explain the genesis or initiation of the disease. Vast amount of information has accumulated, but unfortunately, the cause of atherosclerosis is still not established.

Many theories on the pathogenesis of atherosclerosis have been proposed but favoured today and receiving the greatest attention is the "response-to-injury" hypothesis. This hypothesis best accommodates the various risk factors discussed earlier.

The "response-to-injury" concept is illustrated in Figure 2.5. A lesion is initiated by some form of injury or damage to the endothelial cells, which, under normal conditions, form a complex barrier and are in dynamic equilibrium with their immediate environment. Once injured, the endothelial cells fail in their function and increased adhesion and permeability soon follow. Platelet aggregation and seeping of plasma constituents into the tissues will take place. A tissue response is then triggered and the formation of atherosclerotic plaque is initiated.

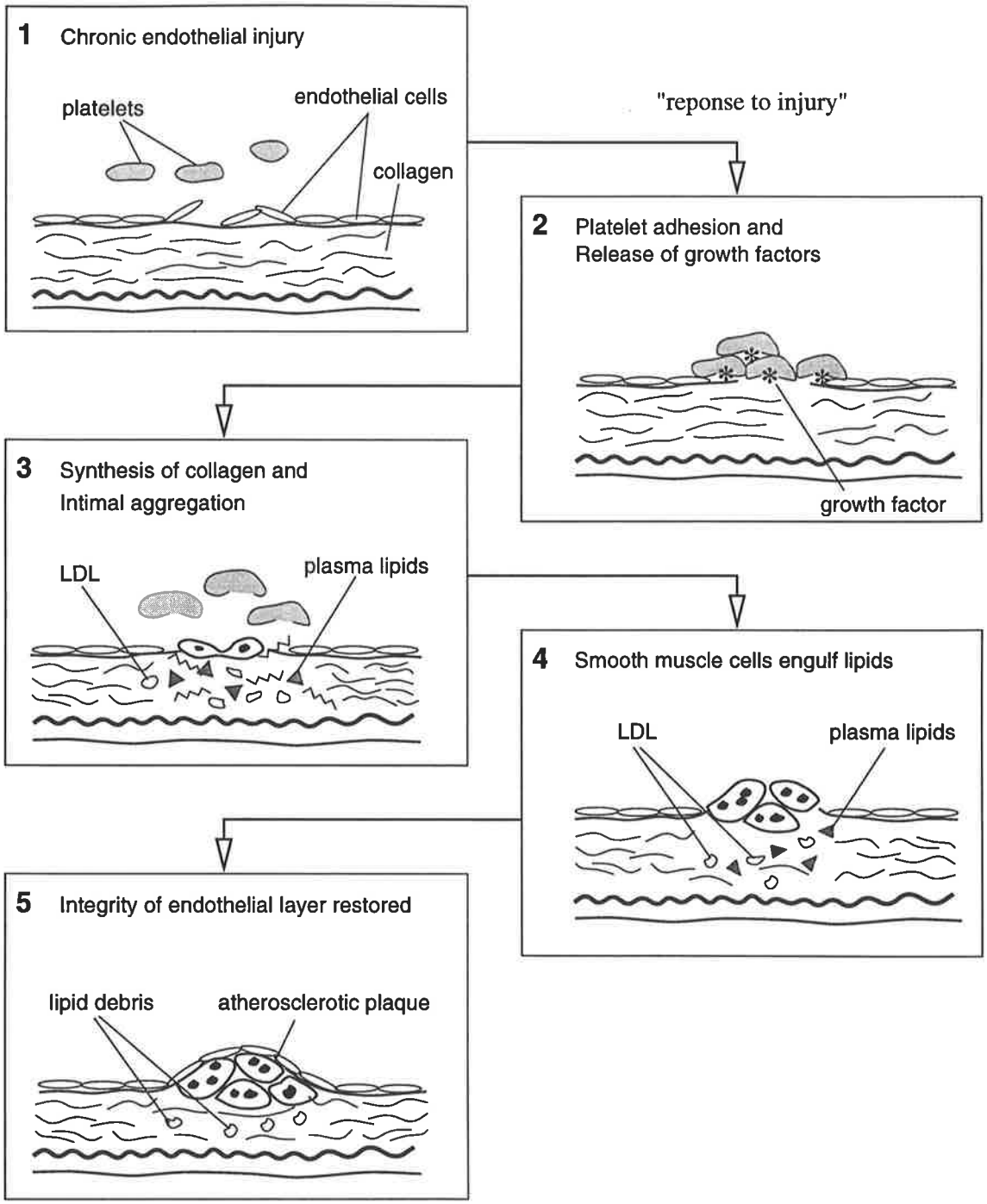

Figure 2.5: Diagram showing the different stages of atherogenesis according to the response to injury hypothesis

Platelets adhere to the vessel wall and release a growth factor that stimulates the smooth muscle cells which then begin to engulf lipids and proliferate. The influx of low-density lipoproteins, or LDL, enhances this reaction. This could explain why a high level of cholesterol is related to the incidence of atherosclerosis.

Regeneration of the endothelial layer will then ensue to restore the integrity of the endothelium. An atherosclerotic plaque is thus formed. Coronary arteries are particularly susceptible to luminal narrowing at a relatively early stage by atherosclerotic plaques.

2.5 Hemodynamics and Atherogenesis

Central to the "response-to-injury" hypothesis is damage to the endothelial lining. Although this hypothesis is able to explain the association of the various risk factors, it fails to explain the cause for the damage of the endothelium. The risk factors may accelerate the atherosclerotic process, but statistical associations of the disease with the risk factors cannot be considered causal relation. Thus, it seems fair to say that the risk factors that have been identified by studies such as the Framingham Study can only be regarded as secondary or modifying influences. The primary cause of the disease would have to be the mechanism which brings about endothelial damage.

Many researchers (for example, Texon 1963; Gessner 1973; Nerem and Cornhill 1980; Glagov *et al* 1988) believe that the fluid dynamics of blood flow, or hemodynamics, could play a key role in causing primary damage to the arterial wall. The main reason for this is the fact that the growth of atherosclerotic plaques occurs chiefly at some favoured sites in the arterial tree. In particular, the sites for predilection are characterised by tapering, curvature, bifurcation and branching. This has led researchers to suggest that mechanical influences such as increased flow velocity, elevated shearing stresses and recirculation and turbulence in flow are

responsible for causing endothelial damage.

However, there are still questions on exactly how these mechanical forces could interact to cause damage to the endothelium (Nerem and Cornhill, 1980). For example, Texon (1963) hypothesised that the suction effect of the lateral pressure at sites of attachment stimulates intimal proliferation (Figure 2.6). However, Gessner (1973) argued that a suction action on the endothelium will exist only if the local pressure beneath the endothelium exceeds the intraluminal pressure, which is unlikely to occur over a significant period of time and hence Texon's suction model is untenable.

From the preceding discussion, it is clear that in order to improve our knowledge on the role of hemodynamics in the genesis and process of atherosclerosis, more quantitative work is needed. There is no doubt that with the advent of high speed digital computers, computational fluid dynamic techniques will play an increasingly significant part in the development of mathematical modelling studies in blood flow problems with the hope of gaining better insight in this area. The next chapter discusses the application of computational fluid dynamic methods to study blood flow using mathematical models.

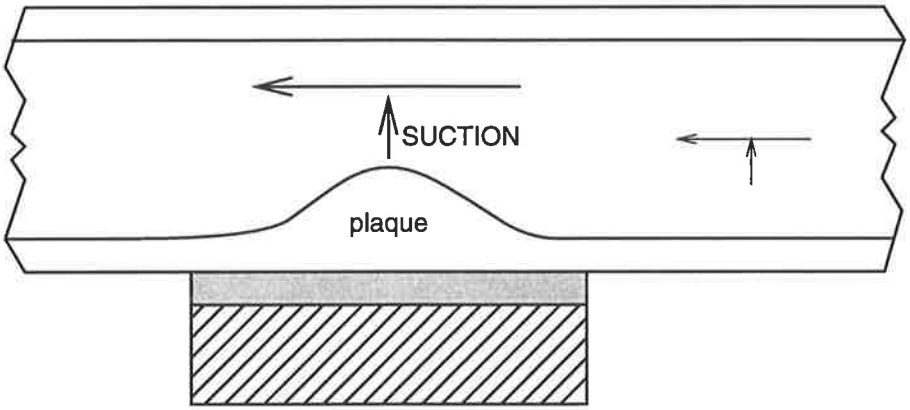

Figure 2.6: Velocity and pressure (suction) changes associated with atherosclerotic plaque at zone of attachment. Texon's model (1963) which is refuted by Gessner (1973).

CHAPTER 3

CFD TECHNIQUES AND APPLICATIONS IN BLOOD FLOW STUDIES

3.1 Introduction

As we have seen from the description of arterial vessels in Chapter 2, arteries are elastic tubes, capable of responding to physical and physiological influences. The blood flowing in these vessels is a complex suspension of red and white corpuscles, platelets and lipid globules in plasma, a colloidal solution of numerous materials. Despite the difficulty arising from these complexities, extensive insight into cardiovascular flows can still be obtained through mathematical modelling by applying computational fluid dynamic, or CFD techniques to simpler physical systems.

The literature contains many examples of mathematical models for various fluid dynamic systems, with analytic or numerical methods of solution. Consequently, this chapter shall be restricted to a discussion at a relatively qualitative level. The more important equations and aspects will be presented as they are needed in later chapters.

In this chapter, the basic fluid laws relating to flow through vessels will first be described. The general principles of CFD techniques will then be presented. Two commercial CFD codes, FIDAP and PHOENICS will be introduced and only briefly described as details of the usage of the these packages can be found in the respective

manuals.

3.2 Fluid Dynamics of Blood Flow

Mathematical studies of blood flow are based on the application of physical principles and equations to describe the behaviour of fluids in tubes. A brief description of some of these principles is presented in this section.

Viscosity of Blood

Viscosity is defined as the property of a fluid that determines its resistance for its own motion. The origin of this resistance can be attributed to adhesive and cohesive forces within the fluid. Mathematically, viscosity is defined as the ratio of shear stress to the velocity gradient (i.e. shear rate) and is usually denoted by μ.

A Newtonian fluid is one with a constant viscosity. Blood, being a suspension of blood cells in plasma, is a non-Newtonian fluid. However, under conditions of relatively high velocity as in the arteries which develop atherosclerosis, and in vessels with diameter larger than 0.5 mm, the viscosity of blood does not alter appreciably (Texon 1963).

Laminar and Turbulent Flow

There are two basic models of viscous fluid motion – laminar flow and turbulent flow (Figure 3.1). For an axisymmetric laminar flow in a pipe, the particles of the fluid follow straight line paths parallel to the pipe axis. Such layered or laminar flow has a parabolic velocity profile. In turbulent flow, the particles follow a random path and only the average motion is along the pipe axis. Laminar flow occurs at velocities up to a certain critical velocity. Above this critical velocity, the flow becomes turbulent. The transition of flow from laminar to turbulent can sometimes be determined by the Reynolds number of the flow.

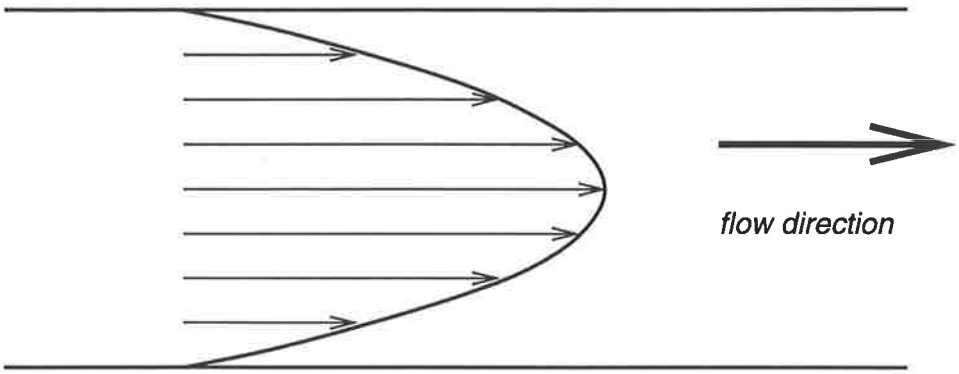

Laminar flow

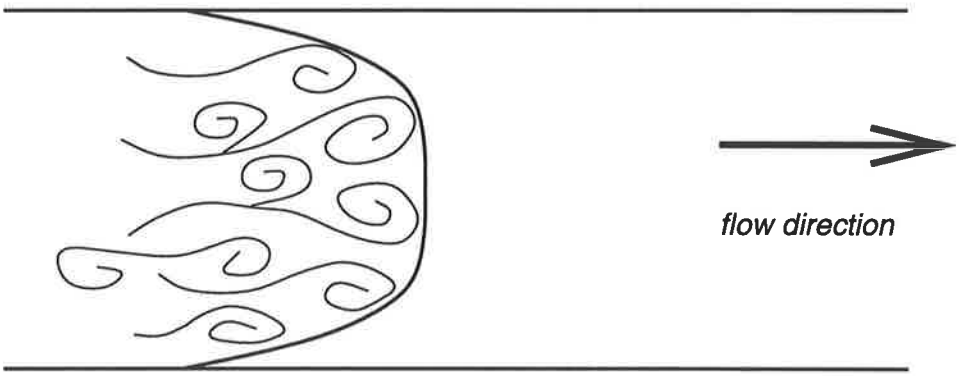

Turbulent flow

Figure 3.1: Velocity profiles of laminar and turbulent flows

The Reynolds number, Re, for flow in a pipe is usually defined as

$$Re = \frac{VD}{\nu} \tag{3.1}$$

where V is the velocity at the center, D is the pipe diameter and ν is the kinematic viscosity of the fluid. The kinematic viscosity is defined as

$$\nu = \frac{\mu}{\rho} \tag{3.2}$$

where ρ is the fluid density.

It has been shown that above a critical Reynolds number, there will be a transition of fluid motion from laminar to turbulent. It is widely accepted that the critical Reynolds number for this transition is 2,000 (McDonald 1960; Mazumdar 1992). In the human circulatory system, the flow of blood is normally laminar. However, irregularities and stenoses in the blood vessels may produce turbulence.

Poiseuille Flow Formula

For flow in a long narrow tube, neglecting end effects, the Poiseuille formula for the relation between the volume of flow, Q, and pressure difference, ΔP is given by

$$Q = \frac{\Delta P \pi R^4}{8\mu L} \tag{3.3}$$

where L and R are the length and radius of the tube respectively.

It follows that the average velocity (which is the volume flow divided by area of cross section of tube) is given by

$$\overline{V} = \frac{\Delta P R^2}{8\mu L} \tag{3.4}$$

The relation between the resistance to volume flow, K, the volume flow and the pressure difference is given by

$$K = \frac{\Delta P}{Q} \tag{3.5}$$

Hence, from Equation (3.3), K may be written as

$$K = \frac{8\mu L}{\pi R^4} \tag{3.6}$$

Thus, it is clear from the equation above that the resistance to volume flow is related to the geometry of the vessel and the viscosity of the flowing fluid but independent of the flow velocity.

Shear Stress

It is usual and reasonable to suppose that the blood in immediate contact with the vessel wall has the same velocity as the vessel wall. This particular type of boundary condition is known as the "no slip condition" and is commonly used in blood flow models. It follows that at the arterial walls, the flowing blood in the vessel will generally have a non-zero velocity gradient, $\frac{du}{dy}$, where u and y are the velocity component and space coordinate respectively, as shown in Figure 3.2.

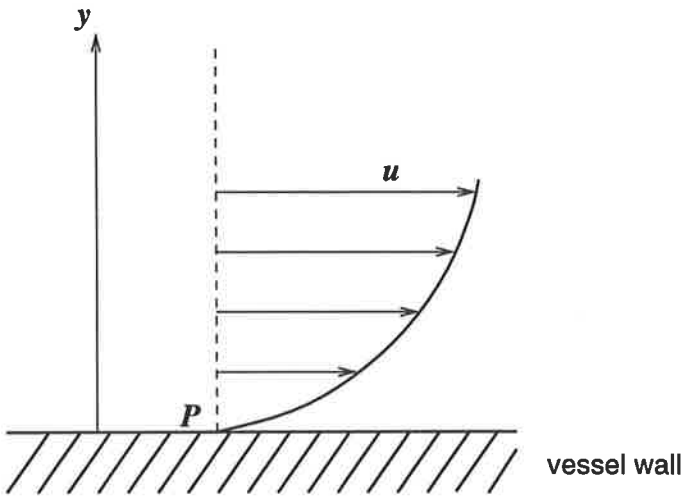

Figure 3.2: Diagram showing the velocity component, u, in the direction of the flow and the space coordinate y. No slip condition is applied at P.

The shear stress, τ, at point P is related to the velocity gradient by

$$\tau = \mu \left. \frac{du}{dy} \right|_P \tag{3.7}$$

where μ is the viscosity of blood.

Shearing stresses on the walls are difficult to measure and very often, in blood flow models, they are derived or estimated from the values of the velocity components using the relationship above.

The various properties of fluids and fluid flow may be applied to the study of blood flow together with the equations governing the motion of fluids. In their most basic form, these governing equations are partial differential equations which, to date, do not have analytic solutions. Numerical methods are often needed to obtain approximate solutions to the equations.

3.3 Computational Fluid Dynamics

Computational Fluid Dynamics (CFD) is the study of numerical approaches for the solution of equations (usually in partial differential form) which govern fluid and heat transfer processes. The governing equations have been known for about 300 years but direct work on them so far has only yielded closed-form analytic solutions for simplified forms of the equations describing flow in simplified geometries.

Major applications of CFD first began to appear in the late 1940's through to the early 1960's. Today, CFD can be viewed as a permanent third alternative in fluid dynamics investigations, along with pure experimental and pure theoretical investigations. An historical account of CFD is available in Roache (1972).

There are several major advantages of CFD compared to experimental fluid dynamics investigations (Fletcher 1988). Firstly, lead time in design and development is significantly reduced. In both *in vivo* and *in vitro* studies, a considerable amount

of time normally has to be spent in designing and developing the experiment. Also, once an experiment is set up, it may be difficult or expensive to alter certain parameter values to create alternative designs. In a CFD study, generally, parameter values may usually be changed without affecting the overall model. In this way, the effects of a particular parameter on the model can be studied and analysed. However, it is possible that in some cases, changes in certain parameter values may render the numerical process unstable. Nevertheless, given a well developed CFD code, models may be designed and suitably redesigned very quickly.

Secondly, CFD provides more detailed and comprehensive flow information. Experiments are very effective for obtaining global information in blood flow models such as total pressure drop across a stenosis or velocity at a particular point in the vessel. However, obtaining detailed velocity and pressure distribution is prohibitively expensive, time consuming and sometimes simply infeasible. CFD, on the other hand, provides this information as part of the solution, permitting a more precise understanding of the flow processes. Thus, a more complete picture of the flow field may be obtained.

Thirdly, CFD is increasingly more cost-effective than experimental investigations. Some *in vitro* experimental set-ups involving laser Doppler anemometry or other similar equipment can be very costly. Improvements in computer hardware performance, on the other hand, are accompanied by lower hardware costs. Thus, costs of computational simulations have decreased significantly. By contrast, costs associated with performing experiments continue to rise.

It must be stressed that this thesis does not suggest that experimental investigations be replaced by CFD studies, the main reason being that constitutive continuum equations used in CFD models are never exact. However, the advantages stated above have made CFD methods increasingly popular as an economically viable alternative and an excellent complement to some experimental methods.

3.4 Basic Principles of CFD

The three fundamental principles which govern the physical aspects of any fluid flow are : (1) conservation of mass (2) conservation of momentum (or Newton's second law of motion) and (3) conservation of energy. These principles may be expressed in terms of mathematical equations, which in the most general form, turn out to be a set of non-linear, coupled partial differential equations. The basic principle behind CFD is replacing the set of partial differential equations with numbers (usually found from a set of algebraic equations) and advancing these numbers in space and/or time to obtain a final numerical description of the complete flow field of interest.

In CFD, when a model is defined, one needs to select the discretisation method which will lead to a numerically solvable set of algebraic equations. Several approaches are available, for example, Finite Difference, Finite Element, Finite Volume, Boundary Element and so on. Whatever the approach, the following general steps are usually involved :

1. The solution domain is first subdivided into a finite number of subdomains (known as elements, cells and so on) to form a computational grid. The approximate solution to the problem will be found at the discrete locations (nodes, grid intersection points or cell centres depending on the chosen method). This step is usually termed the domain discretisation step.

2. All dependent variables are initialised and boundary conditions applied. The initial or boundary values are either known or approximated.

3. The partial differential equations are cast into some form of algebraic equations depending on the finite approximation scheme employed. This is the equations discretisation step. A result of this step is a set of equations of the form,

$$A_c\phi_c + \sum_{nb} A_{nb}\phi_{nb} = Q_c \tag{3.8}$$

where the subscripts c and nb refer to the cell centre and the centres of a certain number of neighbour cells respectively. A's are the coefficients involving geometrical parameters (volume, area or distance), fluid properties (density, viscosity, specific heat, etc.) and also variable values due to the non-linearity of the equations. Q contains all terms which are known or treated as such within one iteration cycle. ϕ is the dependent variable, which may be velocity components or pressure, that we wish to calculate at points on the grid.

4. The computational cycle then begins. This involves calculating new values of the dependent variables based on the initial and boundary conditions while incrementing the independent variables. Some methods of solution make use of a direct solver for the algebraic equations but more commonly applied are iterative methods of solving the algebraic equations.

Although different methods of discretisations of the solution domain and the governing equations will give rise to different numerical schemes, the general steps stated above are usually present in all schemes. The literature has a vast collection of work done in the area of analysis of such numerical schemes of solving partial differential equations. The present study, however, is not concerned with the relative merits of the different methods or with improving computational methods; rather, it is concerned with the application of CFD codes to blood flow problems.

3.5 Commercial CFD Codes

In recent years, many commercial companies have started producing softwares for industrial applications of CFD. The development in computer hardware, especially workstations, has contributed to the overall growing popularity of CFD in industry and research.

While it is beyond doubt that such commercial CFD codes are useful, some cau-

tion is necessary when choosing the code and designing the study. It is especially important to avoid using a CFD code as a "black box" software because the results obtained from these codes are only as valid as the physics incorporated in the governing equations and boundary conditions, and are therefore subject to error. Truncation errors associated with the particular algorithm and grid used to obtain the numerical simulation, as well as round-off errors which accumulate during the computational process, combine to compromise the accuracy of the CFD results. Thus, model validation is an essential component when using CFD codes to ensure that the problem is well represented and that the solutions obtained are feasible and realistic.

Table 3.1 shows some features of some commercial CFD codes. It is not intended here to go into detailed analysis of the various commercial codes. However, it is important to note that most of these codes are specialised for some range of applications, where they would perform better and are easier to set up than others. Therefore, to a certain extent, the choice of which CFD software to use depends on the nature of the problem to be solved.

Table 3.1: Some features of various commercial CFD codes

Features	FLUENT/RAMPANT	TASCflow	flow3D	FIDAP	STAR CD	PHOENICS	SHIPFLOW
Block-structured grid	yes/yes	yes	yes	yes	yes	yes	yes
Unstructured grid	no/yes	no	no	yes	yes	yes	no
Local refinement	no/yes	yes (embedded)	no	yes	yes (adaptive)	yes	no
Discretisation	FV/FV	FV	FV	FE	FV	FV	FD
Interpolation/ Differencing	power-law/ 2nd order polynomials	2nd order skew upwind	UDS	linear and quadratic elements	UDS, LUDS self filtered CDS	UDS, hybrid UDS/CDS	UDS
Turbulence Modelling	k-ϵ	k-ϵ, two layer k-ϵ	k-ϵ	k-ϵ with modifications	k-ϵ (stand. low Re, 2 layer)	mixing length, k-ϵ, algebraic	k-ϵ
Moving grid	no/no	no	no	no	yes	yes	no
Transient flows	yes/yes	yes	yes	yes	yes	yes	no
Two phase flows	yes/yes (E/L,E/E)	yes (E/L)	no	yes (E/L)	yes (E/L)	yes (E/L, E/E)	no
User interface	yes/partial	yes	yes	yes	yes	yes	no

Adapted from Perić (1994) with appropriate updates. (FV = Finite Volume; FE = Finite Element; FD = Finite Difference; UDS = first order upwind scheme; CDS = second order central differencing/linear interpolation; LUDS = second order linear upwind scheme/linear extrapolation; E/E = Eulerian calculation for both phases; E/L = Eulerian calculation of carrying phase, Lagragian calculation of dispersed phase). Code names are trademarks of their respective holders.

In the present study, two commercial CFD codes have been used to construct models of blood flow through stenosed arteries. The first is FIDAP [1], which has been extensively used and tested, and the second is PHOENICS [2].

FIDAP had been used very successfully by researchers such as Johnston and Kilpatrick (1991a, 1991b) in blood flow studies. A model for an axisymmetric flow in a rigid tube can be easily set up in FIDAP. The first model in this study is therefore an axisymmetric model which serves to illustrate the usefulness and effectiveness of appropriate CFD codes in modelling studies. This model is also an extension of the paired stenoses work performed by Johnston and Kilpatrick. For these reasons, FIDAP is a good choice of CFD code for our first model.

The other two models described in this thesis are models in three dimensions. A CFD code which has a good and efficient user interface in terms of model construction and grid generation would be an appropriate choice. In PHOENICS, there are both menu-driven interface and user-defined input files to assist the user in model construction. Furthermore, the grid generation process is aided by a useful feature which assigns colours to the grids or cells according to the orthogonality of the cell, thus providing invaluable information to the user in terms of appropriate grid definition. This is particularly helpful in modelling blood flow in three dimensions as the grid definition in these models can become fairly complicated.

Details of the usage of both FIDAP and PHOENICS may be found in the respective manuals and user guides. In addition, both FIDAP and PHOENICS are equipped with fairly comprehensive "on-line help" systems. Hence, only brief descriptions of the general structure and principles of the two codes are given here.

[1] FIDAP is a trademark of Fluid Dynamics International, Inc.
[2] PHOENICS is a trademark of CHAM, Ltd.

3.5.1 FIDAP : A Brief Description

FIDAP [3] is a general purpose CFD code based on the Finite Element method of solving partial differential equations. It is suitable for simulating viscous incompressible fluid flows, including the effects of heat transfer. Both steady and transient flows can be modelled in arbitrary geometries that may be two-dimensional, axisymmetric or three-dimensional.

The Finite Element Method (FEM) has been successfully applied in the solution of many structural analysis problems. Only recently has the finite element scheme been applied to CFD. FIDAP claims to be the first commercially available general purpose CFD code based on the FEM.

In the FEM, the flow domain is divided into a number of simply shaped regions called finite elements. The elements are identified by the locations of the element corners in space. These points are called nodes or nodal points. The equations of fluid mechanics describing the flow in the entire domain are replaced by a set of algebraic equations having matrix coefficients which are derived by approximating the equations on each element. The FEM is a well established method and further details of its application can be found in the literature.

FIDAP consists of three main modules : FIPREP, FIDAP and FIPOST. FIPREP is a command driver program used to enter all the data required to define the problem. FIDAP is the numerical simulation module which actually performs the computational processing. FIPOST is the post-processing module which includes plotting facilities. The information flow and associated files in a FIDAP run are described in Appendix A.

[3]FIDAP is an acronym for **Flu**Id **D**ynamics **A**nalysis **P**ackage

3.5.2 PHOENICS : A Brief Description

PHOENICS [4] is another general purpose CFD code which simulates fluid flow, heat transfer, chemical reaction and related phenomena. Steady and transient flows, as well as turbulent flows, may be modelled. PHOENICS also comes with a grid refinement facility.

PHOENICS is based on the Finite Volume Method (FVM) of discretising the governing equations. In the FVM, the solution domain is divided into cells, which are topologically Cartesian brick elements. Figure 3.3 shows a typical cell. The scalars are stored at the centre points of each cell and assumed to prevail over the entire cell. The vector quantities are stored at the centre points of the six cell faces.

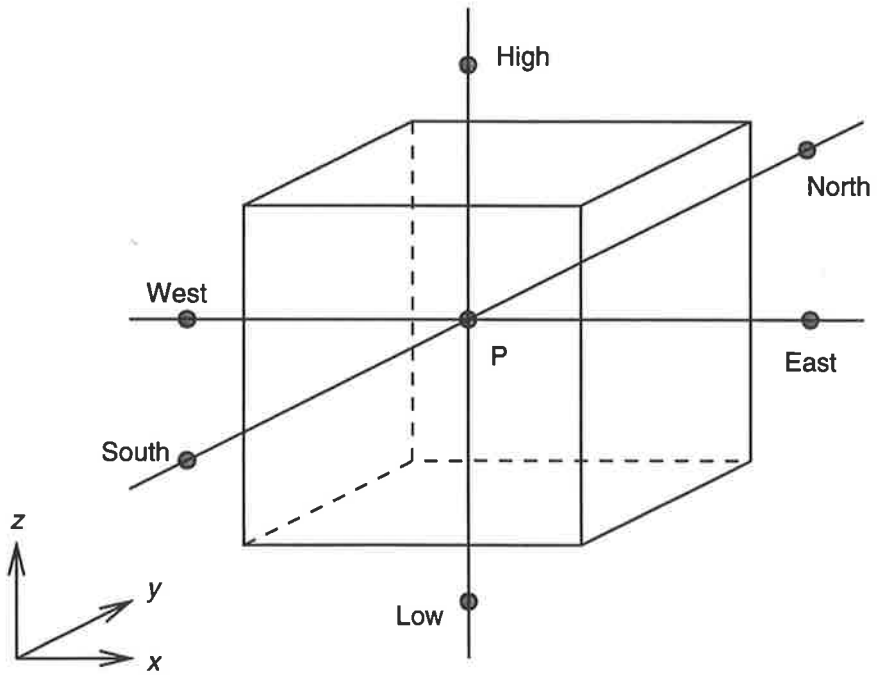

Figure 3.3: A typical cell used in PHOENICS. The cell centre is marked P. The directions W-E, S-N and L-H represent the positive x, y and z directions respectively.

[4]PHOENICS is an acronym for **P**arabolic, **H**yperbolic **O**r **E**lliptic **N**umerical **I**ntegration **C**ode **S**eries

Like FIDAP, PHOENICS is organised as a suite of programs, each with a well defined role. The programs that make up the entire system are SATELLITE, EARTH, PHOTON, PINTO, AUTOPLOT and GUIDE. A description of the roles of these programs and their relationships can be found in Appendix B.

The discretised equations in PHOENICS are solved iteratively using the SIMPLER algorithm developed by Patankar. Details of the scheme can be found in Patankar (1980) where a comprehensive treatment of the SIMPLER algorithm is given.

Mathematical modelling of blood flow through stenosed arteries in precise mathematical terms remains an insurmountable problem. However, with the proper use of CFD codes, it is possible to obtain considerable insight into the mechanics of blood flow in diseased arteries. The next three chapters are reports on three modelling studies using commercial CFD codes.

CHAPTER 4

MODEL I : AXISYMMETRIC TRIPLE STENOSES

4.1 Introduction

In this chapter, we examine a model of blood flow through an artery with three stenoses in series. Although the treatment of the problem considered here is fairly simplistic, it serves to demonstrate the potential effectiveness and usefulness of numerical models in studying blood flow problems. Furthermore, this model is an extension and generalisation of the work on paired stenoses developed by Johnston and Kilpatrick (1991a).

Multiple stenoses in arteries are a common phenomenon and using this model, we examine the effects of three stenoses of differing severity on some of the flow characteristics like pressure drops across the axial distance and streamlines of flow.

A geometrical description of the model is first presented. This is followed by a discussion on the governing equations and the formulation of the problem in FIDAP. Results obtained from the FIDAP code will be presented in the form of pressure drop graphs and streamline plots. A discussion on the clinical significance of the study will then be presented.

4.2 Geometrical Description of Model

Coronary arteries in the human body will generally bend and curve and are rarely symmetrical or even regular in cross section. Figure 4.1 shows the longitudinal section of a typical coronary artery suffering from multiple stenoses. As can be seen from the figure, the physical geometry of an artery can be quite complex. A mathematical model of the actual complex geometry of such arteries is difficult to construct. In order to study the hemodynamics of flow through arteries, one needs to simplify the geometry while keeping the essential features intact.

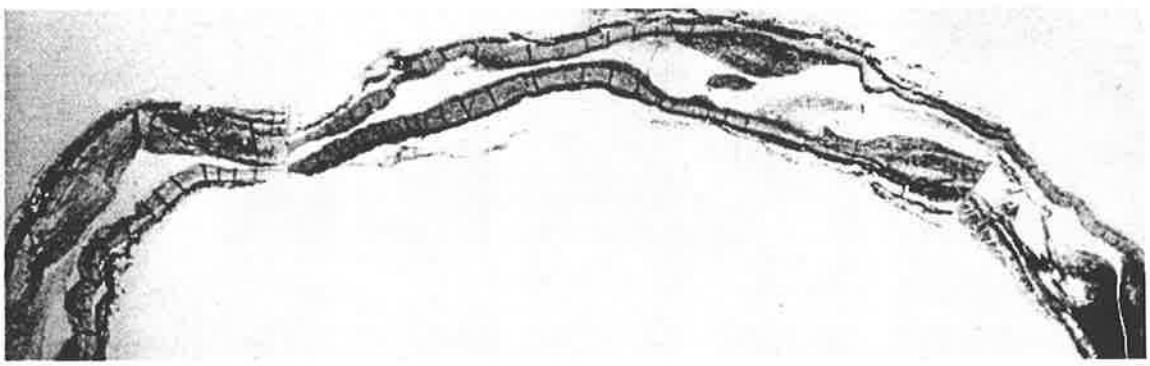

Figure 4.1: Composite Photomicrograph of longitudinal sections of the Left Circumflex Coronary Artery suffering from multiple stenoses. Source : Vlodaver *et al* (1976).

Certain assumptions will have to be made in order to simplify the geometry and construct a model suitable for our purpose. In Chapter 1, we have seen various models and methods of handling such a problem. In this chapter, we wish to study the aspect of varying degrees of stenoses in a multiply stenosed artery while keeping the model relatively simple. This study will not only serve as a starting point for our discussion but also provide an insight into the flow characteristics of blood in an artery that has multiple stenoses, a situation that is not uncommon.

We shall assume the blood vessel to be symmetrical about its axis and having a circular cross section. A typical human coronary artery has a diameter of around 1 to 2 mm and in our study, the diameter of the unobstructed tube will be fixed at 1 mm. Although arteries are seldom perfectly straight, we shall consider a straight tube model here and leave the discussion of curved arteries to a later chapter. We shall also assume the tube to be rigid and thin-walled.

Shape of Stenosis

We now need to decide on the shape of the stenoses in our model. A simple examination of angiograms of stenosed arteries would reveal that stenoses generally do not follow any particular shape or pattern. In his early theoretical models, Young (1968) had proposed a "cosine curve" shape for the stenosis. Various other shapes have since been considered by other investigators such as Mates (1978) and Umezu *et al* (1992). Models of irregular stenoses have also been constructed (Johnston and Kilpatrick 1991b).

Most mathematical studies performed in this area, however, have used the cosine function to describe stenoses as it is a fairly good approximation of the shape of stenoses. Moreover, the cosine function may be handled easily and hence is a simple and convenient way of representing the shape of stenoses. Throughout this study, we will use the cosine function to describe the shape of the stenoses notwithstanding the fact that it is possible to design models with other arbitrary shapes.

Severity of Stenoses

The severity of a stenosis is usually described by the percentage of the cross sectional area occluded. The cross sectional area considered is taken at the narrowest portion (or the "throat") of the blockage.

Consider Figure 4.2 which shows a typical model of a tube with a single stenosis. Suppose R_0 is the radius of the unobstructed tube and δ is the height of the stenosis.

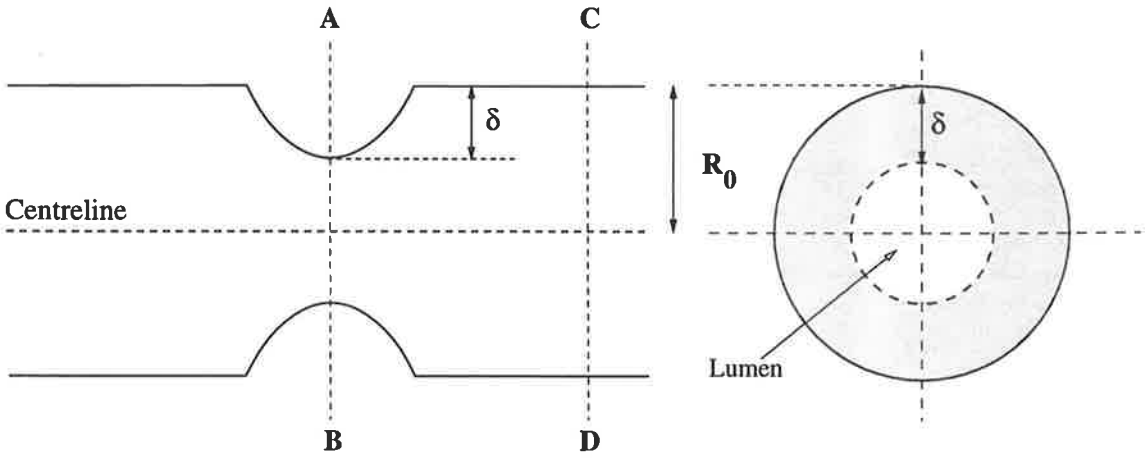

(a) Longitudinal section

(b) Cross section at the throat

Figure 4.2: A single stenosis. (a) Longitudinal section : line AB lies on the narrowest part of the stenosis and line CD lies on the unobstructed part of the tube. (b) Cross section at AB.

Without loss of generality, let R_0, the unobstructed radius of the vessel, be of unit length, i.e. let $R_0 = 1$. Hence, it follows that $0 \leq \delta < 1$. Therefore,

Cross sectional area of lumen across CD $= \pi R_0^2 = \pi$

Cross sectional area of lumen across AB $= \pi(1-\delta)^2$

Hence, the percentage of area occluded is given by

$$\left(\frac{\pi - \pi(1-\delta)^2}{\pi}\right) \times 100$$

$$= 100(1 - (1-\delta)^2)$$

A summary of the relationship between δ, the height of the stenosis, and the percentage of area occluded for an axisymmetric model is given in the Table 4.1.

Table 4.1: Relationship between δ and areal occlusion

δ	Areal Occlusion (%)
0	0
0.1	19
0.2	36
0.3	51
0.4	64
0.5	75
0.6	84
0.7	91
0.8	96
0.9	99

Equations of the Boundary

The model under consideration is shown in Figure 4.3. The figure shows only one "half" of the tube since the tube is assumed to be symmetrical about its axis or centreline. The origin of the cylindrical coordinates, r and z, is placed at the entry point on the centreline of the tube. The three stenoses are placed in series with S_1, S_2 and S_3 representing the positions along the z-axis of the proximal, central and distal stenoses respectively.

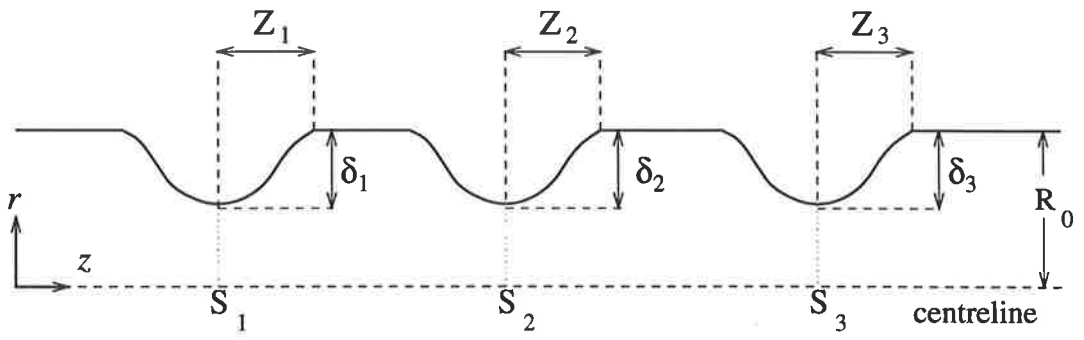

Figure 4.3: Geometry of axi-symmetric triple stenoses model

In the figure, R_0 is the radius of the unobstructed tube and the heights of the

stenoses are denoted by δ_1, δ_2 and δ_3 respectively. Hence, $(R_0 - \delta_1)$, $(R_0 - \delta_2)$ and $(R_0 - \delta_3)$ are the radii of the tube at the narrowest part of the respective blockages. Also, $2Z_1$, $2Z_2$ and $2Z_3$ denote the stenotic lengths of the respective stenoses.

Using the variables described above and a cosine curve shape for the stenoses, the equations representing the boundary may be written as

$$R(z) = \begin{cases} R_0 - \frac{\delta_1}{2}(1 + \cos(\frac{\pi(z-S_1)}{Z_1})), & S_1 - Z_1 < z < S_1 + Z_1 \\ R_0 - \frac{\delta_2}{2}(1 + \cos(\frac{\pi(z-S_2)}{Z_2})), & S_2 - Z_2 < z < S_2 + Z_2 \\ R_0 - \frac{\delta_3}{2}(1 + \cos(\frac{\pi(z-S_3)}{Z_3})), & S_3 - Z_3 < z < S_3 + Z_3 \\ R_0 & \text{otherwise} \end{cases} \tag{4.1}$$

These equations may be written in a more compact form :

$$R(z) = \begin{cases} R_0 - \frac{\delta_i}{2}(1 + \cos(\frac{\pi(z-S_i)}{Z_i})), & S_i - Z_i < z < S_i + Z_i \\ & i = 1, 2, 3 \\ R_0 & \text{otherwise} \end{cases} \tag{4.2}$$

We note that Equation (4.2) is a general form for the mathematical description for the boundary of an axisymmetric model of an artery with three stenoses whose shapes follow a cosine curve. The equation can be further generalised to represent any number of stenoses if we let i range from 1 to n, where n is the number of stenoses in the tube.

By changing the values of δ_i, we can vary the severity of each of the three stenoses. Also, since the S_i's denote the positions of the stenoses along the z-axis, we can also vary the inter-stenotic distances (i.e. $S_{i+1} - S_i$) by varying the values of S_i's.

4.3 Governing Equations

Equations of Motion

In this study, blood has been assumed to be a Newtonian fluid. Although we know that blood, being a suspension of blood cells in plasma, is non-Newtonian in nature, our study models blood flow in arteries whose internal diameter is greater than 500 μm and in such cases, it is reasonable to assume blood to be Newtonian (McDonald 1960). We will also assume the flow to be laminar and steady.

The governing equations for the steady flow of a Newtonian fluid are the continuity equation and the usual Navier-Stokes equations. In cylindrical coordinates, these may be written as (see Mazumdar, *Biofluid Mechanics*, p.12) :

$$\frac{\partial v_r}{\partial r} + \frac{v_r}{r} + \frac{\partial v_z}{\partial z} = 0 \tag{4.3}$$

$$v_r \frac{\partial v_r}{\partial r} + v_z \frac{\partial v_r}{\partial z} = -\frac{1}{\rho}\frac{\partial P}{\partial r} + \nu \left[\frac{\partial^2 v_r}{\partial r^2} + \frac{1}{r}\frac{\partial v_r}{\partial r} - \frac{v_r}{r^2} + \frac{\partial^2 v_r}{\partial z^2} \right] \tag{4.4}$$

$$v_r \frac{\partial v_z}{\partial r} + v_z \frac{\partial v_z}{\partial z} = -\frac{1}{\rho}\frac{\partial P}{\partial z} + \nu \left[\frac{\partial^2 v_z}{\partial r^2} + \frac{1}{r}\frac{\partial v_z}{\partial r} + \frac{\partial^2 v_z}{\partial z^2} \right] \tag{4.5}$$

where r and z are the physical coordinates with the z-axis located along the centreline of the artery. v_r and v_z are respectively the radial and axial components of velocity. P is the pressure and ρ and ν are the density and kinematic viscosity of blood respectively.

Boundary Conditions

The usual no slip condition is applied on the arterial walls. Also, we shall assume that the blood does not penetrate through the walls as it flows along the artery.

Hence, we have

$$v_r = v_z = 0 \quad \text{at} \quad r = R(z) \tag{4.6}$$

Along the line of symmetry, the centreline, the radial component of the velocity and the shear stress vanish since we are assuming an axisymmetric flow. Therefore,

$$v_r = \frac{\partial v_z}{\partial r} = 0 \quad \text{at} \quad r = 0 \tag{4.7}$$

Upstream, the flow is assumed to have a parabolic velocity profile corresponding to a fully developed Poiseuille flow for an incompressible fluid through a circular tube of uniform cross section, i.e.

$$v_z = U(1 - \frac{r^2}{R_0^2}) \tag{4.8}$$

$$v_r = 0 \tag{4.9}$$

where U is the characteristic maximum velocity of the parabolic profile. Downstream, we apply the conditions of zero normal and tangential stress and leave the velocity free.

4.4 Formulation of the problem in FIDAP

To study the effects of relative severity of the stenoses in a triplet on blood flow, we set up models with different combinations of relative severity. Using the usual way of defining the severity of a stenosis by percentage of areal occlusion, we define a 96% areal occlusion to be a *severe* case of stenosis and a 84% areal occlusion to be a *mild* case. The various combinations set up are shown in Table 4.2

Table 4.2: Various combinations of relative severity

CASE	Stenosis 1 Proximal	Stenosis 2 Central	Stenosis 3 Distal
1 (S-S-M)	severe	severe	mild
2 (S-M-S)	severe	mild	severe
3 (S-M-M)	severe	mild	mild
4 (M-S-S)	mild	severe	severe
5 (M-S-M)	mild	severe	mild
6 (M-M-S)	mild	mild	severe
7 (S-S-S)	severe	severe	severe

Stenosis 1 is the proximal narrowing (at S_1 in Figure 4.3)
Stenosis 2 is the central narrowing (at S_2 in Figure 4.3)
Stenosis 3 is the distal narrowing(at S_3 in Figure 4.3)

The main aim of this model is to study the effects of relative severity of three stenoses in a series on the characteristics of blood flow. Therefore, since the case for three mild stenoses (M-M-M) is essentially similar to case 7 (S-S-S), it has not been included in the present study.

The governing equations (4.3), (4.4) and (4.5) may be solved by using the CFD code, FIDAP. In order to apply FIDAP to our problem, we first need to discretise the solution domain. In our model, the solution domain is discretised into 13 quadrilateral regions, labelled a to m, as shown in Figure 4.4. The points, labelled 1 to 28, form the corner-points or "key points" of these quadrilateral regions.

Each of these regions is further discretised into quadrilateral elements. The grids in the vicinity of the stenoses contain more elements than those further away as the values of the variables at these points are expected to change more abruptly and rapidly. In our model, the solution domain of 13 regions has been discretised into a non-uniform grid containing 3132 quadrilateral elements. Figure 4.5 below shows a typical distribution of the elements in regions a, b and c.

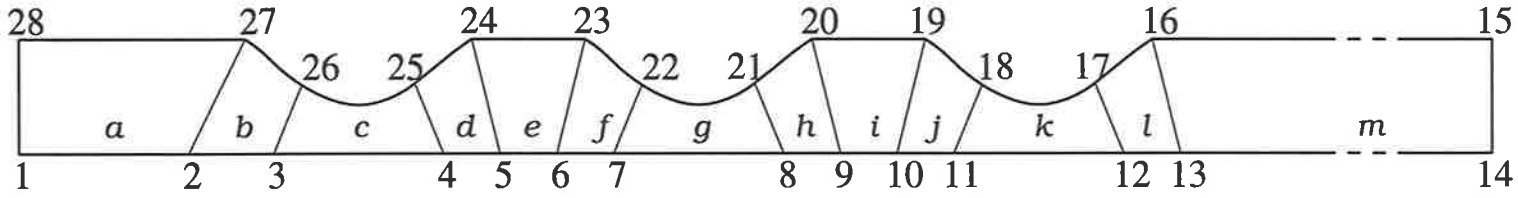

Figure 4.4: Solution domain is discretised into 13 non-uniform regions

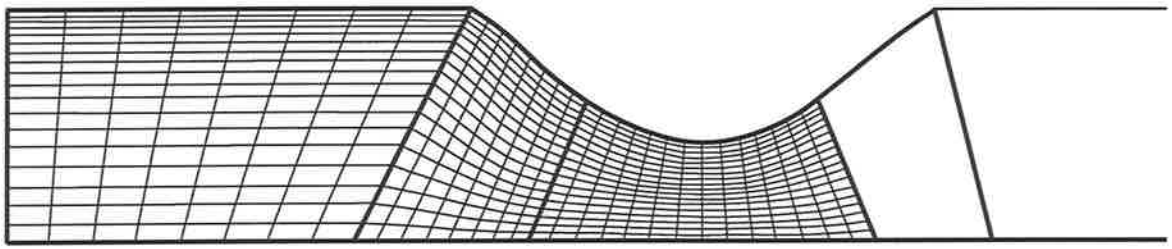

Figure 4.5: Non-uniform grid cells in regions a, b and c

Table 4.3 below gives a summary of the number of cells in each of the 13 regions and the physical and the logical coordinates of the points used in constructing the model.

Table 4.3: Data used in the Triple Stenoses Model

Region	a	b	c	d	e	f	g	h	i	j	k	l	m
Number of Cells	8	8	14	8	12	14	16	14	16	16	18	16	14

Points in the logical (I,J,K) and physical (r, z, θ) domains

	Logical Coordinates			Physical Coordinates		
Point Number	I	J	K	z	r	θ
1	1	1	1	0.00	0.00	0.00
2	3	1	1	1.50	0.00	0.00
3	5	1	1	2.25	0.00	0.00
4	7	1	1	3.75	0.00	0.00
5	9	1	1	4.25	0.00	0.00
6	11	1	1	4.75	0.00	0.00
7	13	1	1	5.25	0.00	0.00
8	15	1	1	6.75	0.00	0.00
9	17	1	1	7.25	0.00	0.00
10	19	1	1	7.75	0.00	0.00
11	21	1	1	8.25	0.00	0.00
12	23	1	1	9.75	0.00	0.00
13	25	1	1	10.25	0.00	0.00
14	27	1	1	20.00	0.00	0.00
15	27	3	1	20.00	1.00	0.00
16	25	3	1	10.00	1.00	0.00
17	23	3	1	9.50	0.434	0.00
18	21	3	1	8.50	0.434	0.00
19	19	3	1	8.00	1.00	0.00
20	17	3	1	7.00	1.00	0.00
21	15	3	1	6.50	0.434	0.00
22	13	3	1	5.50	0.434	0.00
23	11	3	1	5.00	1.00	0.00
24	9	3	1	4.00	1.00	0.00
25	7	3	1	3.50	0.929	0.00
26	5	3	1	2.50	0.929	0.00
27	3	3	1	2.00	1.00	0.00
28	1	3	1	0.00	1.00	0.00

In the present model, there are three curved portions which simulate the proximal, central and distal stenoses along the artery. Using Equation (4.2), we can generate the coordinates of the curves and a typical set is shown in Table 4.4.

Table 4.4: A sample of Coordinates for Curves defined in Triple Stenoses Model

Coordinates of curves defined in model for Case 4 (M-S-S)

Curve 1 (Proximal) Point 27 to Point 24		Curve 2 (Central) Point 23 to Point 20		Curve 3 (Distal) Point 19 to Point 16	
z	r	z	r	z	r
2.1	0.906	5.1	0.875	8.1	0.875
2.2	0.815	5.2	0.753	8.2	0.753
2.3	0.728	5.3	0.637	8.3	0.637
2.4	0.647	5.4	0.530	8.4	0.530
2.5	0.576	5.5	0.434	8.5	0.434
2.6	0.515	5.6	0.353	8.6	0.353
2.7	0.465	5.7	0.287	8.7	0.287
2.8	0.429	5.8	0.239	8.8	0.239
2.9	0.407	5.9	0.210	8.9	0.210
3.0	0.400	6.0	0.200	9.0	0.200
3.1	0.407	6.1	0.210	9.1	0.210
3.2	0.429	6.2	0.239	9.2	0.239
3.3	0.465	6.3	0.287	9.3	0.287
3.4	0.515	6.4	0.353	9.4	0.353
3.5	0.576	6.5	0.434	9.5	0.434
3.6	0.647	6.6	0.530	9.6	0.530
3.7	0.728	6.7	0.637	9.7	0.637
3.8	0.815	6.8	0.753	9.8	0.753
3.9	0.906	6.9	0.875	9.9	0.875

The governing equations were solved numerically using FIDAP (Version 6.01). We set $S_1 - Z_1$ (i.e. location of the beginning of the first stenosis) to be equal to $2R_0$. Also, the downstream boundary conditions were applied at a distance of $10R_0$ from the end of the last stenosis to ensure stability in the numerical process.

In order to compare our results with those obtained by Johnston and Kilpatrick in their paired stenoses model, we have set up our model to be of the same dimension as their model. For all the combinations shown in Table 4.2, we have set $Z_1 = Z_2 = Z_3 = R_0$. Also, the Reynolds number $\left(Re = \frac{\overline{U}D}{\nu}\right)$ was fixed at 100, which is reasonable for an artery of diameter, D, of 1 mm, with blood flowing at an average velocity, $\overline{U}$ of 36 cm/s. The kinematic viscosity of blood, ν, was fixed at $3.6 \times 10^{-6} m^2/s$.

The model was also solved for various inter-stenotic distances to study the effects of varying inter-stenotic lengths on the flow characteristics. A sample input file for the model in FIDAP is given in Appendix C.

4.5 Results and Discussion

In this section, we present and discuss the results of the solution of the model. Pressure drop profiles and streamline plots for all the seven cases considered will be discussed and compared with published work.

Pressure Drop

Figures 4.6 through 4.12 show the pressure profile along the axis of the artery for cases 1 to 7 respectively. In case 1 (Figure 4.6), the proximal and central stenoses are more severe than the distal. We observe from the graph that the pressure drops across the more severe stenoses are larger.

In case 3 (Figure 4.8), a relatively large drop in pressure is observed across the

more severe proximal stenosis. Similar patterns are observed from the other graphs shown. These results seem to imply that in a triplet, the effects of the more severe stenosis are the more dominant ones.

Examining the graph in Figure 4.6 again, we observe that there is a distinct recovery of pressure across the distal stenosis, which in this case is the milder one. In Figures 4.7, 4.8 and 4.10, a similar pressure recovery is present when a mild stenosis follows a more severe one. Such a recovery of pressure is not detected in cases 4, 6 and 7 as can be observed in Figures 4.9, 4.11 and 4.12 because in these cases, there is no mild stenosis following a more severe stenosis.

In fact, by examining the graphs of pressure drops against axial distance for all the seven cases, it would be fair to conclude that whenever there is a milder stenosis following a more severe one, recovery of pressure is observed.

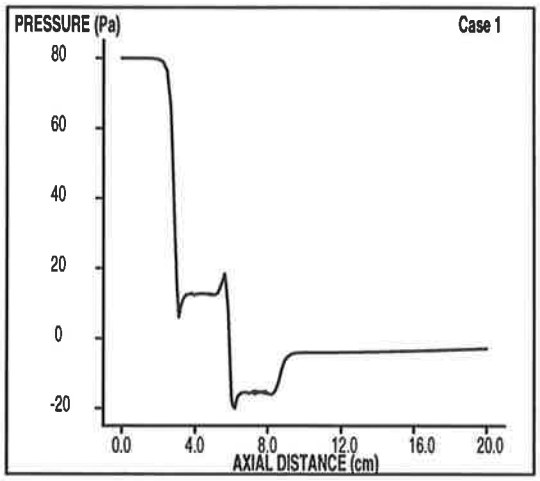

Figure 4.6: Pressure vs Axial Distance for Case 1 (S-S-M)

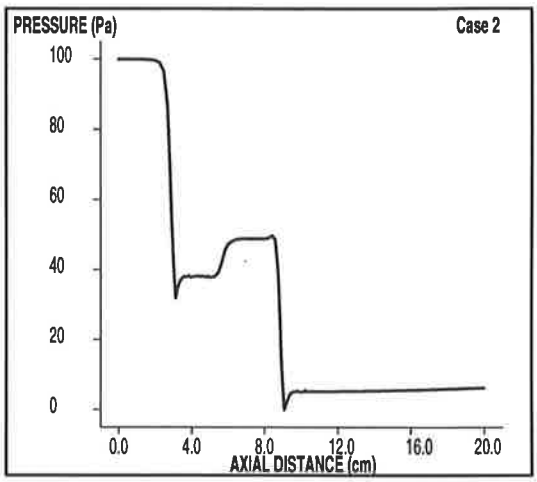

Figure 4.7: Pressure vs Axial Distance for Case 2 (S-M-S)

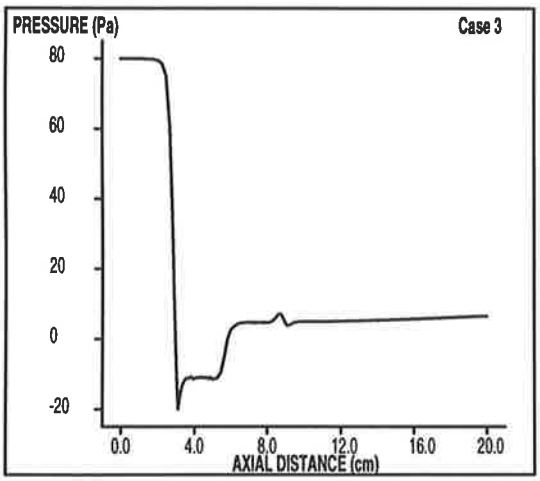

Figure 4.8: Pressure vs Axial Distance for Case 3 (S-M-M)

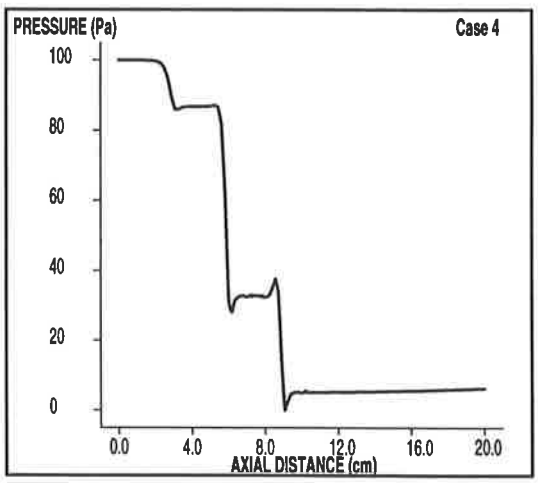

Figure 4.9: Pressure vs Axial Distance for Case 4 (M-S-S)

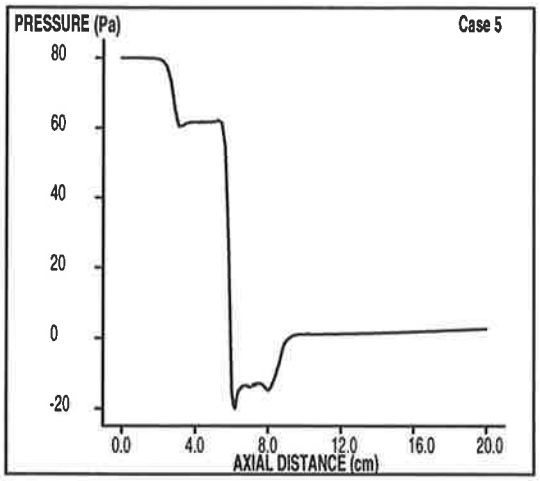

Figure 4.10: Pressure vs Axial Distance for Case 5 (M-S-M)

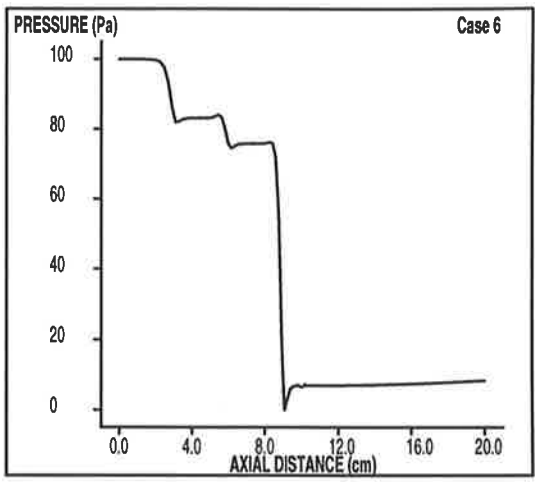

Figure 4.11: Pressure vs Axial Distance for Case 6 (M-M-S)

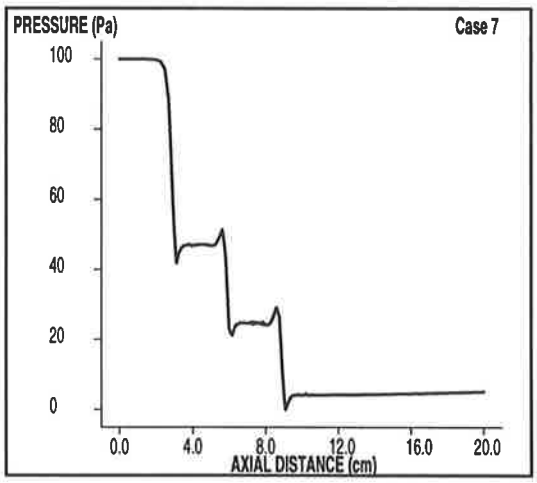

Figure 4.12: Pressure vs Axial Distance for Case 7 (S-S-S)

Streamline Plots

Typical streamline plots showing the recirculating zones are presented in Figures 4.13 through 4.19 for all the seven cases considered. We observe that recirculation is more intense between two severe stenoses than between two mild stenoses. This can be seen by examining the streamlines for cases 1 and 4 (Figures 4.13 and 4.16) and cases 3 and 6 (Figures 4.15 and 4.18). Cases 1 and 4 have two consecutive severe stenoses while cases 3 and 6 have 2 consecutive mild ones.

Recirculation between a mild and a severe stenosis with the milder one upstream is relatively less intense. This can be observed in the streamline plots of cases 4, 5 and 6. However, if a mild stenosis follows a more severe one (as in cases 1, 3 and 5) then there is more intense recirculation between a severe and a mild stenosis. This observation is consistent with the earlier observation made - that a pressure recovery is observed whenever a mild stenosis follows a more severe one.

The presence of more intense recirculation would imply more rapid changes in the flow velocities. This in turn means that higher shearing stresses are exerted on the arterial walls. Hence, the streamline plots show qualitatively that as the severity of a series of stenoses increases, the shearing stresses between the lesions also increases. In addition, the location of the milder stenoses will also have an effect on the shearing stresses. Since it is believed that shearing stresses on the arterial walls may play an important role in the proliferation of arterial diseases as previously discussed, the implication here is that factors such as differences in the severity of the stenoses should be taken into consideration when examining and interpreting angiograms of arteries with multiple stenoses.

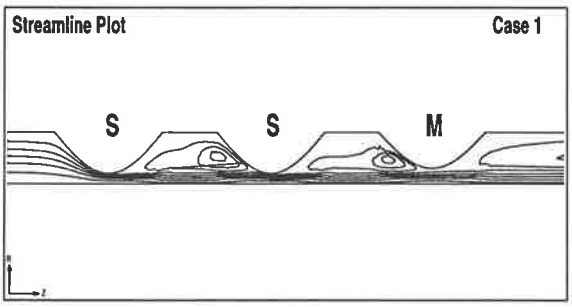

Figure 4.13: Streamline plot for Case 1

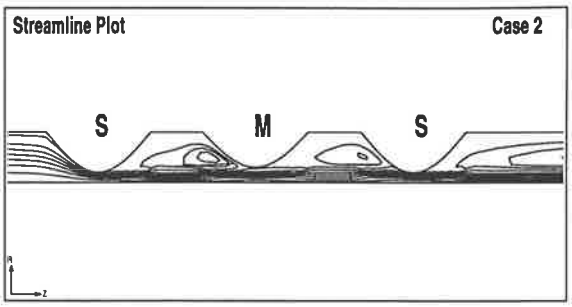

Figure 4.14: Streamline plot for Case 2

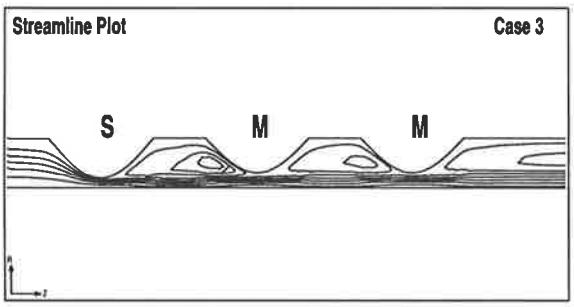

Figure 4.15: Streamline plot for Case 3

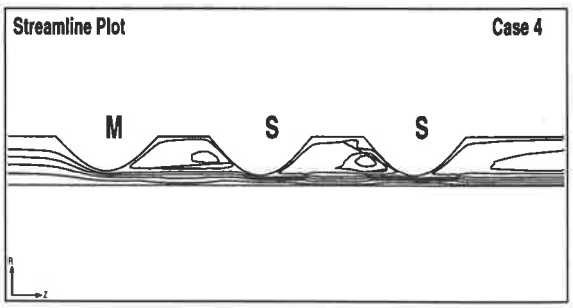

Figure 4.16: Streamline plot for Case 4

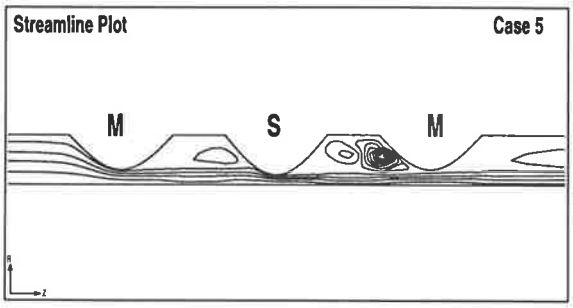

Figure 4.17: Streamline plot for Case 5

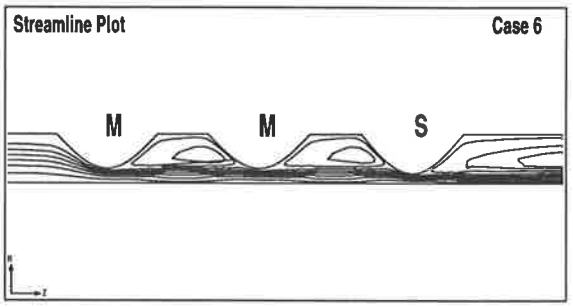

Figure 4.18: Streamline plot for Case 6

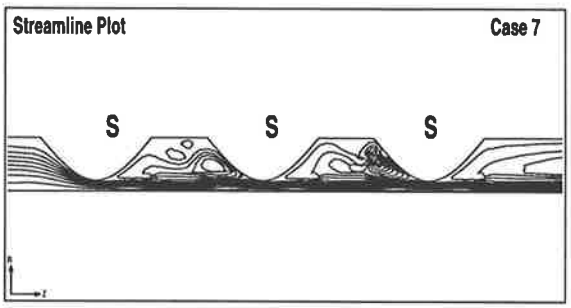

Figure 4.19: Streamline plot for Case 7

The effect of varying the inter-stenotic distance on the pressure drop in the case of triple stenoses was studied by solving the model with various values of S_2 while keeping S_1 and S_3 fixed.

Figure 4.20 shows the variation of the pressure drops across each stenosis and the total pressure drop across the axis with the distance between the central and proximal stenoses (i.e. $S_2 - S_1$) for case 7. It is clear from the figure that in this case, the pressure drops across the proximal, central and distal stenoses as well as that across the entire triplet do not vary appreciably with the position of the central stenosis. In general, it is observed that in a triplet of stenoses, if the distance between the proximal and distal stenoses (i.e. $S_3 - S_1$) is kept constant then varying the position of the central stenosis has no significant effect on the pressure drop.

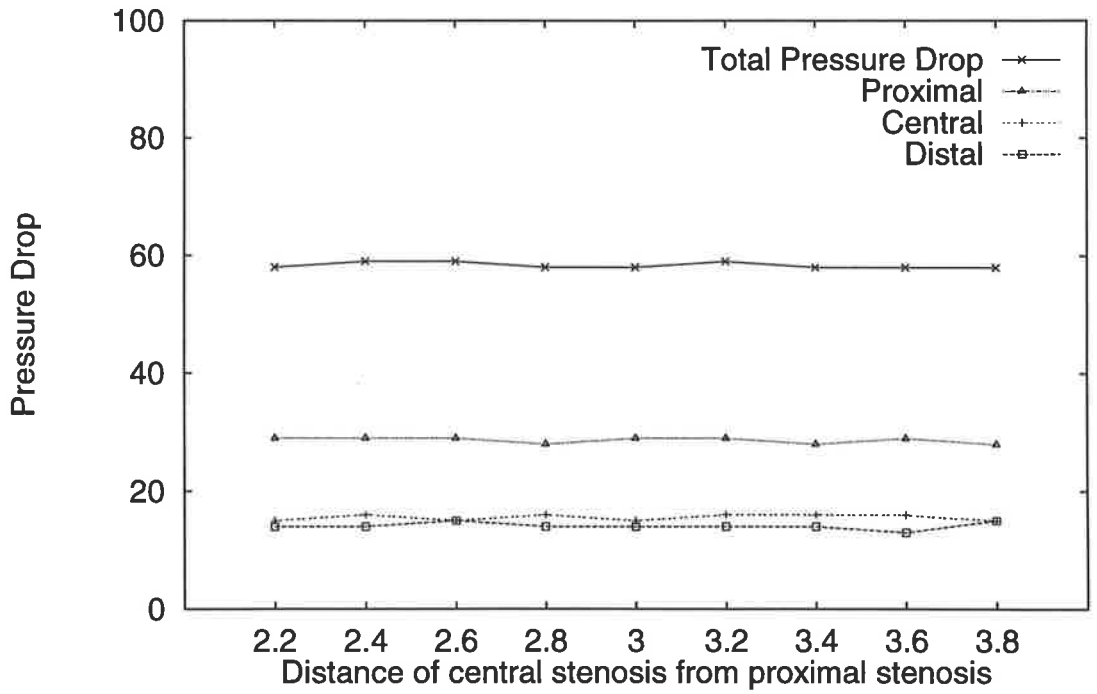

Figure 4.20: Graph showing the variation of pressure drops with the relative position of central stenosis for Case 7

4.6 Conclusion

The results obtained in this study are consistent with those obtained by Johnston and Kilpatrick (1991a) in their study of paired arterial stenoses. In the model considered in this chapter, however, we have looked into the case of varying degrees of stenosis in triplets and have demonstrated its effects on certain flow characteristics. In particular, the following conclusions may be drawn :

1. In a triplet of stenoses, the effects of a milder stenosis are diminished in the presence of a more severe stenosis.

2. Whenever there is a mild stenosis following a more severe one, pressure recovery is observed.

3. Recirculation between stenoses is more intense with a milder stenosis following a more severe one.

4. With two stenoses at a fixed length apart, the presence of a third stenosis in between has no significant effect on the total pressure loss.

It is not uncommon to find multiple stenoses occurring in a single artery. However, despite its common occurrence, studies on multiply stenosed arteries have so far been fairly limited. Most experimental models have been on single stenosis.

Chakravarty and Datta (1990) had used the finite difference formulation to study the dynamic response of blood flow in multiply stenosed arteries. In the study described in this chapter, we have demonstrated with a simple model that the geometrical differences in the narrowings in a triplet have a significant effect on blood flow. In particular, we have shown that the effects of a milder stenosis are considerably diminished in the presence of a more severe stenosis.

However it is important to note that the "mild" stenosis in this model is only mild when compared to the "severe" stenosis. While its effects may have been diminished in the presence of a more severe stenosis, the presence of the milder stenosis should not be overlooked or disregarded.

Also, a pressure recovery is observed whenever a mild stenosis follows a more severe one. This means that the presence of a mild stenosis could in fact help increase or maintain the pressure head needed for flow. The implication here is that in multiple stenoses, the total pressure drop across the stenotic region may not be a good indication of the severity of the blockages.

It is also important to point out that we have assumed a rigid tube in this model. Atherosclerosis usually occurs in older people, and our discussion in Chapter 2 (see page 20) has mentioned that arteries lose their elastance with age. Hence it would not be unreasonable to assume a rigid tube for a model of a stenosed artery.

Although the model discussed here is fairly idealised, it can be easily modified to suit the needs of further investigations. Nevertheless, despite its simplicity, the model has helped us understand and even made it possible to predict various hemodynamic features associated with blood flow in multiply stenosed arteries.

The results from the study presented in this chapter have been published (see Appendix E).

CHAPTER 5

MODEL II : SINGLE STENOSIS IN THREE DIMENSIONS

5.1 Introduction

The model that we have discussed in the previous chapter is an axisymmetric model solved in two dimensions. In reality, blood vessels are seldom symmetrical about their axes and stenoses in them are generally irregular and not symmetrical.

In this chapter, we shall develop a model of blood flow through an artery with a protrusion from one "side" of the arterial wall; that is, the artery has an asymmetrical stenosis. The model is formulated and solved using the CFD code, PHOENICS. Although Dvinsky and Ojha (1994) recently attempted to develop such a model and obtained solutions using the computational code, HEMO, they have not discussed the effects of wall shearing stresses in their study. This is an important aspect because the distribution of shear stress on the arterial walls can have a major influence on the progression of arterial diseases, as pointed out by various researchers such as Young (1968), Nerem (1992) and Fry (1968).

Hence, it is in our interest to understand the effects of stenoses on the shearing stresses on the arterial walls. The model discussed in this chapter attempts to provide a quantitative insight into the effects on various flow characteristics, including the distribution of wall shearing stresses, due to the presence of an asymmetric

stenosis. A geometrical description of the model is first presented. This is followed by a discussion on the formulation of the problem in PHOENICS. Results in terms of pressure drops and velocity fields will be presented together with a discussion on the method used to estimate the shearing stresses on the arterial walls. Important conclusions on the peak wall shear stresses will be made.

5.2 Geometrical Description of Model

Shape of Stenosis

Although stenotic constrictions can take different geometrical forms, Young and Tsai (1973) suggested that they can be grouped into two basic categories : (a) approximately axisymmetric stenosis, and (b) stenosis formed by an isolated surface protuberance from one wall. The model to be discussed here is of the second type of constriction and is geometrically similar to the experimental models used by Young and Tsai. The main difference lies in the shape of the stenosis. In longitudinal section, the stenosis shape in their model follows an arc whereas the stenosis in the model here follows a more conventional and realistic cosine curve shape.

A representation of the model in longitudinal and cross sections is given in Figure 5.1. The model basically consists of a straight rigid tube having a circular cross section with a protuberance from one wall. The side of the wall with the protuberance is labelled Side A and the other unstenosed side is labelled Side B, as shown in Figure 5.1a. The height of this protrusion is h and the physical radius of the unobstructed part of the artery is R_0. The stenosis has a length of $2Z_0$. The cross section at the throat of the stenosis, that is, the narrowest part of the vessel, is shown in Figure 5.1b and Figure 5.1c shows a typical cross section through the stenotic region.

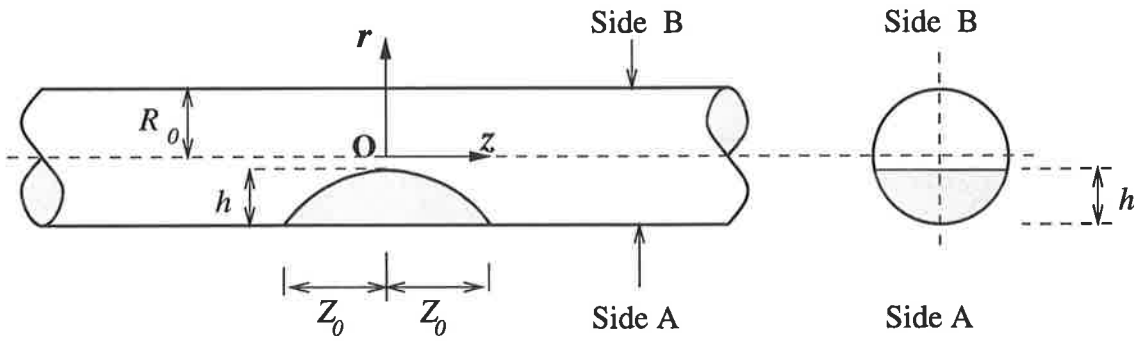

(a) Longitudinal section through axis

(b) cross section through origin

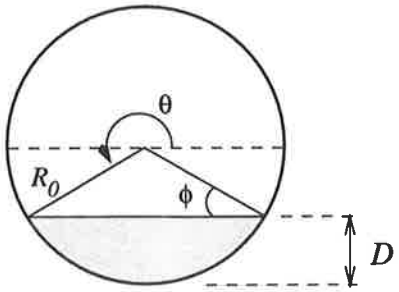

(c) Typical cross section through stenotic region

Figure 5.1: Geometry of the asymmetric stenosis model

Equation of the Boundary

The equation for the wall boundary is best described using cylindrical polar coordinates (R, θ, Z) with its origin situated at O as shown in Figure 5.1a. R is the radial distance from the axis of the tube, Z is the axial distance from the origin and θ is the angle from the "horizontal" plane as shown in Figure 5.1c.

Introducing the following dimensionless variables,

$$r = \frac{R}{R_0} \quad , \quad d = \frac{D}{R_0} \quad , \quad z = \frac{Z}{R_0} \quad , \quad z_0 = \frac{Z_0}{R_0} \quad , \quad \delta = \frac{h}{R_0}$$

the boundary may be described by the following equation,

$$R(r,\theta,z) = \begin{cases} 1 & , \text{ for } |z| \geq z_0 \\ \dfrac{1-d}{-\sin\theta} & , \text{ for } |z| < z_0 \text{ and } \theta < -\phi \text{ , } \theta > \pi + \phi \\ 1 & , \text{ for } |z| < z_0 \end{cases} \tag{5.1}$$

where ϕ and d are given by,

$$\phi = \arcsin(1-d) \tag{5.2}$$

$$d = \delta \cos\left(\frac{\pi z}{2z_0}\right) \tag{5.3}$$

Percent Stenosis

For this asymmetric model, the percent stenosis defined in the previous chapter needs to be modified. As usual, we define the percent stenosis (or degree of stenosis) as the percentage of cross sectional area occluded at the throat of the stenosis. Using dimensionless variables, this corresponds to the cross section of the artery at z=0. It can be easily shown that the percentage areal occlusion for a stenosis with dimensionless height, δ, is given by :

$$\frac{\arccos(1-\delta) - (1-\delta)\sqrt{2\delta - \delta^2}}{\pi} \times 100\% \tag{5.4}$$

Equations of Motion

The equations governing the motion of fluid in the model are the continuity equation and the steady Navier-Stokes equations. In cylindrical polar coordinates, these may be written as (see Dinnar, *Cardiovascular Fluid Dynamics*, p. 87) :

$$\frac{\partial v_z}{\partial z} + \frac{1}{r}\frac{\partial}{\partial r}(v_r r) + \frac{1}{r}\frac{\partial v_\theta}{\partial \theta} = 0 \tag{5.5}$$

$$\begin{aligned} v_r\frac{\partial v_r}{\partial r} + \frac{v_\theta}{r}\frac{\partial v_r}{\partial \theta} + v_z\frac{\partial v_r}{\partial z} - \frac{v_r^2}{r} = \\ -\frac{1}{\rho}\frac{\partial p}{\partial r} + \nu\left(\frac{\partial^2 v_r}{\partial r^2} + \frac{1}{r}\frac{\partial v_r}{\partial r} - \frac{v_r}{r^2} + \frac{1}{r^2}\frac{\partial^2 v_r}{\partial \theta^2} - \frac{2}{r^2}\frac{\partial v_\theta}{\partial \theta} + \frac{\partial^2 v_r}{\partial z^2}\right) \end{aligned} \tag{5.6}$$

$$\begin{aligned} v_r\frac{\partial v_\theta}{\partial r} + \frac{v_\theta}{r}\frac{\partial v_\theta}{\partial \theta} + v_z\frac{\partial v_\theta}{\partial z} + \frac{v_\theta v_r}{r} = \\ -\frac{1}{\rho r}\frac{\partial p}{\partial \theta} + \nu\left(\frac{\partial^2 v_\theta}{\partial r^2} + \frac{1}{r}\frac{\partial v_\theta}{\partial r} - \frac{v_\theta}{r^2} + \frac{1}{r^2}\frac{\partial^2 v_\theta}{\partial \theta^2} + \frac{2}{r^2}\frac{\partial v_r}{\partial \theta} + \frac{\partial^2 v_\theta}{\partial z^2}\right) \end{aligned} \tag{5.7}$$

$$\begin{aligned} v_r\frac{\partial v_z}{\partial r} + \frac{v_\theta}{r}\frac{\partial v_z}{\partial \theta} + v_z\frac{\partial v_z}{\partial z} = \\ -\frac{1}{\rho}\frac{\partial p}{\partial z} + \nu\left(\frac{\partial^2 v_z}{\partial r^2} + \frac{1}{r}\frac{\partial v_z}{\partial r} + \frac{1}{r^2}\frac{\partial^2 v_z}{\partial \theta^2} + \frac{\partial^2 v_z}{\partial z^2}\right) \end{aligned} \tag{5.8}$$

where v_r, v_z and v_θ are the radial, axial and circumferential components of the fluid velocity respectively, ρ is the density of the fluid and p is the dimensionless pressure across the region of flow. It should be noted that for an axisymmetric case, as discussed in the previous chapter, the circumferential component and the derivative in that direction vanish. That is, $v_\theta = 0$ and $\frac{\partial}{\partial \theta} = 0$ and the above equations would reduce to Equations (4.3), (4.4) and (4.5). The present model, however, is a

three dimensional model. Thus, no assumption about the circumferential velocities is made and all the terms in the equations are retained.

Boundary Conditions

The following boundary conditions are applied :

1. No slip condition is applied at the arterial walls, that is,

$$v_r = v_z = v_\theta = 0 \tag{5.9}$$

2. At the inlet, a "paraboloid" velocity profile representing Poiseuille flow is applied, that is,

$$v_r = v_\theta = 0 \tag{5.10}$$

$$v_z = W_i \left(1 - r^2\right) \tag{5.11}$$

where W_i is the maximum axial velocity at the inlet.

3. At the outlet, we prescribe zero pressure and leave the velocity components free.

The physical dimensions of the model have been chosen to coincide with those commonly used by other researchers in their modelling studies of coronary arteries. In particular, R_0, the unobstructed radius, is fixed at 1.54 mm, as used by Johnston and Kilpatrick (1991) and Back *et al* (1984). Also, Z_0 is fixed at 2.31 mm, or $\frac{3}{2}R_0$. This corresponds to setting the stenotic length to three times the radius, which is a reasonable and realistic assumption. The physical dimensions and boundary conditions for the model are summarised in Figure 5.2 below.

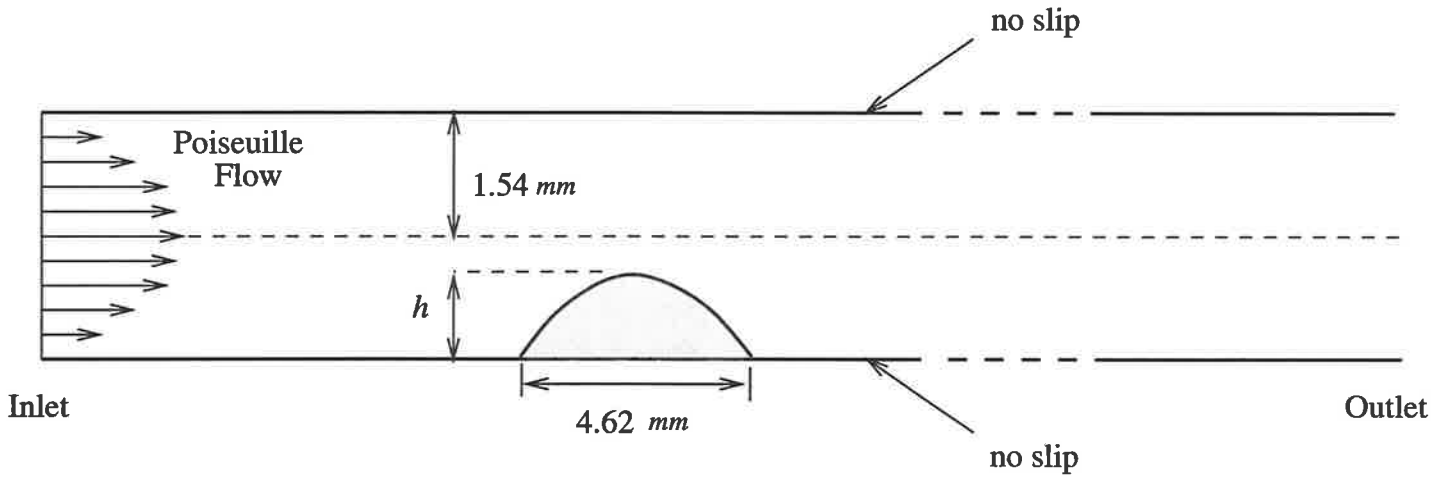

Figure 5.2: Physical dimensions and boundary conditions of the model

5.3 Formulation of the problem in PHOENICS

The equations governing the flow of fluid in the model described here are non-linear and coupled. As stated before, no analytical solution to the equations has yet been found. In the previous chapter, we have employed the CFD code, FIDAP to solve the equations for an axisymmetric model. For the model described in this chapter, we shall use PHOENICS (Version 2.0) to solve the governing equations.

A computational mesh must first be constructed. This can be done with the aid of grid generation programs and one such program (called SATELLITE) is provided in PHOENICS. For the purpose of grid generation and describing the grid, we shall define two new space coordinates, x and y, which are perpendicular to the z direction as shown in Figure 5.3a.

In the present study, the solution domain was discretised into $10 \times 10 \times 110$ cells in the x, y and z directions respectively, making a total of 11,000 non-uniform cells. More cells were placed in the vicinity of the stenosis as we expect a higher rate of change in the variables in that region. Thus, we have a finer grid in the region $z = \pm 1.5$. The grid density in the stenotic section is twice that on the upstream section and four times that on the downstream section. A section of the final grid system is shown in Figure 5.3. Figure 5.3a shows the inside view of the stenosis shape and Figure 5.3b shows the longitudinal section of the grid on the plane at which $\theta = \frac{\pi}{2}$.

After some preliminary studies, it was decided that the inlet could be placed about ten radii distance upstream from the start of the stenosis and the outlet could be placed about forty radii distance downstream from the stenosis. These dimensions ensured that fully developed Poiseuille flow was re-established at the outlet.

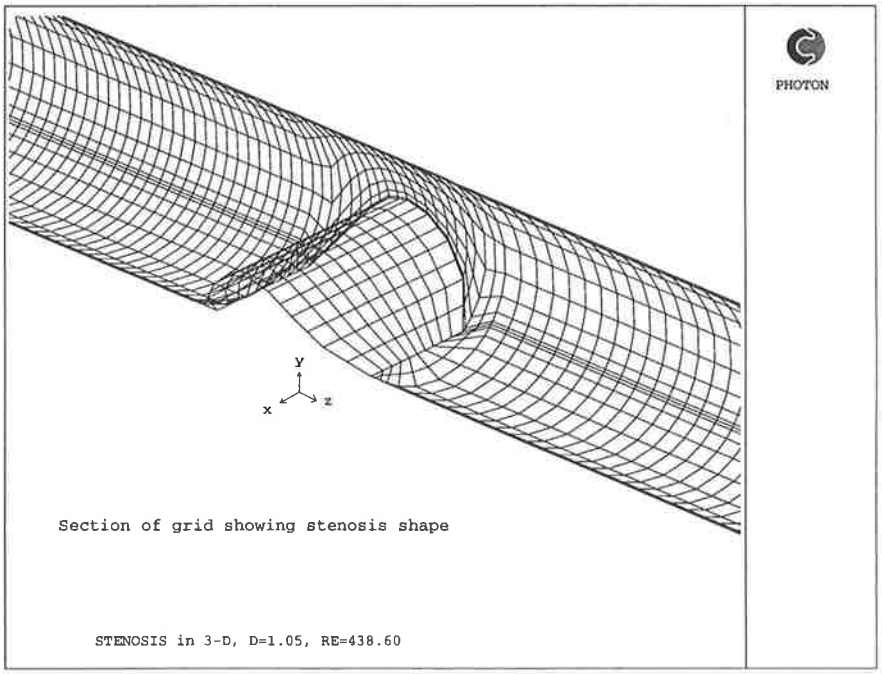

(a) Inside View

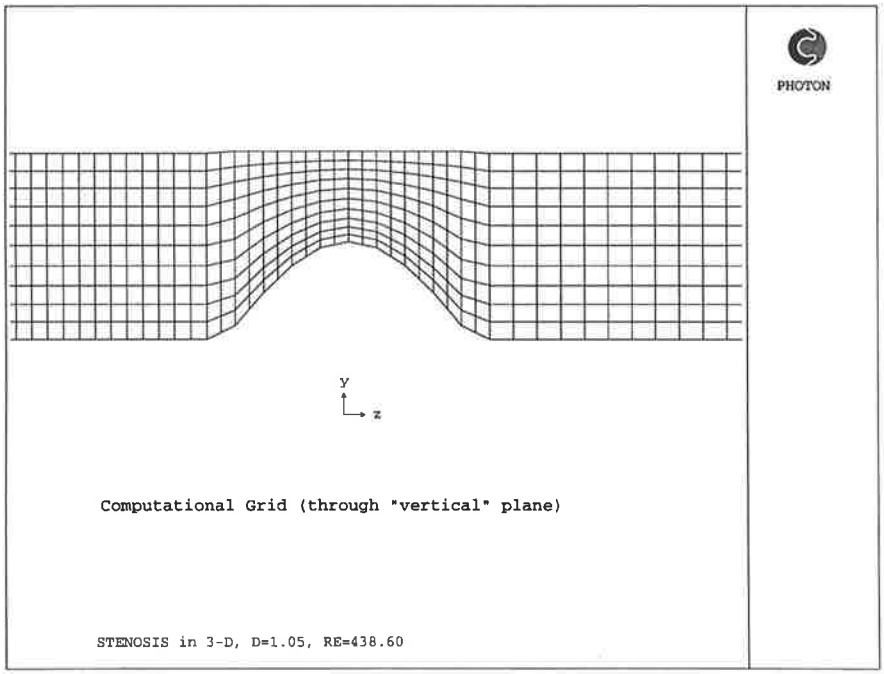

(b) Longitudinal view at $\theta = \frac{\pi}{2}$

Figure 5.3: The computational grid

Models with three different degrees of stenosis, namely, 53.18%, 65.75% and 77.65% areal occlusion, were set up. These correspond to δ values of 1.05, 1.25 and 1.45 respectively. The inlet was placed at $z = -12.0$ and the outlet at $z = 40.0$. The kinematic viscosity of blood, ν, was taken to be $3.6 \times 10^{-6} m^2/s$.

The Reynolds number, Re, in this model is defined as

$$Re = \frac{2R_0 W_0}{\nu} \tag{5.12}$$

where W_0 is the mean axial velocity and the tube diameter is given by $2R_0$, i.e. 3.08 cm. Using this definition, W_0 was varied to give a range of values of Re. Each of the models was solved for Re ranging from about 100 to 700, corresponding to mean axial velocities of between 11.69 cm/s and 81.82 cm/s.

In addition, in order to compare our results with available data, we have constructed a model with an 89% stenosis. This model has a stenosis whose shape follows an arc, as in model M5 of Young and Tsai's (1973) study.

An example of an input data file in PHOENICS for the model described is given in Appendix D. A typical run took about 55 to 65 minutes to converge. Convergence is considered reached when the relative errors for all the variables are within 1 percent. This is usually aided by the use of successive over-relaxation. In PHOENICS, the relaxation factor may be altered at any time during the numerical computation process and typical relaxation factors used in our simulations range between 0.5 to 0.75. Generally, about 200 to 250 sweeps are required to achieve convergence in all cases in this study.

5.4 Results and Discussion

After each successful PHOENICS run, values of the velocity components and pressure at each cell in the entire solution domain are found and stored. Converged solutions for steady laminar blood flow through a straight artery with a stenosis were obtained for Re = 105.33, 173.33, 210.67, 316.00, 438.60, 526.32, 614.04 and 701.75 (corresponding to steady flow rates of 0.0550, 0.0906, 0.1101, 0.1651, 0.2292, 0.2750, 0.3208 and 0.3667 lt/min respectively). Several important aspects of the results for models with 53.18%, 65.75% and 77.65% stenosis are summarised in Table 5.1.

In addition, from the results, we are able to obtain information on pressure drops across a length of the artery as well as plot the velocity profiles for the stenosis models. Also, shearing stresses on the arterial walls can be approximated from the numerical solutions. This provides useful and important information as shearing stresses are difficult to measure in an experimental set-up. In this section, we shall discuss the results of this modelling study in terms of pressure drop, velocity field and the wall shearing stresses.

Table 5.1: Summary of Model II solutions

Reynolds number	105.33	173.33	210.67	316.00	438.60	526.32	614.04	701.75
Inflow Velocity, W_0 (cm/s)	12.31	20.26	24.62	36.94	51.26	61.52	71.77	82.02
Steady flow rate (cc/s)	0.9173	1.5094	1.8346	2.7519	3.8196	4.5835	5.3474	6.1112
Steady flow rate (lt/min)	0.0550	0.0906	0.1101	0.1651	0.2292	0.2750	0.3208	0.3667
MAXIMUM AXIAL VELOCITY ($\frac{W}{W_0}$)								
53.18% stenosis	2.0345	1.8597	1.8922	1.8878	1.8566	1.8325	1.8173	1.8055
65.75% stenosis	2.6535	2.5152	2.4535	2.4641	2.4134	2.3847	2.3677	2.3533
77.65% stenosis	3.8766	3.6805	3.6320	3.6402	3.5408	3.4972	3.4673	3.4428
MAXIMUM WALL SHEAR STRESS								
53.18% stenosis								
Side A	6.5115	7.2073	8.0058	9.7791	11.0263	11.5423	11.8580	12.1010
Side B	3.1566	3.3131	3.6490	4.0931	4.4496	4.6997	4.8918	5.0870
65.75% stenosis								
Side A	10.6510	11.9683	12.5908	15.6298	17.8385	18.6897	19.2693	19.6446
Side B	5.6564	6.4923	6.7985	7.7347	8.5459	9.0780	9.6437	10.1171
77.65% stenosis								
Side A	20.7607	23.1777	24.5984	30.2151	34.3056	35.4957	36.2499	36.7170
Side B	11.7714	13.8589	14.6105	17.2245	20.2524	21.9143	23.2015	24.1727

5.4.1 Pressure Drop

Pressure drops are calculated by differencing the axial pressures at $z = -12.0$ and $z = 20.0$ at $\theta = \frac{\pi}{2}$. The full influence of the constriction would have thus been included. The graph of pressure drop against Reynolds number for the 89% stenosis model is shown in Figure 5.4 together with the experimental data from Young and Tsai (1973).

It can be seen from the graph that the pressure drop generally decreases with increasing Reynolds number. In the 89% model, because of the severe constriction, the numerical computation became unstable at Reynolds numbers higher than 700. Therefore, it was only possible to obtain results for Reynolds numbers below 700 for this percent stenosis. Nevertheless, a comparison between the results obtained and those from Young and Tsai's experiment can still be made. From the graph, it can be seen that generally there is a good agreement between the reported experimental data and the computed results of the present model.

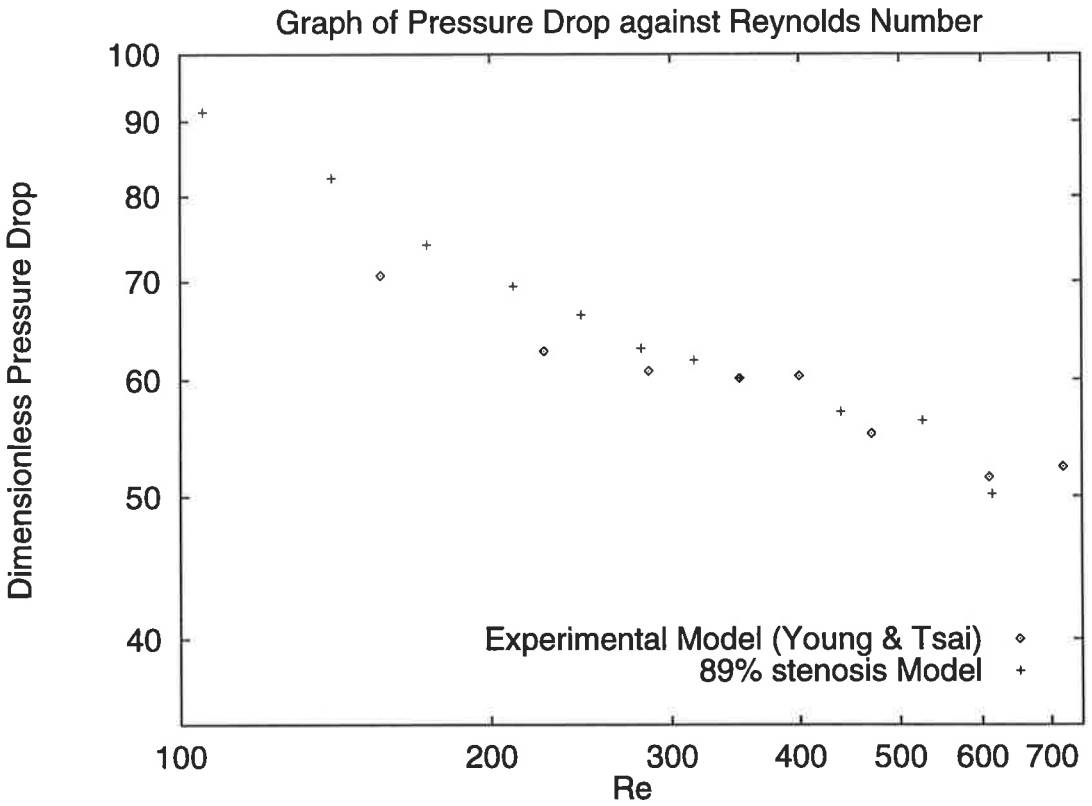

Figure 5.4: Graph showing pressure drop against Re for 89% stenosis in present study and Model M5 in Young and Tsai's study

The dimensionless pressure drop for flow across a stenosis may also be approximated by the equation proposed by Young and Tsai (1973) :

$$\frac{\Delta p}{\rho U^2} = \frac{K_v}{Re} + \frac{K_t}{2}\left(\frac{A_0}{A_1} - 1\right)^2 \tag{5.13}$$

where A_0 is the area of the stenosed vessel at the throat of the stenosis and A_1 is the area of the unobstructed vessel. K_v and K_t are constants related to the geometry of the model. In this study, K_v and K_t are chosen so as to give the best fit of data from our numerical simulation.

It would also be interesting to compare the pressure drops calculated from the simulations with that for a Poiseuille flow across an unobstructed tube. To do this, we first need to obtain a relationship between the dimensionless pressure drop and the Reynolds number for a Poiseuille flow in a straight tube. Using Equations (3.2) and (3.4), for Poiseuille flow in a straight tube, the relationship between the mean axial velocity, W_0, and the pressure drop, ΔP, across the length, L, of the tube may be written as

$$W_0 = \frac{\Delta P R_0^2}{8\nu\rho L} \tag{5.14}$$

where R_0 is the radius of the tube, ρ and ν are the density and kinematic viscosity of the fluid.

From Equations (5.12) and (5.14), we obtain

$$\frac{\Delta P}{\rho W_0^2} = \frac{16L}{R_0}\left(\frac{1}{Re}\right) \tag{5.15}$$

Hence, the following Poiseuille relationship between dimensionless pressure drop

$\left(\frac{\Delta P}{\rho W_0^2}\right)$ and Reynolds number, Re, across a dimensionless length $\left(\Delta z = \frac{L}{R_0}\right)$ is given by

$$\frac{\Delta P}{\rho W_0^2} = \frac{16\Delta z}{Re} \tag{5.16}$$

Pressure drops for all three cases of stenosis severity considered here are shown in Figure 5.5. The line marked "Poiseuille flow" in the figure refers to the variation of pressure drop with Reynolds number for flow in the unobstructed tube and is presented in the graph as a reference. This is given by Equation (5.16) with $\Delta z = 32$. The graph shows an increase in the pressure drops with increase in percent stenosis. In each case, the data points deviate from a straight line at higher Reynolds numbers.

As mentioned in Chapter 3, the resistance to flow, K, is related to the pressure drop, ΔP, and the volume flow rate, Q, by Equation (3.5), which is

$$K = \frac{\Delta P}{Q}.$$

This implies that given a constant flow rate, increase in pressure drop represents an increase in flow resistance across the length.

As we can see from Figure 5.5, at a fixed Reynolds number, the presence of a stenosis increases the pressure drop, and hence flow resistance, across it. Although compensatory mechanisms such as vasodilatation and secondary circulation may be present in the vascular system, it would not be unreasonable to conclude that there is a tendency for severe stenoses to impede the flow of blood and hence reduce blood supply to the regions.

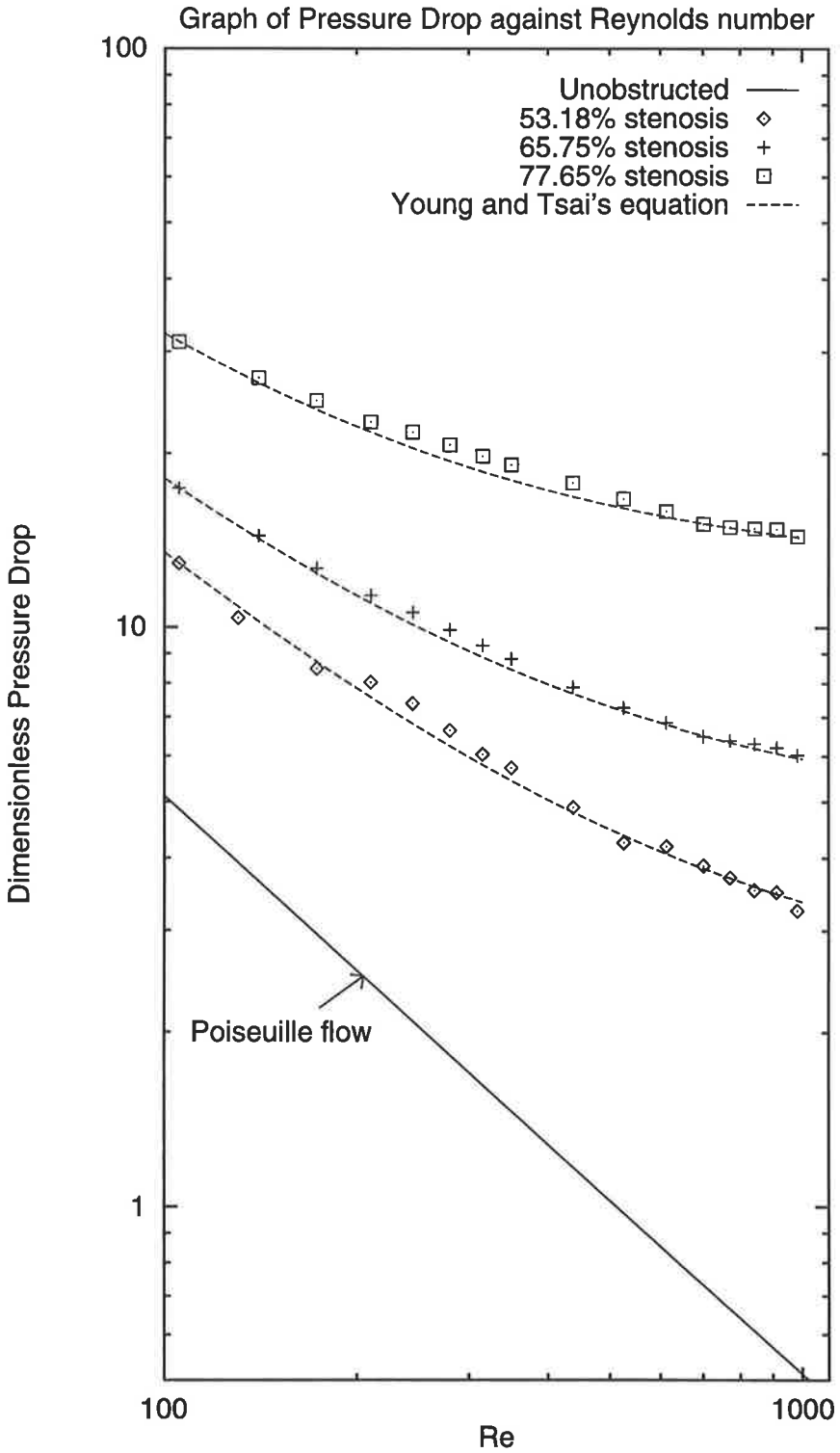

Figure 5.5: Graph showing pressure drop against Re. Dotted lines are curves plotted using Equation (5.13) for pressure drop.

5.4.2 Velocity Field

In general, in a three dimensional model, it is no longer suitable to examine the flow patterns using streamline plots. This is because the fluid particles are not restricted to a single plane in a three dimensional model. In the present study, we overcome this difficulty by examining the velocity profiles for the flow instead of studying the streamlines, in a selected section on a chosen plane. Although any plane may be chosen in principle, in this section, we have restricted the discussion to the velocity profiles on the plane $\theta = \frac{\pi}{2}$ for a section of the artery between z = -3.5 and z = 10.0.

Figures 5.6, 5.7 and 5.8 show these profiles at selected locations along the axial distance for models with 53.18%, 67.75% and 77.76% stenosis respectively.

In the figures, the velocities have been scaled upstream at $z = -3.5$ in order that comparison between the cases can be made. The profiles show fully developed Poiseuille flow prior to the stenosis. At the throat of the stenosis, the axial velocity increases rapidly and backflow is detected immediately after the stenosis.

In each case, the velocity profile is not symmetrical at the stenosis and in the downstream vicinity of the stenosis. However, they return to the initial parabolic shape, representing Poiseuille flow again, a certain distance downstream from the stenosis. This distance for recovery is longer for higher Reynolds numbers, which is what we would expect. It is also clear from the figures that the magnitude of backflow increases with increase in percent stenosis.

While velocity profiles may provide graphic qualitative descriptions of the flow patterns, it is equally useful to obtain quantitative information on the forces acting on the arterial walls. This is discussed in the next subsection.

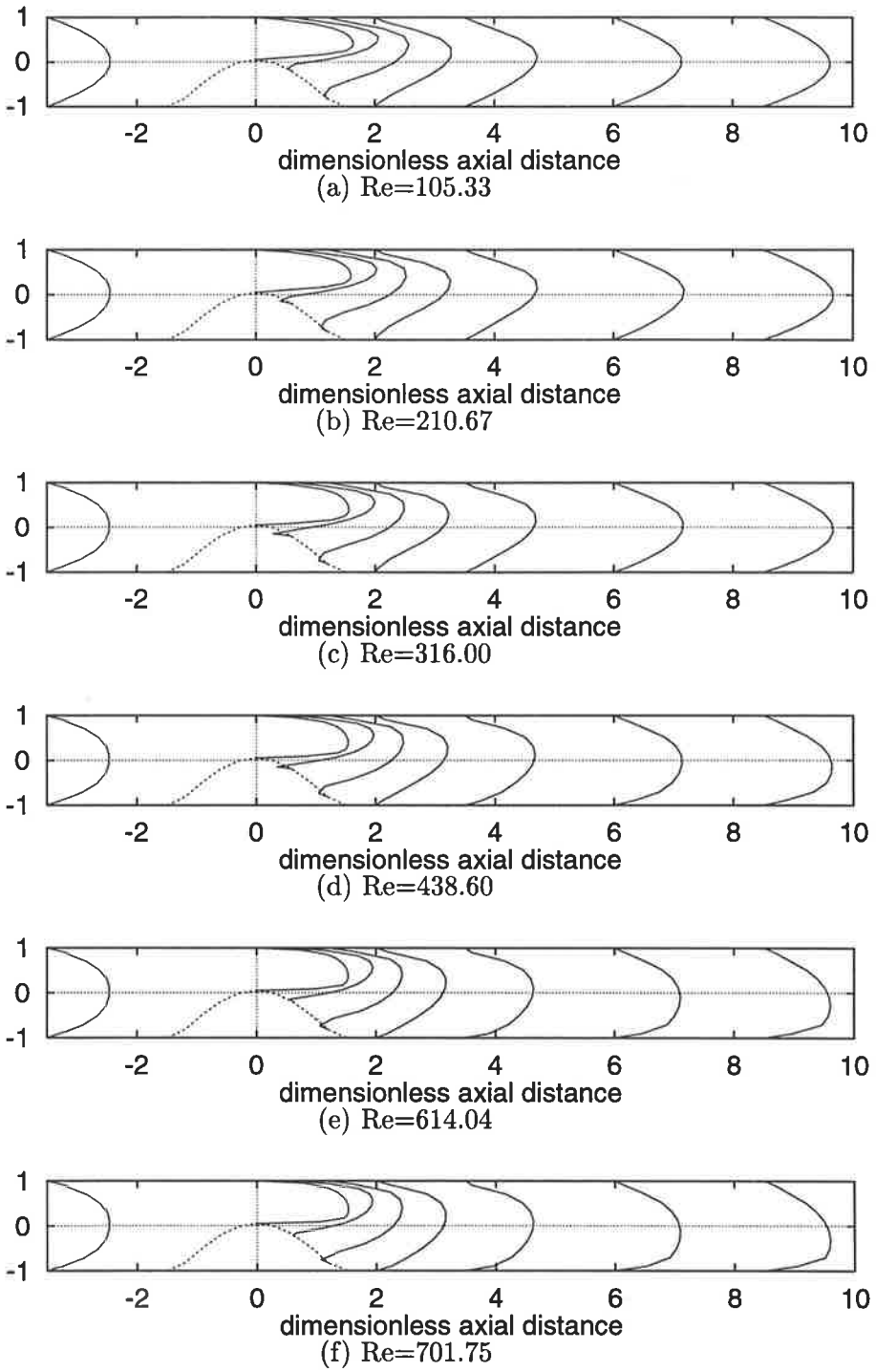

Figure 5.6: Velocity profiles for model with 53.18% stenosis at various Reynolds numbers

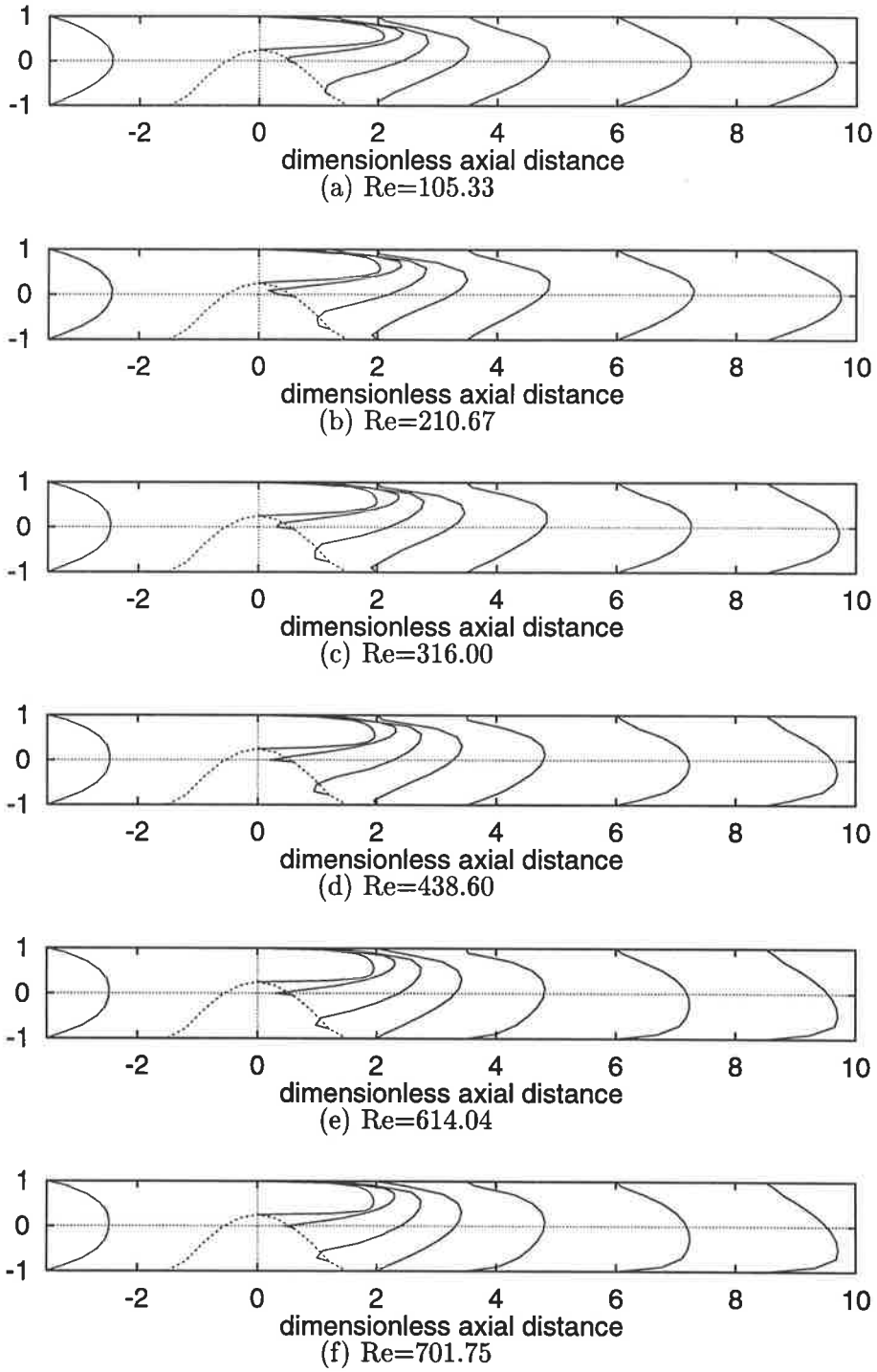

Figure 5.7: Velocity profiles for model with 67.75% stenosis at various Reynolds numbers

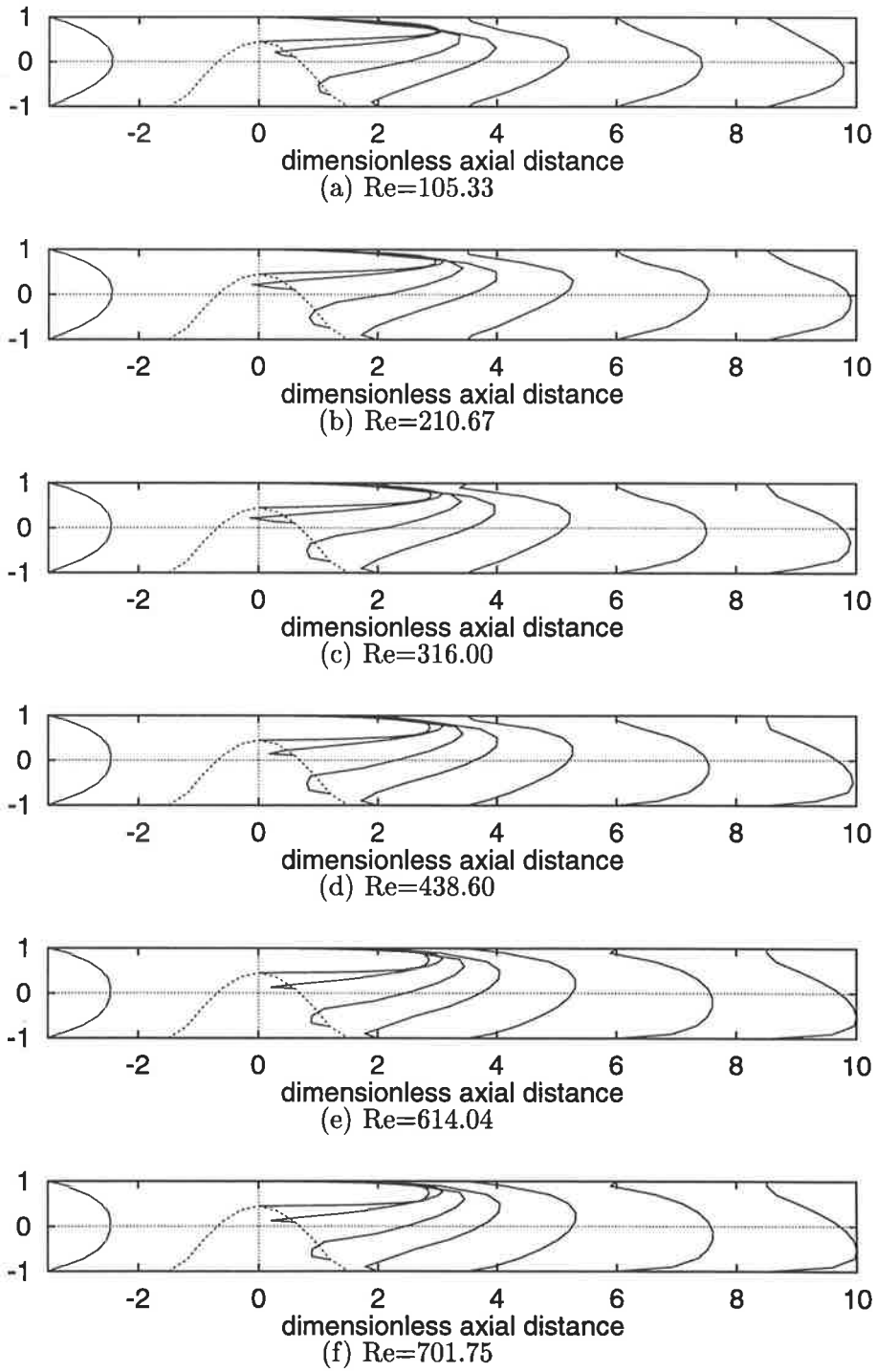

Figure 5.8: Velocity profiles for model with 77.65% stenosis at various Reynolds numbers

5.4.3 Wall Shear Stress

For incompressible fluids with no slip condition at the rigid wall, the dimensional wall shear stress, τ_w, is given by :

$$\tau_w = \mu \frac{\partial \mathbf{u_t}}{\partial \mathbf{n}}\bigg|_{wall} \tag{5.17}$$

where $\frac{\partial \mathbf{u_t}}{\partial \mathbf{n}}$ is the partial derivative of the tangential velocity with respect to the unit normal vector, $\mathbf{n}$, at the wall in physical units and μ is the viscosity of the fluid.

The value of $\frac{\partial \mathbf{u_t}}{\partial \mathbf{n}}$ may be approximated by finding an estimate for the first derivative of the velocity profile at the wall with respect to a unit vector perpendicular to the wall as shown in Figure 5.9. The two values of axial velocity components closest to the wall (w_1 and w_2) and the no slip condition at the wall ($w_0 = 0$) constitute the values needed to fit a quadratic curve. The first derivative at the wall of the resulting quadratic function then gives an approximate value for $\frac{\partial \mathbf{u_t}}{\partial \mathbf{n}}$ which is then non-dimensionalised by scaling it with respect to the wall shear stress for Poiseuille flow at the unobstructed section of the artery.

As the model studied here is not symmetrical about the axis of the artery, it would be interesting to compare the shearing stresses on "opposite sides" of the artery. Labelling "Side A" as the side with the stenosis and "Side B" as the side with no protuberance (see Figure 5.1), graphs of shearing stresses along the walls at $\theta = \frac{\pi}{2}$ are obtained. Figures 5.10, 5.11 and 5.12 show the variation of wall shear stress along the axial distance for models with 53.18%, 65.75% and 77.65% stenoses respectively for a range of Reynolds numbers.

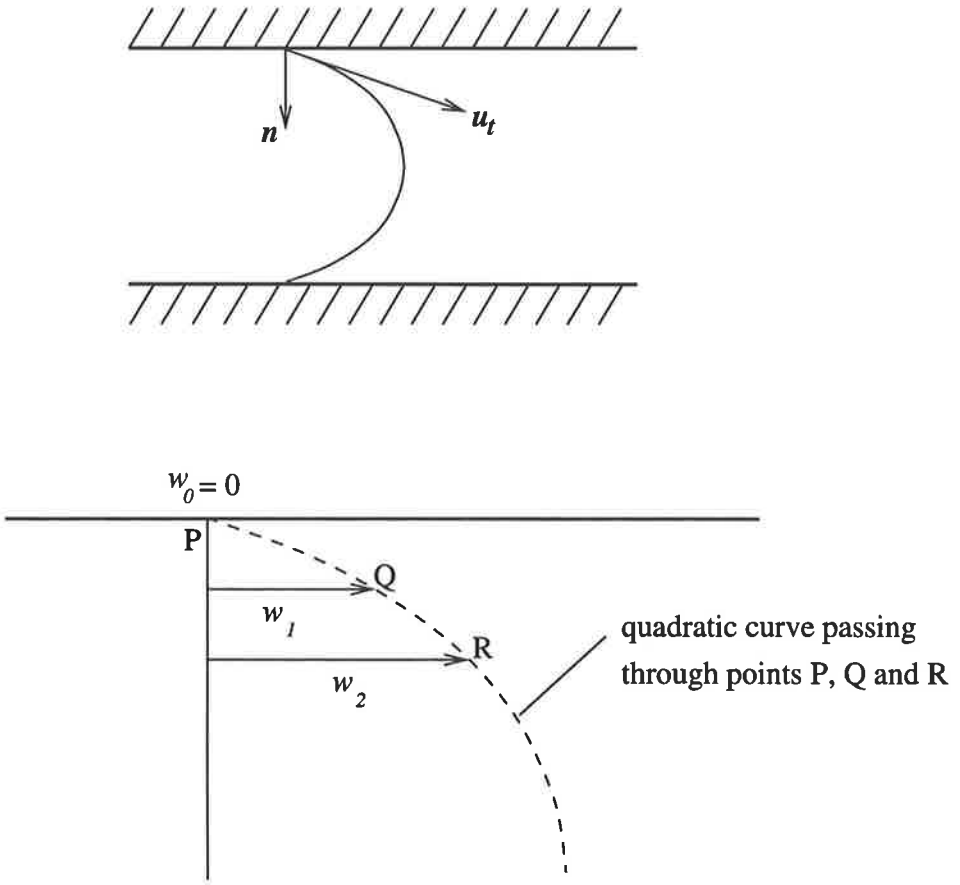

Figure 5.9: Diagram showing the tangential velocity at the wall. The term $\frac{\partial u_t}{\partial n}$ is approximated by the first derivative of the fitted quadratic curve at the wall.

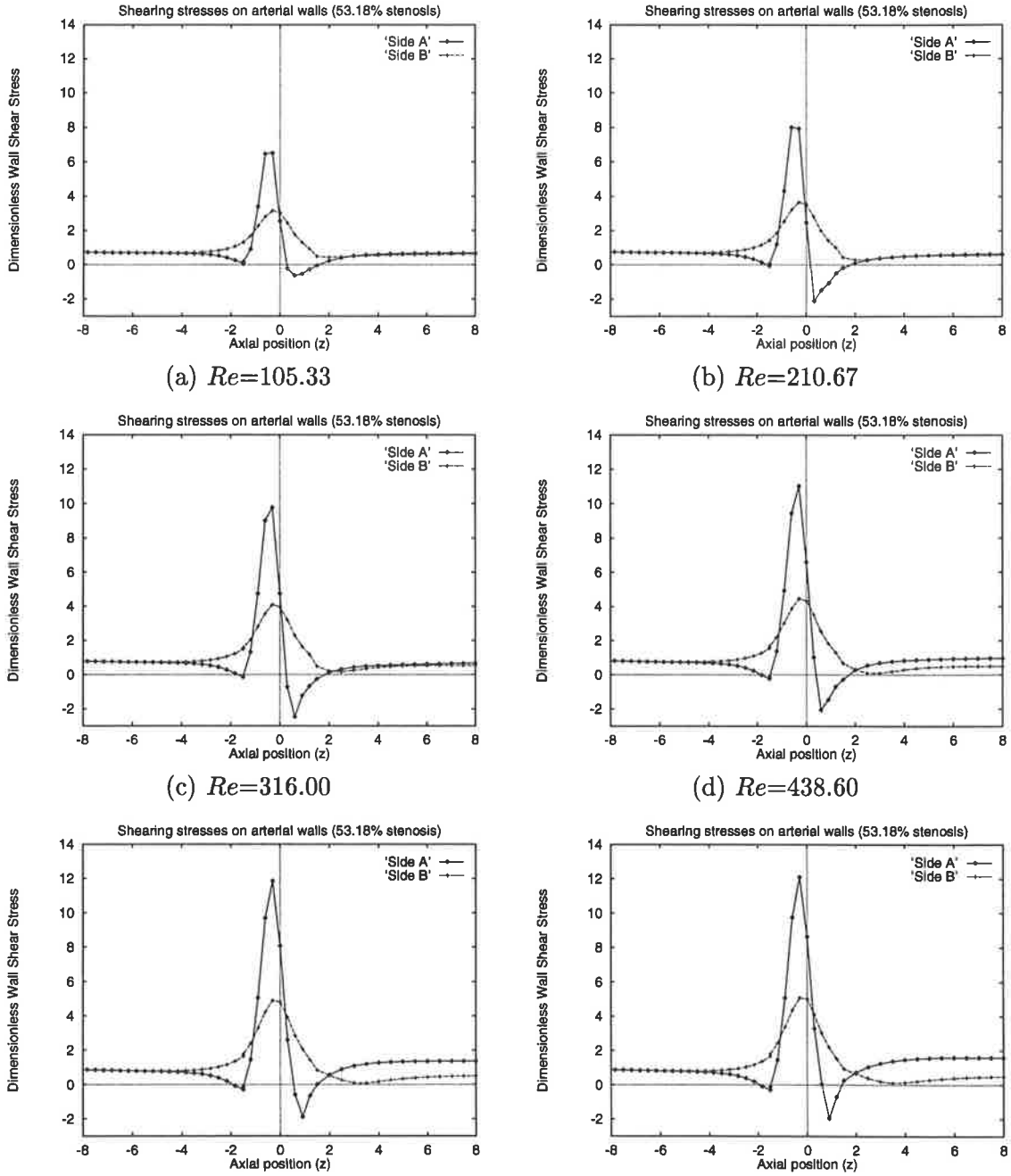

(a) Re=105.33 (b) Re=210.67

(c) Re=316.00 (d) Re=438.60

(e) Re=614.04 (f) Re=701.75

Figure 5.10: Shearing stresses on the wall in the axial direction for model with 53.18% stenosis at various Reynolds numbers

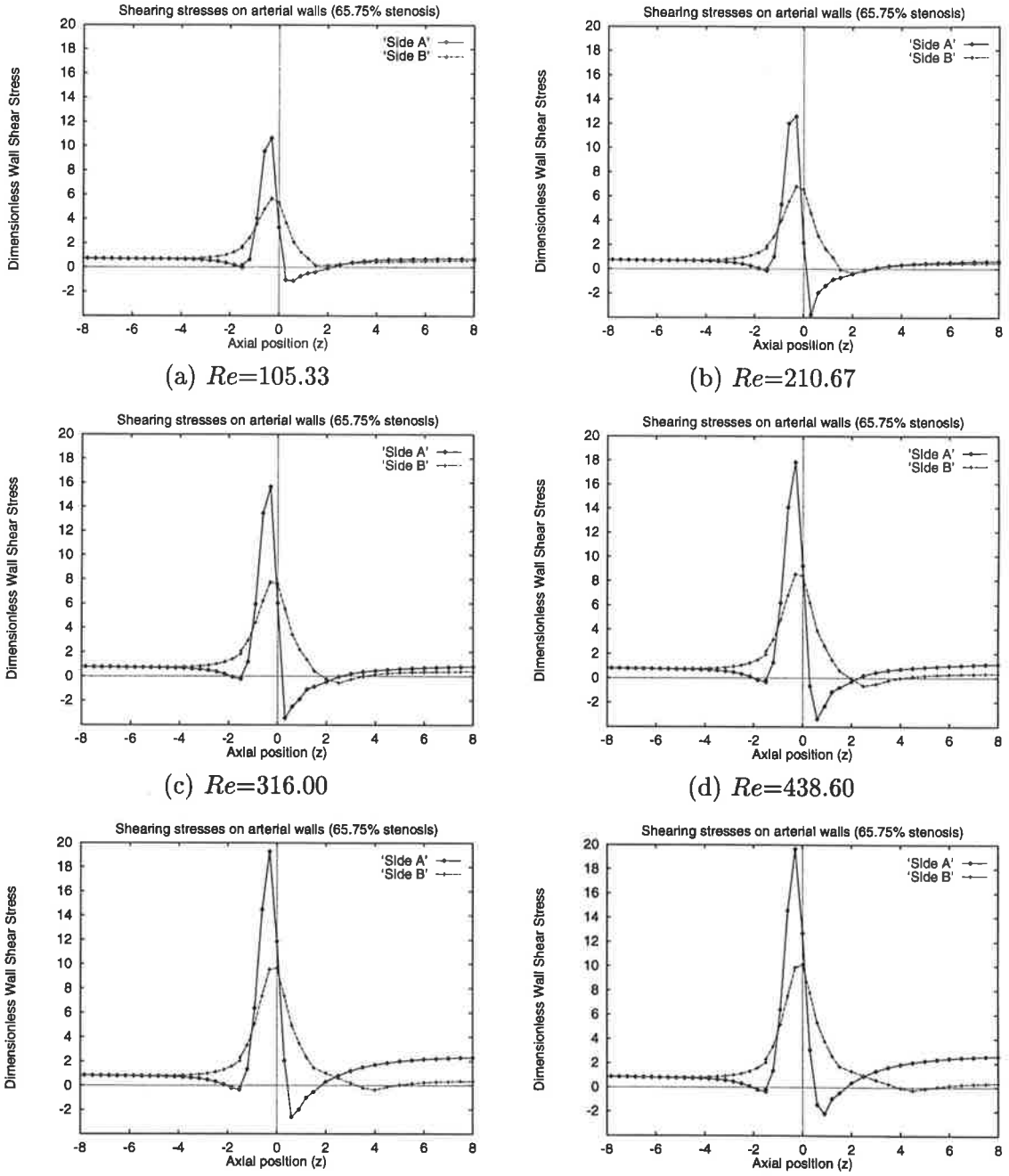

(a) Re=105.33

(b) Re=210.67

(c) Re=316.00

(d) Re=438.60

(e) Re=614.04

(f) Re=701.75

Figure 5.11: Shearing stresses on the wall in the axial direction for model with 65.75% stenosis at various Reynolds numbers

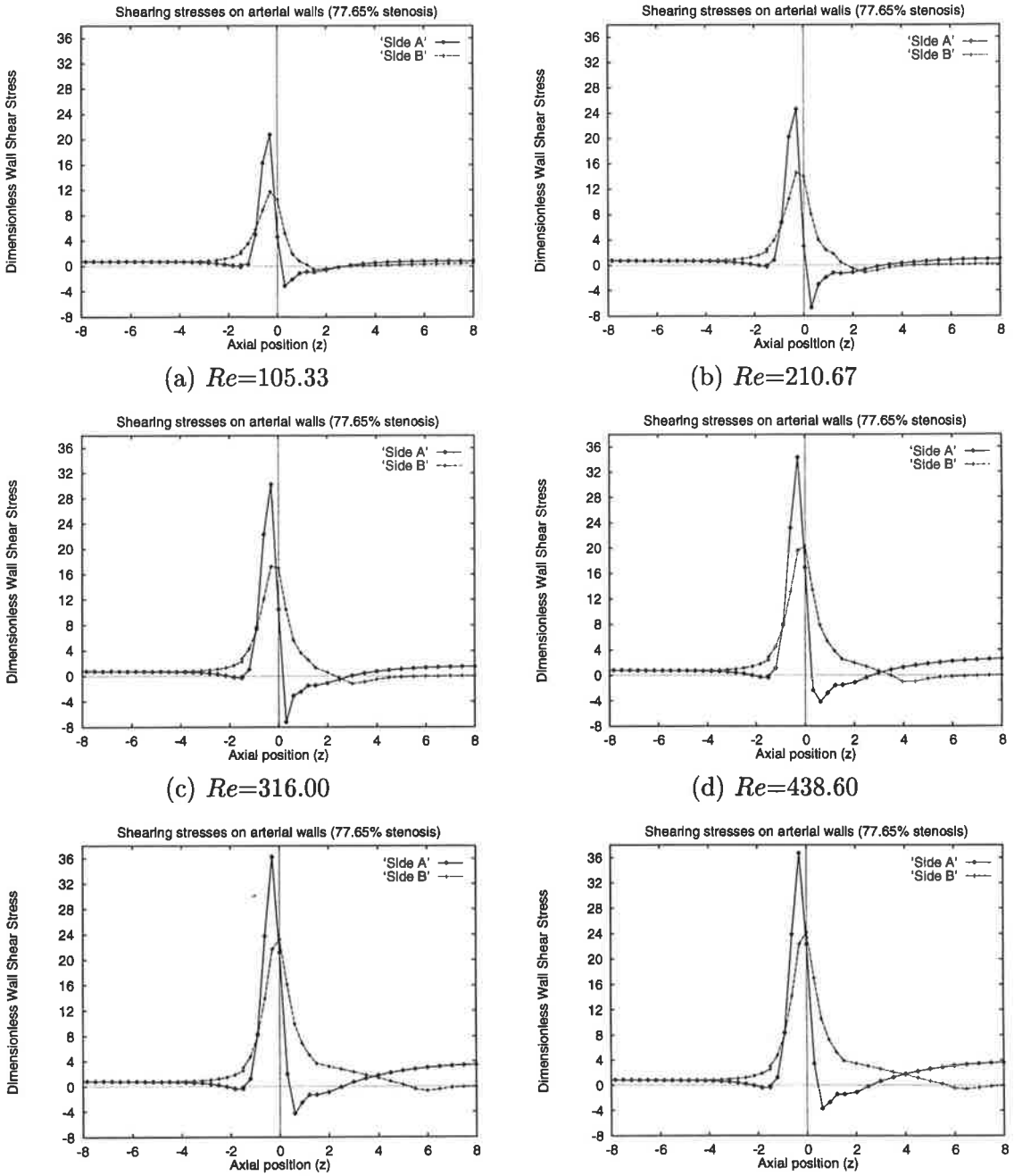

(a) Re=105.33

(b) Re=210.67

(c) Re=316.00

(d) Re=438.60

(e) Re=614.04

(f) Re=701.75

Figure 5.12: Shearing stresses on the wall in the axial direction for model with 77.65% stenosis at various Reynolds numbers

As can be seen from the graphs, maximum shear stresses on both Side A and Side B are reached just before the throat of the stenosis (at $z = 0$) as is the case in other published works (see, for example, Morgan and Young, 1974). Distinct differences are observed in the shear stress distribution on the opposite sides of the walls. On Side B, there is generally no significant negative shear stress. This implies that no flow separation and no backflow occur on this side of the wall. On Side A, however, there is clearly a region of negative shear stress in all cases. It is thus quite apparent that flow separation occurs chiefly on Side A, the stenosed side.

The peak shear stress on Side A (S_A) is higher than that on Side B (S_B) in all cases. Hence, for the range of Reynolds numbers considered in our study, the shear stress ratio $\frac{S_A}{S_B}$ is above 1 in all the models considered. Figure 5.13 below depicts the variation of $\frac{S_A}{S_B}$ with Reynolds number for all three cases of percent stenosis considered.

As can been seen from the graph in Figure 5.13, the ratio $\frac{S_A}{S_B}$ typically takes values between 1.5 and 2.5 for percent stenosis ranging from about 53% to 78%. Also, this ratio generally decreases with increase in the severity of the stenosis. For a mild stenosis (for example, 53.18%), the shear stress ratio may be as high as 2.5 at Reynolds numbers around 400. It appears that when the stenosis is mild, the stenotic side experiences a significantly higher shear stress than the other unprotruded side. As the stenosis becomes more severe, however, this difference is gradually reduced, indicating that the shear stress on the unprotruded side gradually becomes just as significant.

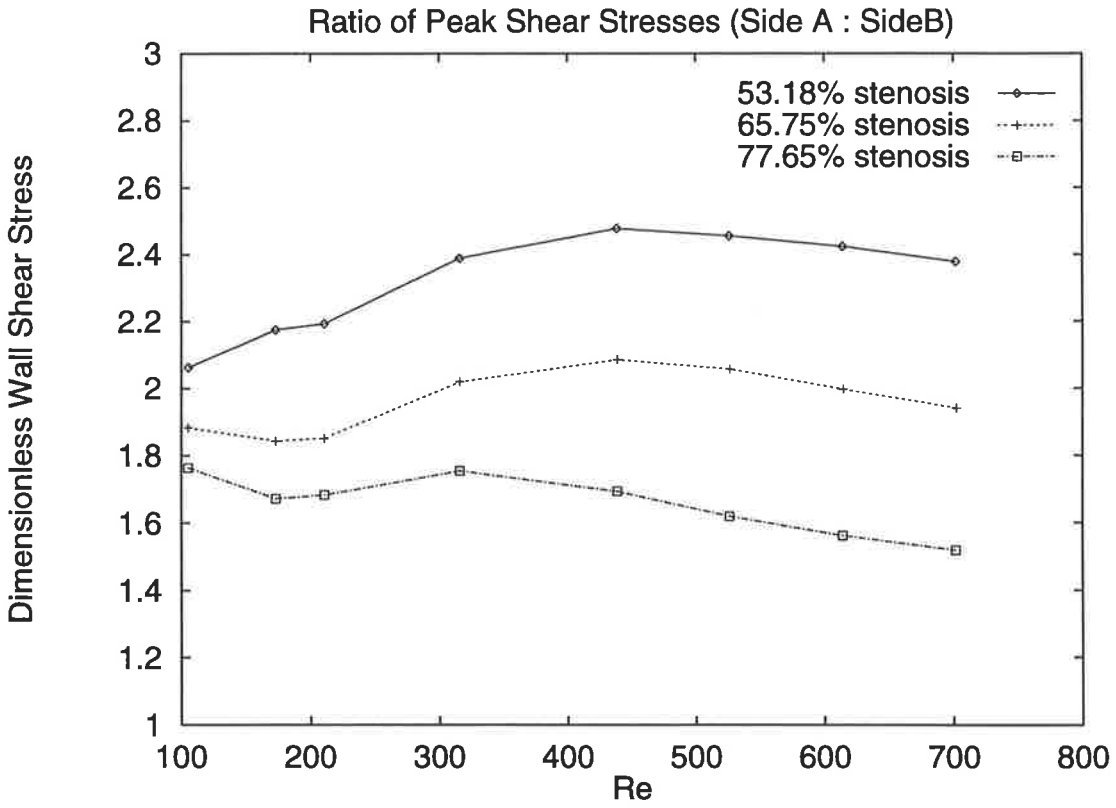

Figure 5.13: Graph showing variations of the ratio of peak shear stress on Side A to peak shear stress on Side B (i.e. S_A/S_B) for the three cases of percent stenosis

It is believed that high shear stress on the arterial walls can cause damage to the endothelium (Fry 1968). Although this could not explain the genesis of atherosclerosis, the relatively higher shear stress on the stenotic side could be an important contributing factor to the progressive growth of the stenotic plaque. Shearing stresses on the vessel wall may cause morphological changes to the endothelium. Although the specific role of wall shear stress in the atherosclerotic process has not been clearly established, the present study indicates that there is a distinct and significant difference in the elevated shear stresses on the opposite sides of the walls in an asymmetric stenosis. The shear stress ratio, $\frac{S_A}{S_B}$, may play an important role in the hemodynamics of the atherosclerotic process.

5.5 Conclusion

In this chapter, we have constructed and obtained solutions for a mathematical model in three dimensions for blood flow through an asymmetric stenosis using a computational fluid dynamic code, PHOENICS. Models for three different degrees of stenosis are studied for a range of moderate Reynolds numbers.

The results have been presented in the form of pressure drops, velocity profiles and shearing stresses on the arterial wall. Comparisons of the pressure drop graphs in this study with those obtained by Young and Tsai (1973) have shown good agreement.

One of the main objectives of this modelling study is to examine the differences in the wall shear stress on the opposite sides of the walls in an artery with asymmetric stenoses. The results from this study confirm that the wall with the stenosis experiences a higher wall shear stress than the other unprotruded side. The ratio of the peak shearing stress on the stenotic side to that on the unprotruded side of the arterial wall can be as high as 2.5 times depending on the percent stenosis as

well as the Reynolds number. In general, a more severe stenosis has a lower ratio. Also, it is found that the ratio generally remains unchanged or varies only slightly with the Reynolds number for the range considered. Furthermore, the severity of the asymmetric stenosis has a more significant effect on the peak shear stress ratio than the Reynolds number.

The results from this chapter have provided quantitative information on the effects of an asymmetric stenosis on the flow of blood, particularly with regards to shearing stresses on the arterial walls. In general, we do not expect stenoses in arteries to conform to any shape, much less to be perfectly symmetrical about the axis as many previous models have assumed. By considering an asymmetric stenosis in a model in three dimensions, we have made the model more realistic and shown that the dynamics of blood flow are significantly altered by the geometry of the narrowing.

The results from the study presented in this chapter have been accepted for publication and will appear in the journal, *Mathematical and Computer Modelling.*

CHAPTER 6

MODEL III : CURVED ARTERY MODEL IN THREE DIMENSIONS

6.1 Introduction

In the previous chapter, we have seen how computational fluid dynamic techniques may be efficiently used to construct more realistic models in three dimensions to study the flow of blood in arteries. The model described earlier has made it possible to study of the effects of asymmetrical stenoses on blood flow characteristics.

However, blood vessels often bend and curve as they traverse around organs. It has been shown that such bends and curvatures in arteries are one of the sites of predilection and may be an important factor in the pathogenesis of arterial diseases (Texon 1963; Nerem and Cornhill 1980). Therefore, it would be desirable to construct a curved artery model and examine the effects of curvature on the flow conditions.

In this chapter, we first present a geometrical description of a curved artery model. Using PHOENICS, the model is solved for degrees of stenosis up to 70% for Reynolds number ranging from 100 to 1200. Results in terms of pressure drops, velocity fields and shearing stresses will be presented. In addition, secondary flow phenomena will also be discussed in detail.

6.2 Description of the Model

Development of the Model

Figure 6.1 shows angiograms of typical coronary arteries of a person suffering from a coronary disease. As can be observed from the figure, coronary arteries are generally not straight conduits. In fact, they usually curve and bend in some tortuous manner. Also, it is not uncommon to find stenoses on the bends of such arteries as can be observed from the angiograms in Figure 6.1

Sabbah *et al* (1984), Altobelli and Nerem (1985) and Back *et al* (1992) and are among the earlier investigators to have studied flow in curved tubes simulating blood flow in a curved artery. The experiments they performed have shown that the flow conditions are significantly altered by the presence of curvature.

Perktold *et al* (1991) developed a model of flow in a slightly bent tube with very gradual tapering and demonstrated the presence of secondary flow phenomena. Padmanabhan and Jayaraman (1984) constructed a model of flow in a curved tube with constriction and, using a perturbation method, produced an analytical solution to their model. However, their method of solution can only handle flow with low Reynolds numbers (Re = 20 - 100). Furthermore, their model has assumed an axially symmetrical stenosis. Asakura and Karino, (1990) in their modelling study using flow visualisation techniques, observed that the asymmetry in the stenoses at bends and bifurcations has a significant effect on flow conditions.

UNIVERSITY OF ADELAIDE

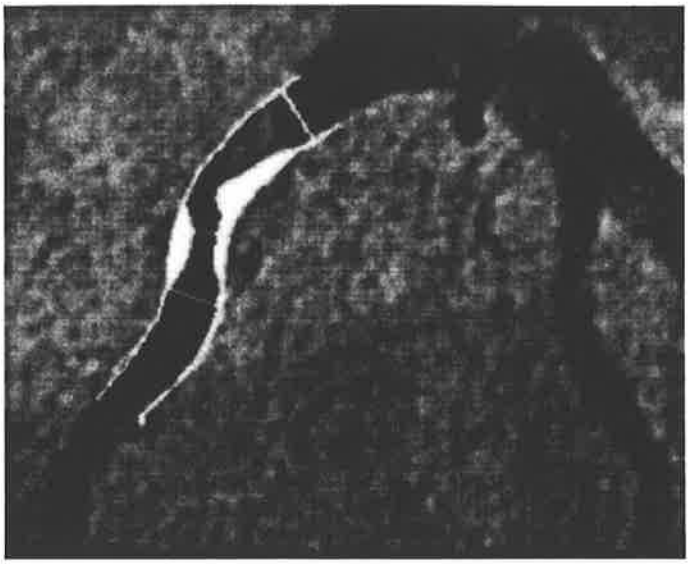

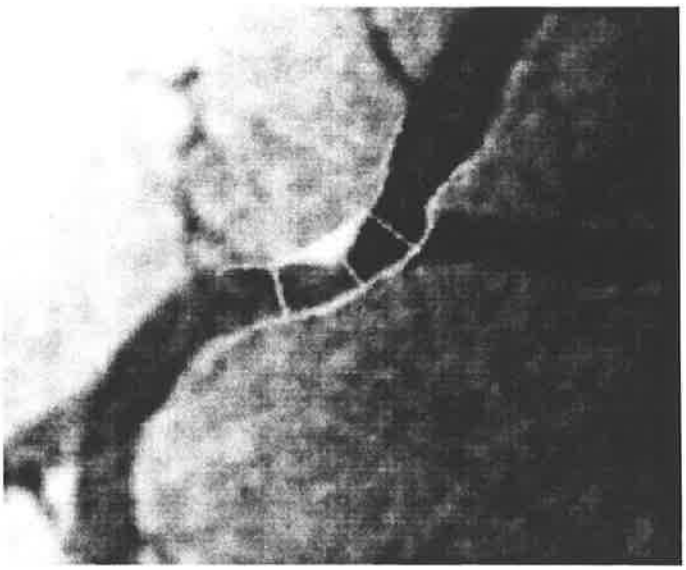

Figure 6.1: Typical angiograms showing the stenoses at bends of tortuous arteries. The images shown here are digitally scanned from angiograms obtained from the Wakefield Hospital, Adelaide.

In recent years, many flow visualisation studies using artery casts have been carried out to provide a realistic investigation of flow patterns in blood vessels. In particular, Back *et al* (1992) had used a highly curved atherosclerotic coronary artery cast with a significant "s" shaped reverse curvature in their experimental study. They were able to measure wall pressure using pressure probes and had demonstrated secondary flow phenomena in the vicinity of the bend.

The basic geometry of the model developed in the present study is similar to that of the artery cast used by Back *et al.* This is so because some form of comparison may be made between the results. Figure 6.2 shows the general geometrical form of our model.

As we shall be using the computer code, PHOENICS, to generate the model, the body fitted coordinate system (r, z, α) is used only for the purpose of describing the model and presenting the results. In this system, r is the radial distance from the centreline of the vessel, α is the angle subtended from the vertical, and z represents the axial coordinate from the entry point following the shape of the centreline. r_w and r_c are the radius of the tube and the radius of curvature respectively, and θ is the angle of curvature as shown in the figure. L_1 and L_3 are lengths of the tube prior to and immediately after the bend. L_2 is the length of the curved portion.

We introduce a non-dimensional length, s, which is defined as

$$s = \frac{z}{r_w} \tag{6.1}$$

Thus, s represents the dimensionless distance from the entry point measured along the centreline of the artery. In Figure 6.2, the values of s at certain points of interest are shown.

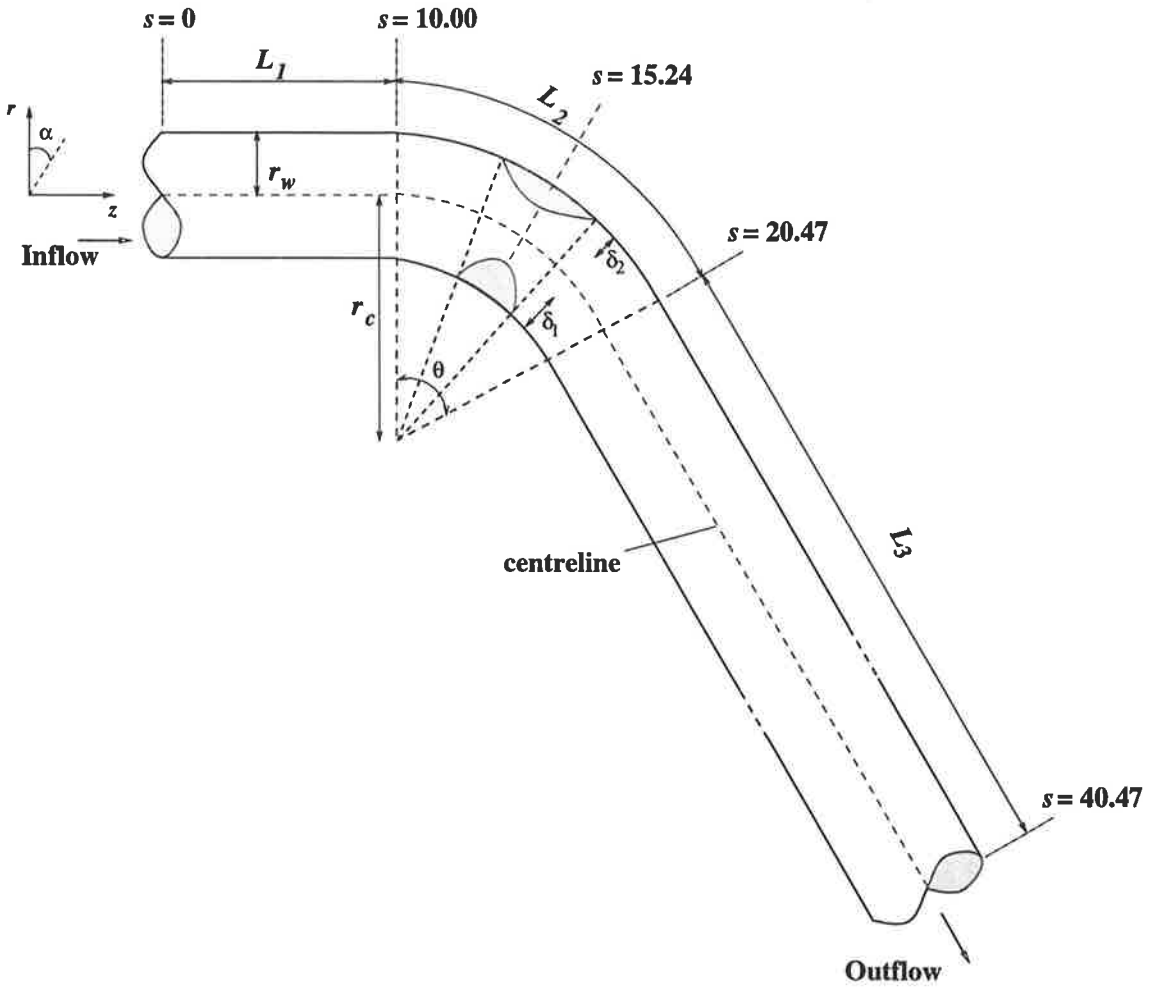

Figure 6.2: Geometrical representation of the Curved Artery Model with non-symmetric stenoses. s is the dimensionless distance measured from the entrance, along the centreline. The throat of the stenosis is located at s= 15.24.

Percent Stenosis

The stenoses in our curved artery model are situated centrally on the bend. In general, stenotic plaques can grow from either side of the wall even though it seems more common to find atherosclerotic plaques on the inner side of the curved artery. In the present model, δ_1 is the height of the protrusion from the inner wall (i.e. inner side of the bend) and δ_2 is that from the outer wall. This is designed so that we have a more general case.

The degree of stenosis is determined by the percentage of cross sectional area occluded at the throat (i.e. narrowest part) of the stenosis. Figure 6.3 below shows the cross section of the model at s=15.24 for a general case. The shaded regions represent the occluded or blocked area. It should be noted that the model here suggests that the cross section of the lumen at the stenotic region is not circular. In fact, it is not uncommon to find slit-like luminal cross sections at stenotic segments of pathologic arteries (see Becker and Anderson 1983).

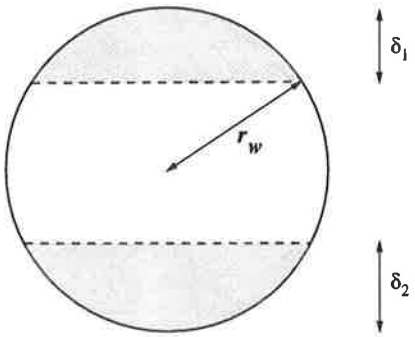

Figure 6.3: Cross section of model at the narrowest portion of the stenosis

It can be shown, as an extension to Equation (5.4), that for $r_w = 1$, the percentage of area occluded is given by

$$\frac{1}{\pi}\sum_{i=1}^{2}\left(\arccos(1-\delta_i) - (1-\delta_i)\sqrt{2\delta_i - \delta_i^2}\right) \times 100\% \tag{6.2}$$

Governing Equations and Boundary Conditions

As can be seen from the description of the model above, there are a number of geometrical parameters that can be varied. In this study, we wish to concentrate on the effects of non-symmetric stenoses in curved arteries on blood flow and have hence kept some of these parameters fixed.

The governing equations for the flow are the full Navier-Stokes equations for a Newtonian fluid. This is justified as the non-Newtonian effects only become significant in vessels with a diameter of less than 500 μm. In all our models, we have set the radius of the unobstructed part of the artery, r_w, to be 1.54 mm, which is a reasonable value for a typical right coronary artery of man and is the same value used in Model II. We have also assumed the tube to be rigid as it has been shown that for a stenosed artery, elasticity effects are negligible (Padmanabhan and Devanathan 1981). At the vessel walls, no slip and no penetration conditions apply.

The angle of curvature, θ, is fixed at 60^o. This is a reasonable value for a typical coronary artery. Also, λ, defined as the ratio of r_c to r_w, is fixed at approximately 10. Hence, the length of the curved segment, L_2, is approximately 16.13 mm.

According to Chang and Tarbell (1988), the placement of the entry of the flow prior to the curved segment may be decided using the following entry length correlation,

$$\gamma_D = 49 Re^{1/3} \lambda^{-1/2} \tag{6.3}$$

where γ_D is the entry length in degrees of axial curvature. In the present model, for $Re = 100$ to $Re = 1200$, γ_D ranges from 71.92^o to 154.95^o, corresponding to about 1.2 to 2.6 times θ. Hence, for this study, it is justified to place a fully developed inflow at about 5 tube diameters from beginning of the curvature. Thus, L_1 is fixed at 15.4 mm.

The length of tube downstream from the curvature is chosen to ensure that a

fully developed flow is re-established. After some preliminary studies, it was decided that L_3 could be fixed at around 30.8 mm.

6.3 Formulation of the problem in PHOENICS

To study the effects of stenoses in curved arteries on blood flow, three groups of models have been set up. Group A models a curved artery without any constriction, Group B models a protrusion from the inner wall of the curvature and Group C models protrusions from both the inner and the outer walls of the curvature. Varying degrees of stenosis have been modelled and Table 6.1 shows the set of models presented in this study. Each of the models set up (A, B1 to B10, C1 to C6) was solved for Reynolds numbers ranging from 100 to 1200. Models B5 to B10 have been set up to have the same degree of stenosis as Models C1 to C6.

Table 6.1: Models of different degrees of stenosis

Model	δ_1/r_w	δ_2/r_w	Percent Stenosis (%)
A	0.0	0.0	0
B1	0.8500	0.0	40.49
B2	1.0500	0.0	53.18
B3	1.2500	0.0	65.75
B4	1.4500	0.0	77.65
B5	0.9039	0.0	43.89
B6	0.9639	0.0	47.70
B7	1.0352	0.0	52.24
B8	1.1208	0.0	57.67
B9	1.2031	0.0	62.84
B10	1.2978	0.0	68.67
C1	0.8500	0.15	43.89
C2	0.8500	0.25	47.70
C3	0.8500	0.35	52.24
C4	0.8500	0.45	57.67
C5	0.8500	0.55	62.84
C6	0.8500	0.65	68.67

The governing equations of the flow may be solved using PHOENICS (Version 2.0). In order to apply PHOENICS to the model, the solution domains of each set must first be discretised. For a preliminary run, the solution domain was first discretised into 8,000 non-uniform cells. This was subsequently refined to give a total of 32,000 cells.

The reason for using a coarse grid as a preliminary step is that it allows salient features of the flow to be determined fairly speedily. Grid refinement then follows to ensure that the solutions obtained are as "grid independent" as possible. However, it must be noted that increasing the discretisation of the domain will also increase the computational expense. Both computer run-time as well as computer storage requirement are likely to increase. Hence, an optimal value of 32,000 cells was decided after a number of experimental runs.

The grids generated in this set of models are curvilinear grids, which conform to the shape of the body of the model. This system of grid formation is often called the Body-Fitted Coordinate (or BFC) system. Figures 6.4 through 6.8 show some examples of the discretised sections for Model B1.

Figure 6.4 and 6.5 show part of the computational grid in longitudinal section and a cross section at an unstenosed portion respectively. It is highly desirable to have "orthogonal" grid cells (that is, grid cells with edges at right angles) with an aspect ratio as close to unity as possible. However, this is sometimes difficult to achieve in practice. The PHOENICS grid generation program includes a facility which colour-codes grid cells as they are formed, giving information about the geometrical suitability of the grid. Using this facility as an aid, the grids were generated with as high a degree of orthogonality as possible. Figures 6.6, 6.7 and 6.8 show the transition of the grid cell distribution at three different points on the curved and stenosed portion of the artery.

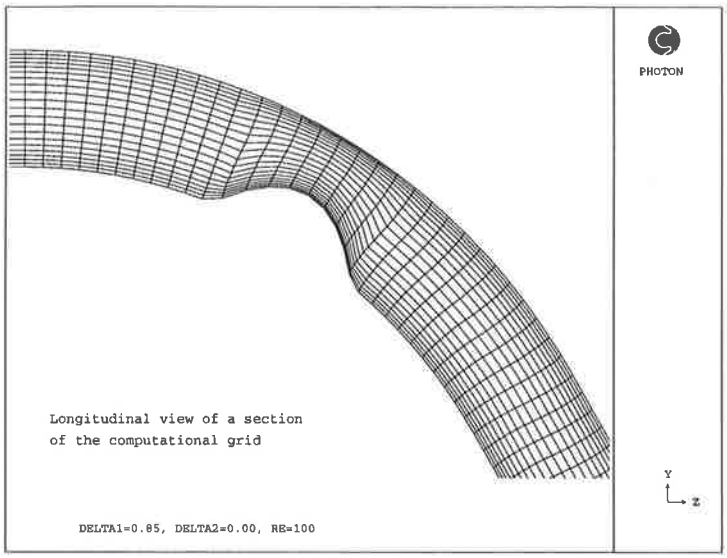

Figure 6.4: A segment of the grid for Model B1 in longitudinal section

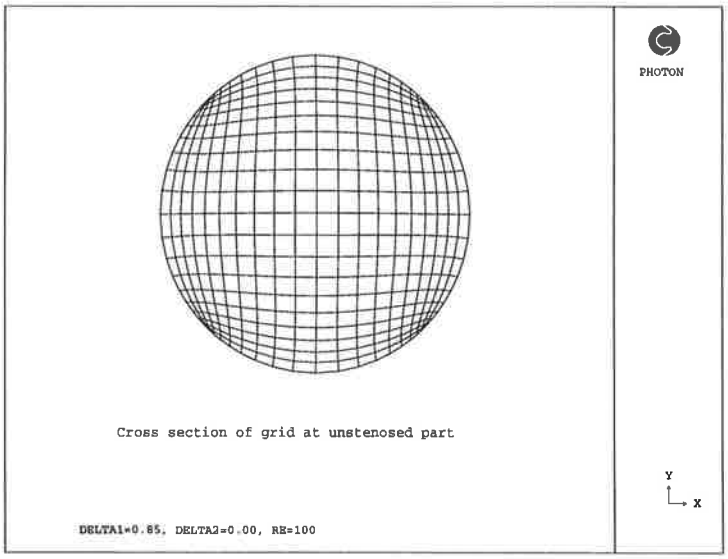

Figure 6.5: Cross section of grid for Model B1 at unobstructed part

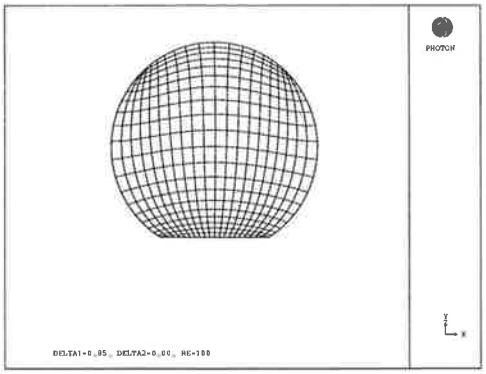

Figure 6.6: Cross section of grid for Model B1 at $s = 14.19$

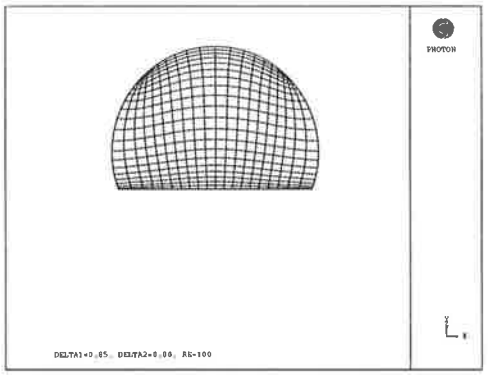

Figure 6.7: Cross section of grid for Model B1 at $s = 14.89$

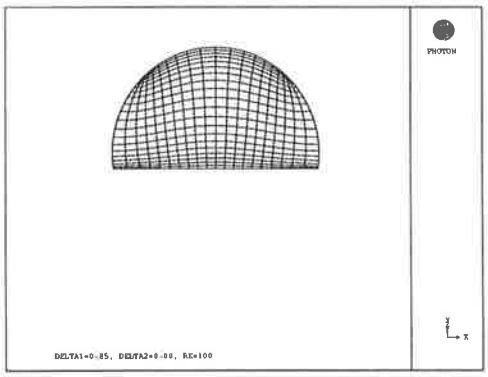

Figure 6.8: Cross section of grid for Model B1 at $s = 15.59$

6.4 Results and Discussion

In all the models considered (A, B1 to B10, C1 to C6), the unobstructed radius, r_w, is fixed at 1.54 mm. The stenotic length of the inner stenosis is approximately 3.14 mm and the outer stenosis, if present, has a length of about 3.84 mm. The viscosity and density of blood is taken to be $3.6 \times 10^{-6} m^2/s$ and 1.06 kg/m^3 respectively.

A typical PHOENICS run for models in Groups A and B took between 80 to 90 minutes to converge. Models in Group C took an average of about 120 minutes for convergence. Convergence is considered reached when the relative errors for all the variables are within 1 percent. This is usually aided by the use of successive over-relaxation. In PHOENICS, the relaxation factor may be altered at any time during the numerical computation process and typical relaxation factors used in the simulations in the present study range between 0.5 and 0.85. Generally, for models in Groups A and B, about 500 sweeps are required to achieve convergence whereas Group C models may take up to 2900 sweeps.

The models are solved for Reynolds numbers ranging from 100 to 1200 corresponding to flow rates ranging from 0.0523 to 0.6434 lt/min. In this section, we present the results obtained for the models. As it is not possible to report all the findings, only representative results demonstrating the essential features of the study will be presented in detail.

6.4.1 Pressure Drop

A graph showing the variation of pressure drop with Reynolds number for Models A, B1 and C4 is given in Figure 6.9. Pressure drops are calculated by taking the pressure difference between $s = 1.0$ and $s = 29.0$, i.e. approximately 8 to 9 radii distance from each end of the curvature. Also shown in the graph for reference is

the Poiseuille flow relation for a straight unobstructed tube given by the equation,

$$\frac{\Delta P}{\rho U^2} = \frac{32}{Re}\Delta s \tag{6.4}$$

where left hand term is the non-dimensionalised pressure drop across Δs, the dimensionless length of tube in consideration.

In general, it can be seen that the calculated pressure drops for the models in all the three Groups are higher than that in the unobstructed Poiseuille flow. This difference, which translates to the relative flow resistance, progressively increases with increasing Reynolds number.

For Group A, (i.e. curved artery with no constriction), the relative flow resistance is about 12.7 percent higher at $Re = 100$, and about 67.5 percent higher at $Re = 500$ than a straight unobstructed tube. This compares fairly well with the 14 percent and 70 percent respectively reported by Back *et al* (1992) in their experimental study using a curved artery cast of man. The slight discrepancy may be attributed to the fact that the artery cast model had a second bend and that contributed to the overall resistance.

The graph shows that the presence of even a mild stenosis in the curved segment increases the relative flow resistance quite significantly. In particular, for a 40.49 % stenosis from one wall (the inner wall of the curvature), at $Re = 500$, the relative flow resistance is 26.52 percent higher than in a curved unobstructed artery. For the same Reynolds number, a 57.67 % stenosis with narrowings on both walls, the relative flow resistance is increased by 42.65 percent.

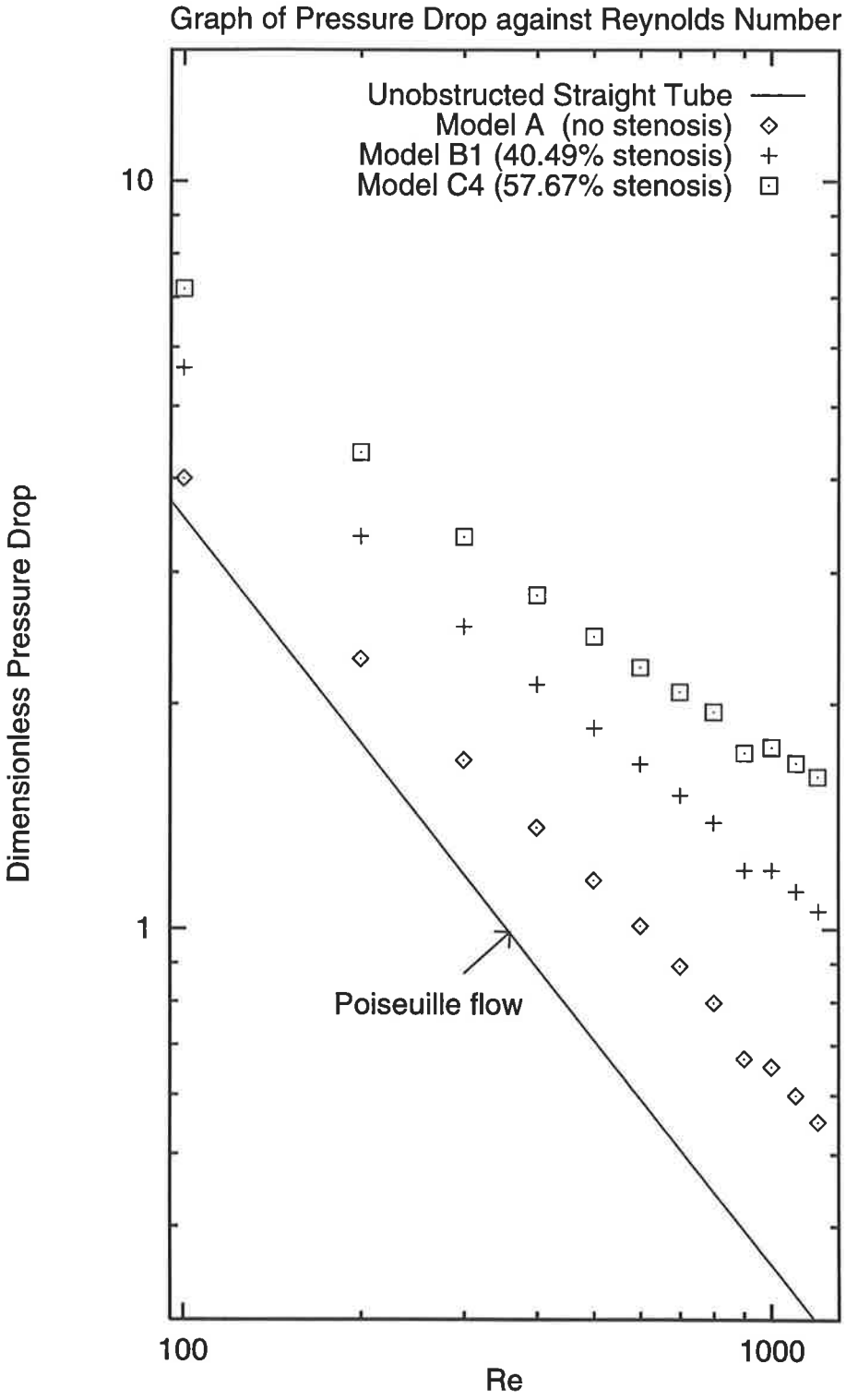

Figure 6.9: Graph of dimensionless pressure drop against *Re* for Models A, B1 and C4. Model B1 has protrusion from inner wall only and Model C4 has protrusions from both inner and outer walls.

May *et al* (1963) proposed that the relationship between the total pressure drop and percent stenosis for an axi-symmetric stenosis in a straight tube may be described by the equation,

$$\Delta P = \frac{8\mu L}{R^2} V \left(\frac{A_1}{A_2}\right)^2 + \frac{4.8\mu}{R} V \left(\frac{A_1}{A_2}\right)^{3/2} + \rho V^2 \left(\frac{A_1}{A_2}\right)^2 \tag{6.5}$$

where the symbols take the following meanings :

ΔP = total pressure drop

μ = viscosity of blood

ρ = density of blood

L = length of stenosis

R = radius of unstenosed lumen

A_1 = cross sectional luminal area of unstenosed vessel

A_2 = cross sectional luminal area of stenosis

V = blood velocity in pre-stenotic segment

It was also found that a constant V does not interfere with the proper interpretation of this relationship (May *et al* 1963) and Equation (6.5) is essentially a function of $\left(\frac{A_1}{A_2}\right)^2$. Although the equation is for a straight tube, it would be interesting to compare it with our results. Figure 6.10 below shows a graph of pressure drop against percent stenosis for models in Group B and Group C at $Re = 400$.

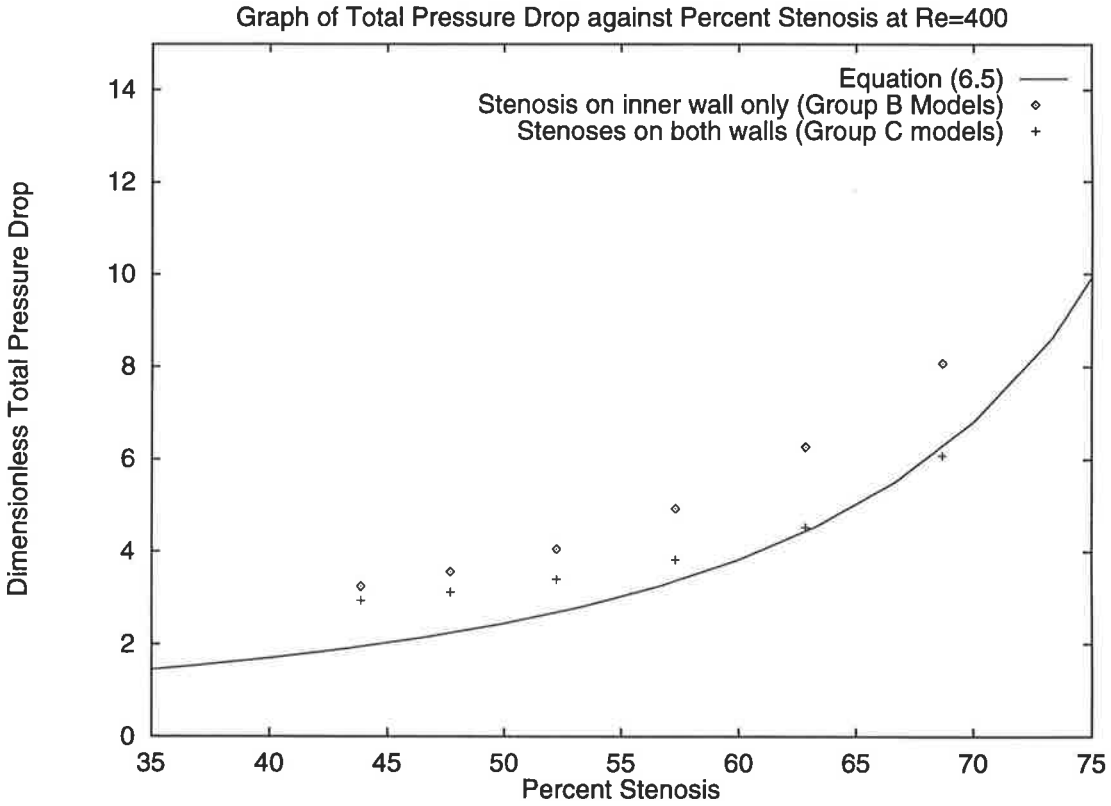

Figure 6.10: Comparison of pressure drops in present curved artery model (for Models B5 to B10 and C1 to C6) with Equation (6.5) at $Re = 400$

Although the actual values of pressure drops may be fairly low in the range of percent stenosis considered, we can observe from the graph in Figure 6.10 that the pressure drop, and hence the relative flow resistance, for flow in a curved artery with stenoses generally increases with increase in percent stenosis. Also, flow resistances in models with only protrusions from only the inner wall (Group B models) are higher than that in models with protrusions from both walls (Group C models). For the range of percent stenosis considered here, the pressure drops in Group B models are between 10 to 38 percent higher than pressure drops in Group C models, showing that asymmetry of the stenosis has a significant effect on the pressure drops.

6.4.2 Velocity Field

Maximum Relative Axial Velocity

After each successful PHOENICS run, values of the velocity components in each grid cell in the entire flow domain are found and stored. A summary of the maximum relative velocity is given in Table 6.2. Relative axial velocity is calculated by dividing the axial component of the velocity (W) in the direction of the body-fitted coordinate, z, by the maximum axial velocity at the inflow (W_i).

It was observed that in general, the maximum $\frac{W}{W_i}$ in each case occurred on the $\alpha = 0$ plane, i.e. the "vertical" plane passing through the centreline of the tube (see Figure 6.2). Hence, the values reported in Table 6.2 are computed maximum values on the $\alpha = 0$ plane. For Model A, the maximum $\frac{W}{W_i}$ occurs near $s = 13.89$. For models in Groups B and C, it occurs at or immediately after the throat of the stenosis (near $s = 15.24$). The results also show that in general, there is only a slight decrease in the maximum $\frac{W}{W_i}$ with increasing Reynolds number, although this is not significant.

A qualitative comparison may be made with the experimental study by Talbort and Gong (1983). In their investigation of flow through curved pipes, it was reported that there is a shift of maximum axial velocity along the pipe from the inner wall towards the outer wall at locations downstream of the bend. This agrees qualitatively with the results in the present study (as shall be seen later when velocity profiles are examined in detail). However, quantitative comparisons are not possible in this case because the flow conditions in their experiments are significantly different from those used here.

Table 6.2: Summary of Maximum Relative Axial Velocities for Models A, B1 to B4 and C1 to C6

Reynolds number	100	200	400	500	700	800	1000	1100
Inflow Velocity, W_0 (cm/s)	11.69	23.38	46.75	54.44	81.82	93.51	116.88	128.57
Steady flow rate (cc/s)	0.8710	1.7420	3.4832	4.3541	6.0961	6.9671	8.7083	9.5792
Steady flow rate (lt/min)	0.0523	0.1045	0.2090	0.2612	0.3658	0.4180	0.5225	0.5748
MAXIMUM RELATIVE AXIAL VELOCITY ($\frac{W}{W_i}$)								
Unstenosed								
Model A	1.2455	1.2199	1.1659	1.1480	1.1226	1.1135	1.0990	1.0933
Stenosis on inner wall								
40.49% (Model B1)	1.2455	1.2195	1.1747	1.1620	1.1375	1.1266	1.1066	1.0985
53.18% (Model B2)	1.5056	1.4802	1.4212	1.4122	1.4029	1.3913	1.3773	1.3625
65.75% (Model B3)	2.0066	1.9512	1.8801	1.8705	1.8517	1.8432	1.8267	1.8118
77.65% (Model B4)	3.0062	2.8922	2.8080	2.7701	2.7034	2.6847	2.5970	2.5421
43.89% (Model B5)	1.3026	1.2701	1.2233	1.2092	1.1799	1.1697	1.1564	1.1566
47.70% (Model B6)	1.3674	1.3545	1.2868	1.2702	1.2575	1.2560	1.2540	1.2519
52.24% (Model B7)	1.4712	1.4323	1.3976	1.4110	1.4294	1.4207	1.4063	1.3881
57.67% (Model B8)	1.5446	1.5142	1.5500	1.5605	1.5517	1.5325	1.5091	1.5032
62.84% (Model B9)	1.6675	1.7067	1.7420	1.7197	1.6975	1.6741	1.6481	1.6430
68.67% (Model B10)	1.8082	1.8748	1.9376	1.9157	1.8592	1.8373	1.8186	1.8081
Stenoses on both walls								
43.89% (Model C1)	1.2453	1.2125	1.1657	1.1514	1.1224	1.1123	1.0987	1.0992
47.70% (Model C2)	1.3084	1.2951	1.2277	1.2111	1.1985	1.1970	1.1954	1.1930
52.24% (Model C3)	1.4633	1.4242	1.3896	1.4031	1.4214	1.4127	1.3984	1.3803
57.67% (Model C4)	1.6674	1.6372	1.6728	1.6834	1.6745	1.6554	1.6318	1.6261
62.84% (Model C5)	1.9377	1.9770	2.0123	1.9901	1.9629	1.9445	1.9185	1.9133
68.67% (Model C6)	2.3155	2.3822	2.4449	2.4231	2.3666	2.3446	2.3258	2.3153

Axial Velocity Profiles

Experiments like those performed by Sabbah *et al* (1984) using flow visualisation techniques and by Back *et al* (1992) using artery casts may provide some information on the flow behaviour of blood in curved arteries. However, the numerical solutions obtained from the present study using CFD codes can give a more complete picture of the flow field in the entire flow domain. Furthermore, there is total flexibility in the display of these information. To facilitate a closer examination of the flow velocities of the models, axial velocity profiles were computed at several locations in the flow field on the $\alpha = 0$ plane. The six locations chosen for the present analysis are shown in Figure 6.11. Also, it should be noted that in our models, the curvature lies between $s = 10.00$ and 20.47, and the stenosis, if present, stretches from approximately $s = 13.49$ to about $s = 16.98$.

The velocity profiles were computed for a selection of cases at $Re = 400$ (i.e. at a physiologic flow rate of 0.209 lt/min) to illustrate the general trend of the flow behaviour. The profiles for Models A, B3 and C1 computed at locations $s =$ 5.00, 13.39, 15.24, 16.98, 18.73 and 33.81, are shown in Figures 6.12 to 6.14. In addition, for comparison between cases, Figure 6.15 shows the axial velocity profiles for Models A, B8 and C4, at two locations in the stenotic region. In all the figures mentioned, the outer wall is at +1.54 mm from the centreline and the inner wall is at -1.54 mm distance from the centreline.

In Figure 6.12a (Model A), we observe a shift in the maximum axial velocity towards the outer wall as the flow enters the curvature. The skewness and asymmetry in the profile is maintained after the bend (e.g. at $s = 18.73$) but the profile gradually returns to the normal Poiseuille flow profile further downstream (Figure 6.12b). This agrees qualitatively with results from studies by Perktold *et al* (1991) and Talbort and Gong (1983).

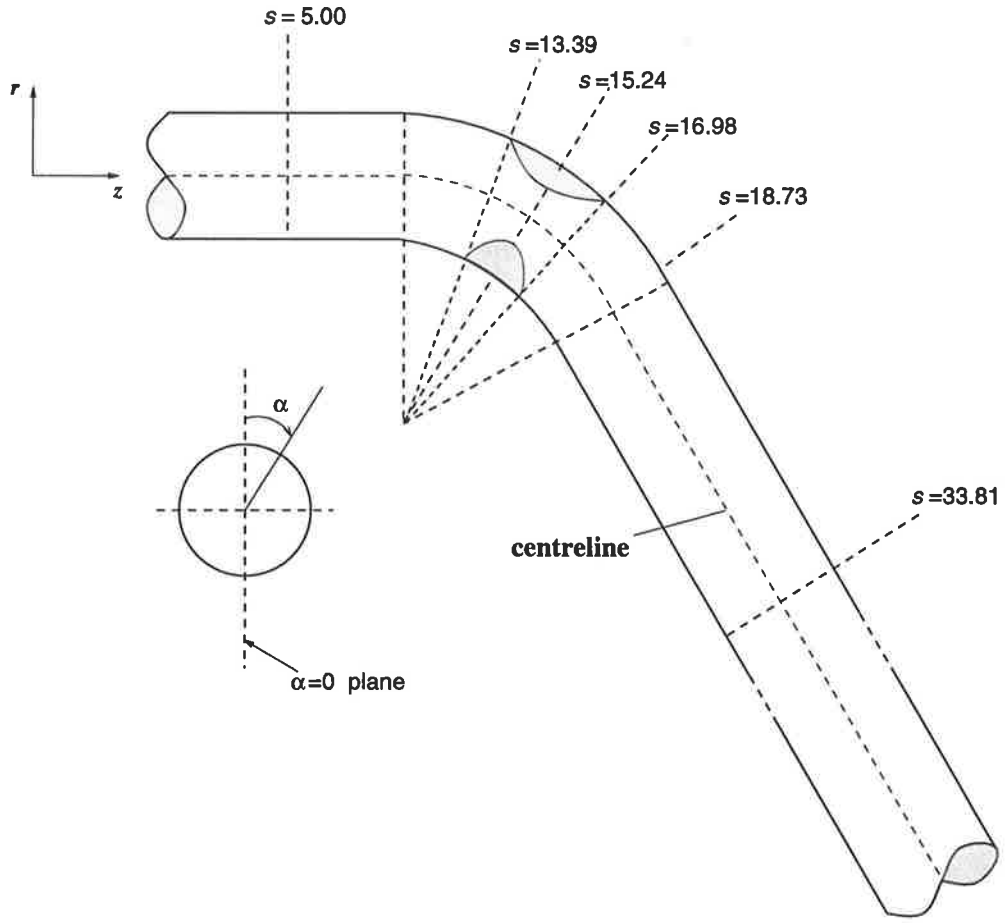

Figure 6.11: Cross sections at which the axial velocity profiles are computed in graph. Axial distances are dimensionless and measured from the inflow boundary.

Figure 6.13 shows the axial velocity profiles for Model B3, which is a curved artery with a protrusion from the inner wall at 65.76% stenosis. In Figure 6.13a, we observe a similar trend of a shift of maximum axial velocity towards the outer wall as the blood flows through the curved portion. In addition, because of the stenosis on the inner wall, there is a significant increase in the axial velocity of up to about $1.9W_i$ near the throat of the stenosis (at $s = 15.24$). Furthermore, Figure 6.13b indicates that there is a clear region of reverse flow on the inner wall at the post-stenotic region.

Figure 6.14 shows the axial velocity profiles for Model C1, which is a curved artery with protrusions from both the inner and outer walls at 43.89% stenosis. With a lower percent stenosis, the maximum axial velocity at the throat is not significantly increased although the shift towards the outer wall is still evident (Figure 6.14a). No reverse flow is observed for this case in the downstream portion of the artery. This could be due to the fact that the percent stenosis in this case is quite mild (43.89%).

A comparison of the velocity profiles between cases in the different groups of models can be made by examining Figure 6.15. It should be noted that Model B8 and C4 have different geometries but the same degree of stenosis (at 57.67%). Profile for Model A is given in the figure as a reference.

From Figure 6.15a, we observe that at the throat of the stenosis, Model C4 has a slightly higher maximum axial velocity ($1.7W_i$) compared to Model B8 ($1.55W_i$)[1] even though both have the same percent stenosis of 57.76%. Downstream of the stenosis, reverse flows are present for both B8 and C4, although the magnitude of backflow is higher in C4. Also, in both cases, backflow only occurs on the inner wall (Figure 6.15b). This trend is also present in all the other corresponding cases in Groups B and C.

[1]This can also be observed from Table 6.2 on page 116.

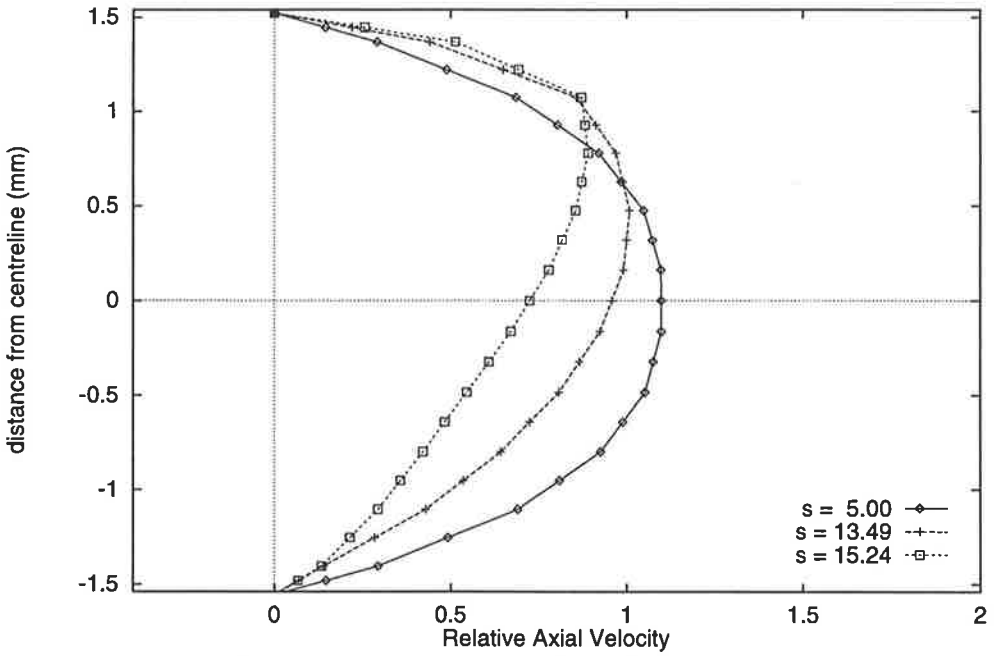

(a) Velocity profiles at $s = 5.00$, 13.49 and 15.24

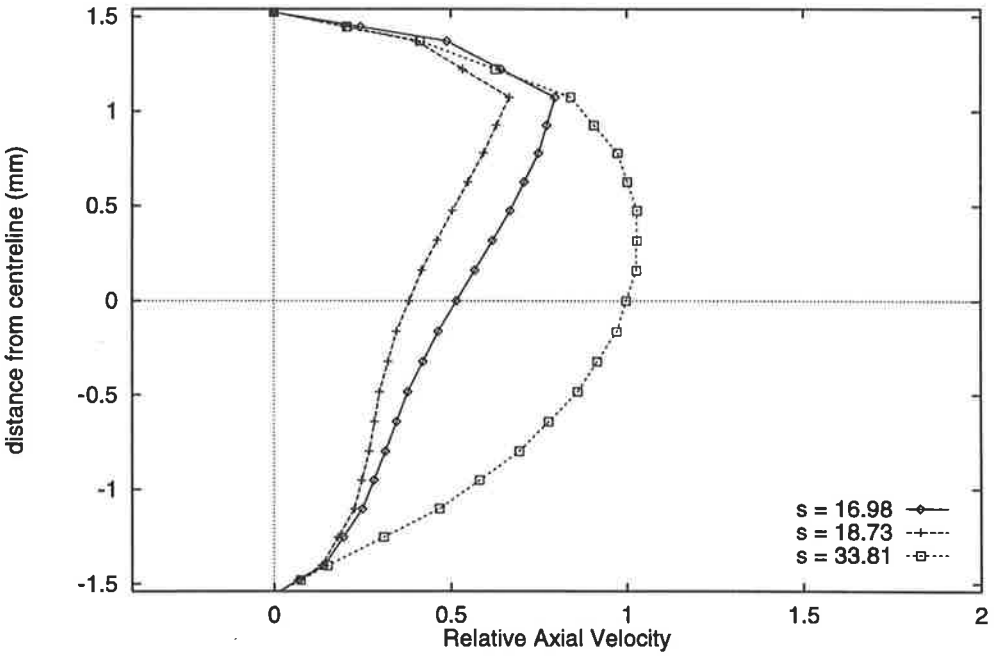

(b) Velocity profiles at $s = 16.98$, 18.73 and 33.81

Figure 6.12: Axial velocity profiles at $\alpha = 0$ for Model A (curved artery with no stenosis) at various locations (see Figure 6.11) along the artery at $Re = 400$

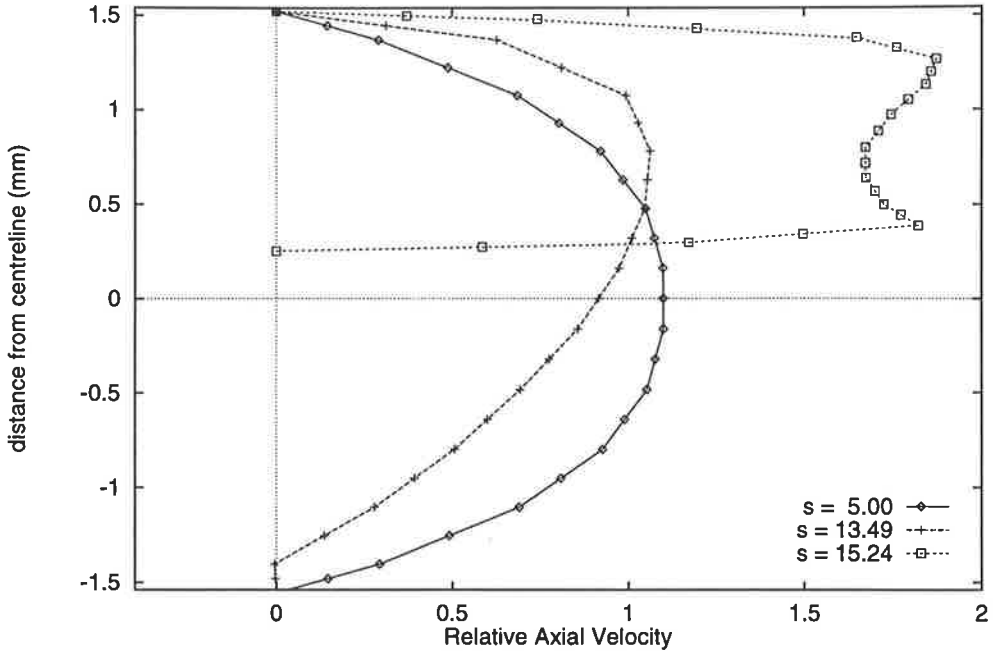

(a) Velocity profiles at $s = 5.00$, 13.49 and 15.24

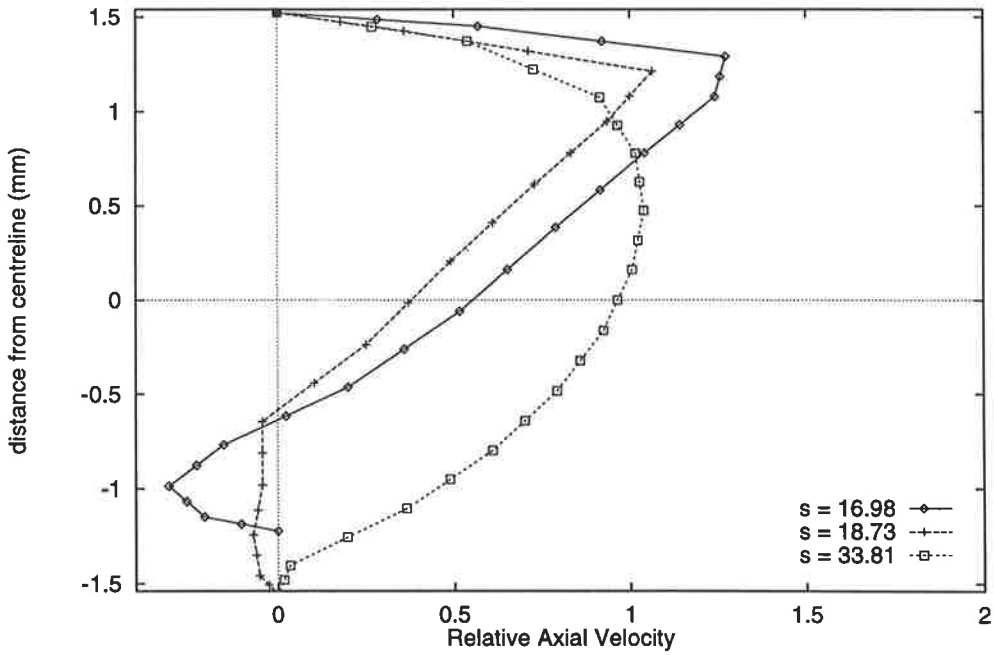

(b) Velocity profiles at $s = 16.98$, 18.73 and 33.81

Figure 6.13: Axial velocity profiles at $\alpha = 0$ for Model B3 (curved artery with one protrusion of 65.76% stenosis) at various locations (see Figure 6.11) along the artery at $Re = 400$

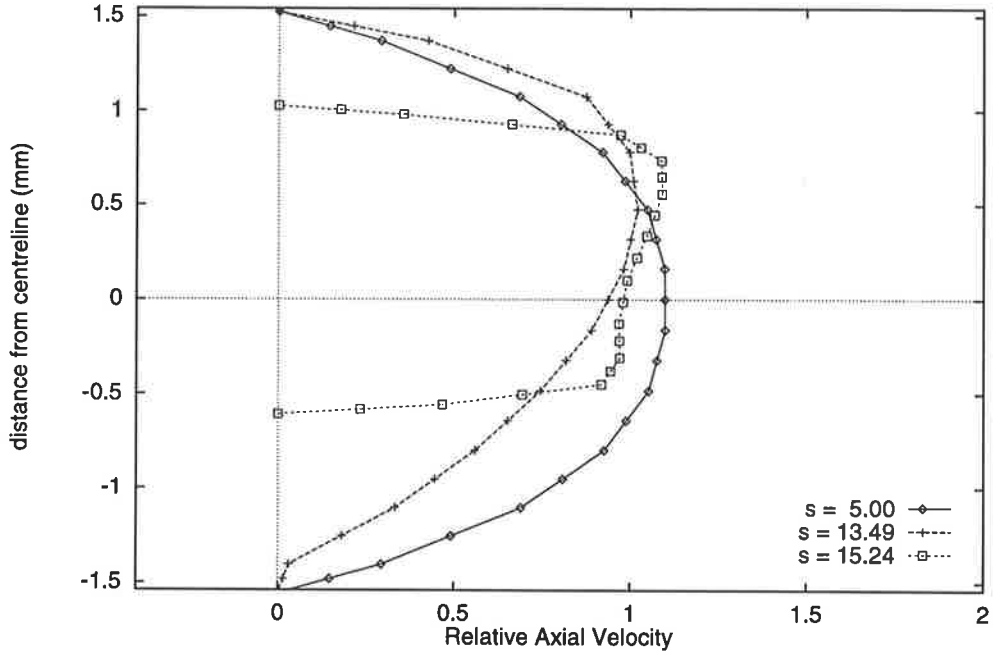

(a) Velocity profiles at $s = 5.00$, 13.49 and 15.24

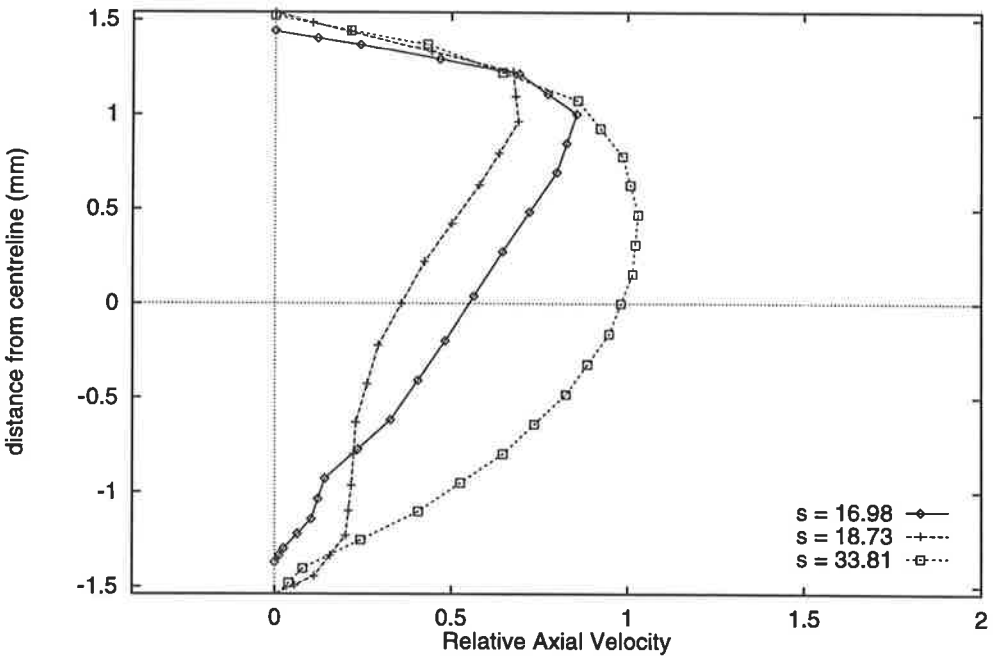

(b) Velocity profiles at $s = 16.98$, 18.73 and 33.81

Figure 6.14: Axial velocity profiles at $\alpha = 0$ for Model C1 (curved artery with protrusions from both walls, 43.89% stenosis) at various locations (see Figure 6.11) along the artery at $Re = 400$

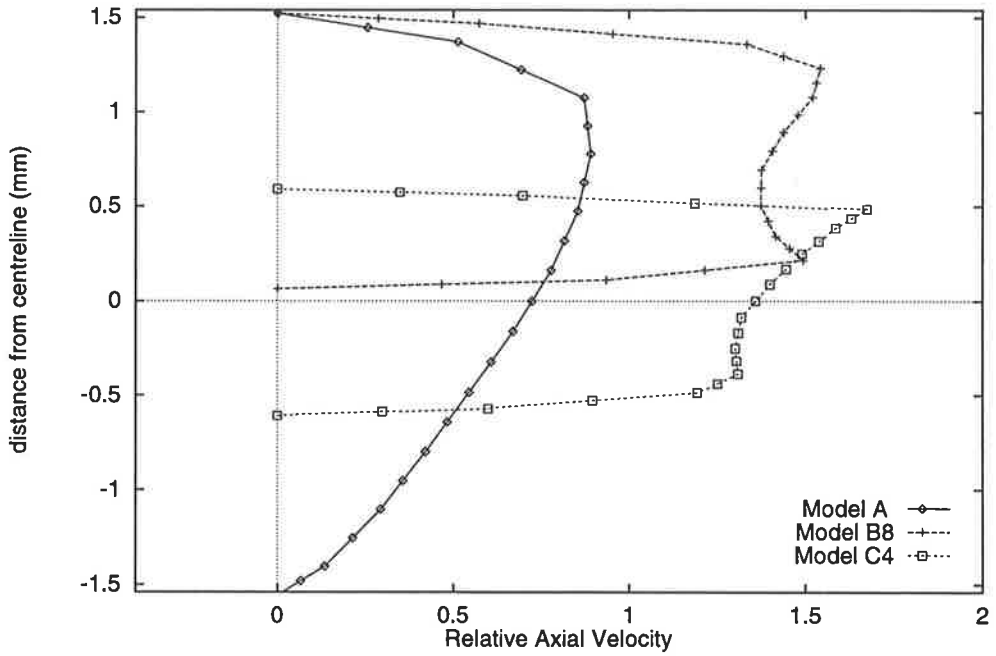

(a) Velocity profiles at $s = 15.24$

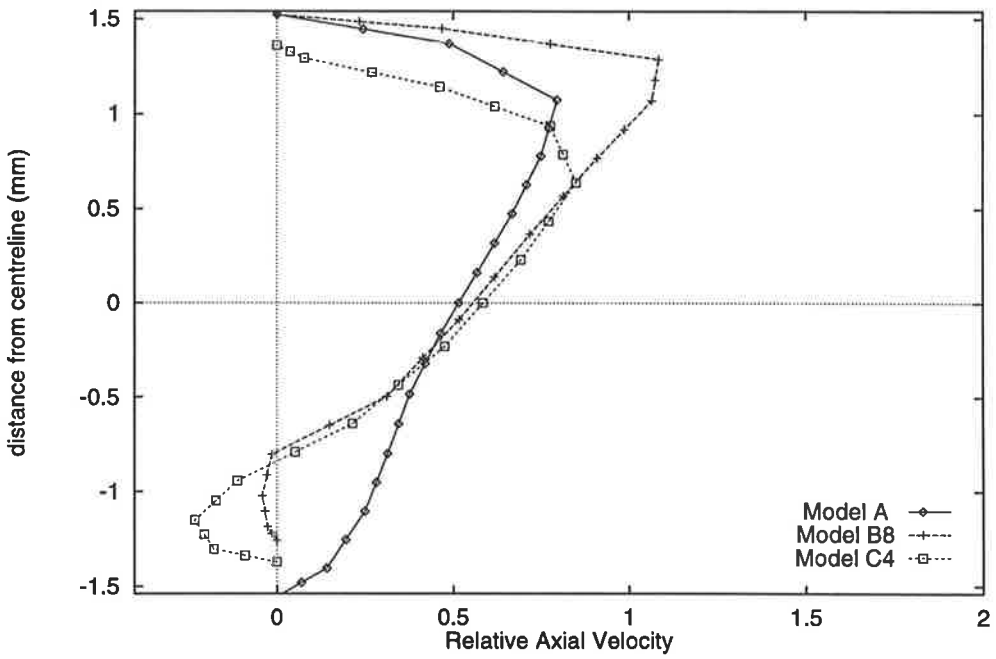

(b) Velocity profiles at $s = 16.98$

Figure 6.15: Comparison of axial velocity profiles at $\alpha = 0$ for Models A, B8 and C4 at two selected locations at $Re = 400$. B8 and C4 are models with 56.67% stenosis.

Secondary Flow Velocity

In curved passages, a velocity component occurs in the plane perpendicular to the flow axis. This movement is known as secondary flow. In the core of a curved tube, the secondary motion is directed towards the outer wall of the bend and circumferentially back near the side wall. A detailed description of this phenomenon has been given by several authors, such as Pedley (1980) and Berger *et al* (1983).

The influence of the secondary motion on the primary flow and, consequently, on the flow patterns of blood in arteries could play an important role in the initiation of endothelial damage or the genesis of other arterial disorders (Nerem 1992). In the straight tube model described in Chapter 5, such secondary flow motion was either not present or very insignificant in comparison with the axial velocity. However, the curved artery models described in this chapter reveal that secondary flow motion significantly contributes to the overall flow patterns. As it is not possible to report all findings, a representative selection of cases (namely, Models A, B1 and C4) will be discussed in some detail here and general conclusions, where appropriate, will be made.

A summary of the maximum secondary velocity expressed as a percentage of the maximum axial velocity for Models A, B1 and C4 at various locations in the bend of the models for Reynolds numbers 400 and 700 is given in Table 6.3. The case for Model B8, which has the same percent stenosis as C4, (i.e. 57.76%) at Reynolds number 400 is included in the table for comparison with Model C4.

For the sake of convenience in the discussion to follow, we shall define σ as

$$\sigma = \frac{\text{Maximum Secondary Velocity}}{\text{Maximum Axial Velocity}} \times 100\%$$

Table 6.3: Maximum Secondary Velocity (as a percentage of Maximum Axial Velocity and computed at various locations on the curved segment) for Models A, B1 and C4 at $Re = 400$ and 700 and for Model B8 at $Re = 400$

$$\sigma = \frac{\text{Maximum Secondary Velocity}}{\text{Maximum Axial Velocity}} \times 100\%$$

% stenosis =	Model A 0%		Model B1 40.49%		Model C4 57.76%		Model B8 57.76%
s Re=	700	400	700	400	700	400	400
12.09	2.9	2.9	2.9	2.8	2.9	2.8	2.8
13.84	2.7	2.8	2.8	3.0	2.8	2.9	3.1
14.54	2.6	2.7	3.0	3.2	3.3	3.5	3.8
15.24	2.5	2.7	3.3	3.5	4.2	4.4	5.1
15.93	2.5	2.7	3.1	3.3	3.7	3.9	4.2
16.63	2.5	2.7	2.8	3.0	3.0	3.4	3.6
17.33	2.5	2.7	2.6	2.9	2.7	3.1	3.3
18.73	2.4	2.7	2.4	2.8	2.5	2.9	3.1

It is clear from the table that there is only a very slight difference in the σ values (generally less than 0.4%) at different Reynolds numbers for each of the Models A, B1 and C4. This agrees qualitatively with the results of Perktold *et al* (1991) in their curved tube model of the Left Main Coronary Artery with slight tapering.

At different locations along the curved segment, σ remains fairly constant in Model A, where there is no stenosis. However, in both Models B1 and C4, the value of σ increases gradually as the flow approaches the throat of the stenosis and decreases gradually downstream of the stenosis. This shows that stenoses on the bends of arteries can alter the flow conditions to some extent.

At $Re = 400$, the σ values for Model B8 show a similar trend. Moreover, in comparison to Model C4 (which has the same degree of stenosis), the σ value in Model B8 increases more rapidly and attains a slightly higher maximum value ($\sigma = 5.1$ at $s = 15.24$). In fact, this general trend prevails in the other corresponding cases;

that is, the σ values in the stenotic region of Group B models are comparatively higher than those in the corresponding Group C models.

The main difference between B8 and C4 lies in the geometry of the models. Model B8 has a protrusion from the inner wall and C4 has protrusions from both inner and outer walls. The results reported seem to suggest that the presence of a stenosis on the outer wall helps in lowering the effects of increased secondary flow velocities brought about by the stenosis on the inner wall of the bend.

Although the models set up here are realistic, experiments in similar geometrical conditions are not available in the literature for quantitative comparisons. However, qualitative agreement between the data reported here and the experiments by Talbort and Gong (1983) as well as Perktold *et al* (1991) suggests a reasonable validity of the models.

Secondary flow fields can also be examined qualitatively in a more graphic manner. The post processor (PHOTON) in PHOENICS allows plots of the velocity field to be created in views from different angles at different locations. Figure 6.16 shows the locations chosen for the plots to be presented here. The directions in which the plots are viewed are perpendicular to the plane of interest and are indicated by the arrows in Figure 6.16

Figures 6.17 to 6.22 show plots of the secondary velocity fields for Models A, B1 and C4. As there is no significant difference in the secondary flow field at different Reynolds numbers (in the range considered in this study), only flow fields at $Re = 400$ are examined. The plots have been generated at locations $s = 12.09$, 13.84, 15.24 and 17.33 to provide a comprehensive representation in the curved segment although in principle, any location on the modelled artery may be chosen. In all the figures of secondary flow fields to be presented, the cross sections are drawn with the outer wall at the top and the inner wall at the bottom of each figure.

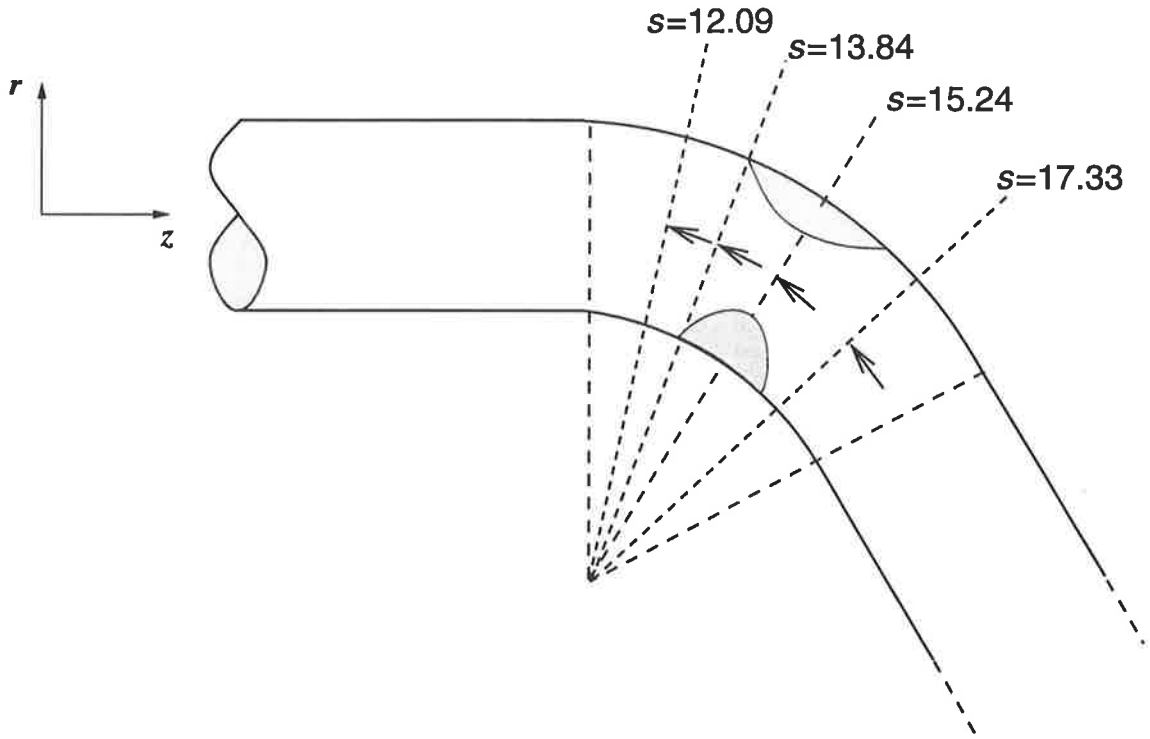

Figure 6.16: Locations on the curve segment where secondary velocity fields are plotted. The arrows indicate the directions in which these plots are viewed.

From Figures 6.17 and 6.18, the gradual development of secondary flow motion in Model A may be observed. As the flow enters the curved segment (at $s = 12.09$), secondary motion becomes evident, and gradually becomes more intense. This is maintained in the latter part of the curvature (Figure 6.18) with little significant change in the intensity of the flow motion or the magnitude of the flow velocities.

The secondary flow fields for Model B1 are shown in Figures 6.19 and 6.20. As in the case for Model A, secondary flow begins to develop as the flow enters the curved segment ($s = 12.09$) and increases in intensity. In Figure 6.20a, at the throat of the stenosis ($s = 15.24$), we observe the development of a fairly significant flow velocity in a direction perpendicular to the axis of the primary flow along the stenosed wall. This may have a significant effect on the stenotic plaque formed. This suggests that lesions on the inner walls of curved segments of arteries are under an added influence from the secondary flow motion.

Figures 6.21 and 6.22 depict the secondary flow fields for Model C4. Secondary flow motion begins to develop as the flow enters the curvature ($s = 12.09$) and becomes quite complex as it approaches the stenotic region. The expected secondary flow motion (from inner to outer wall in the core of the vessel and back circumferentially along the sides) is accompanied by a flow motion near the outer wall in the opposite direction (i.e. directed towards the inner wall in the core) as shown in Figure 6.21b. This continues to develop into a complex flow pattern as the flow approaches the throat of the stenosis (Figure 6.22a). As the flow leaves the stenotic region, the general flow direction is towards the inner wall of the bend.

Although quantitative analysis of the flow field from these graphic plots is not possible, these figures give a very clear qualitative view of the flow patterns associated with secondary flow motion. A quantitative analysis of the shearing stresses on the walls is more useful and will be carried out below.

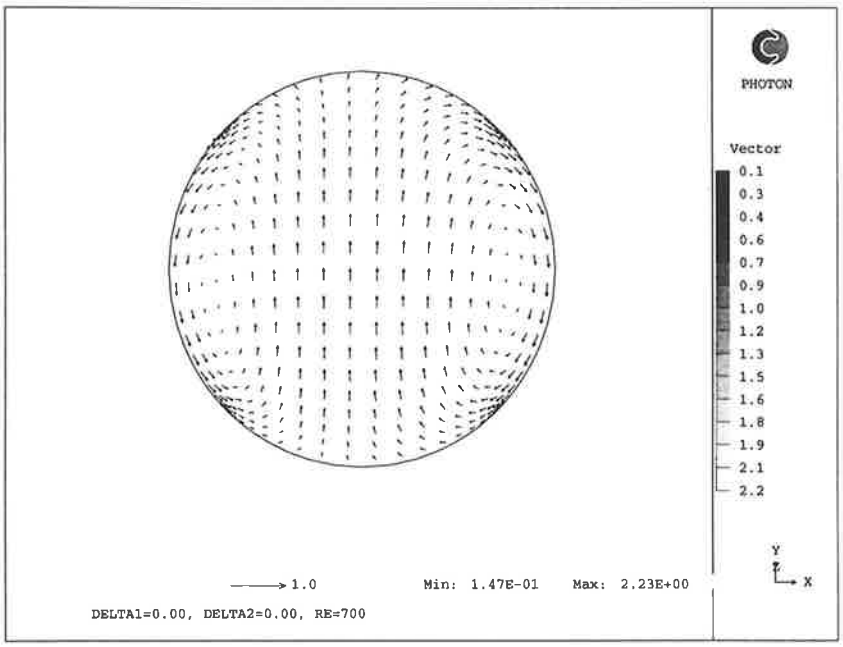

(a) $s = 12.09$

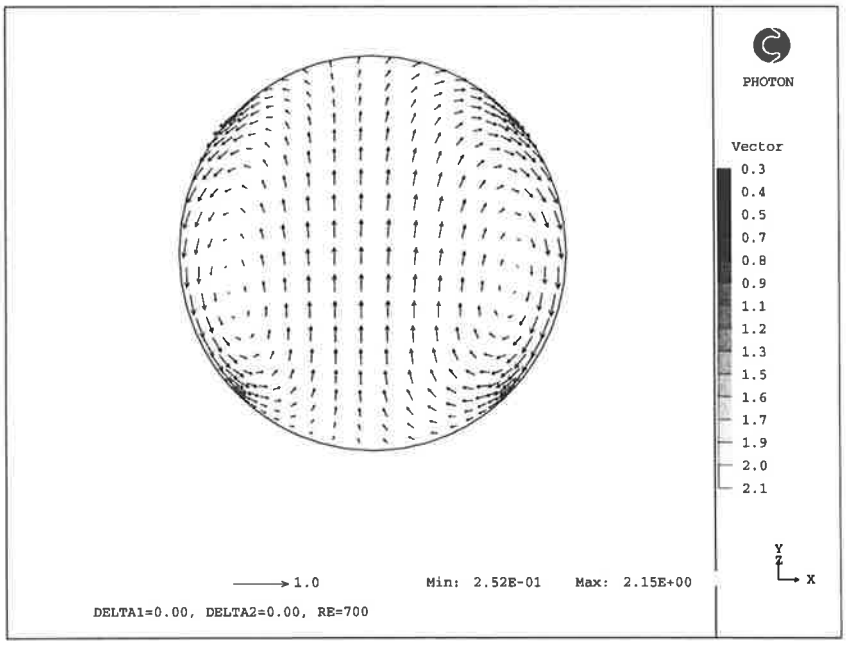

(b) $s = 13.84$

Figure 6.17: Secondary velocity vector field for Model A (curved artery with no constriction) at s=12.09 and 13.84 and for $Re = 700$

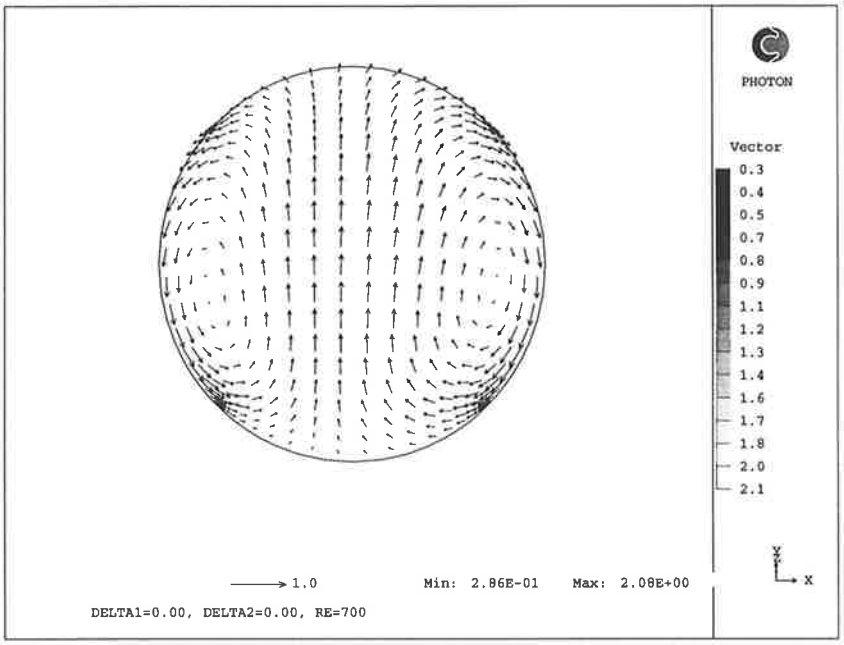

(a) $s = 15.24$

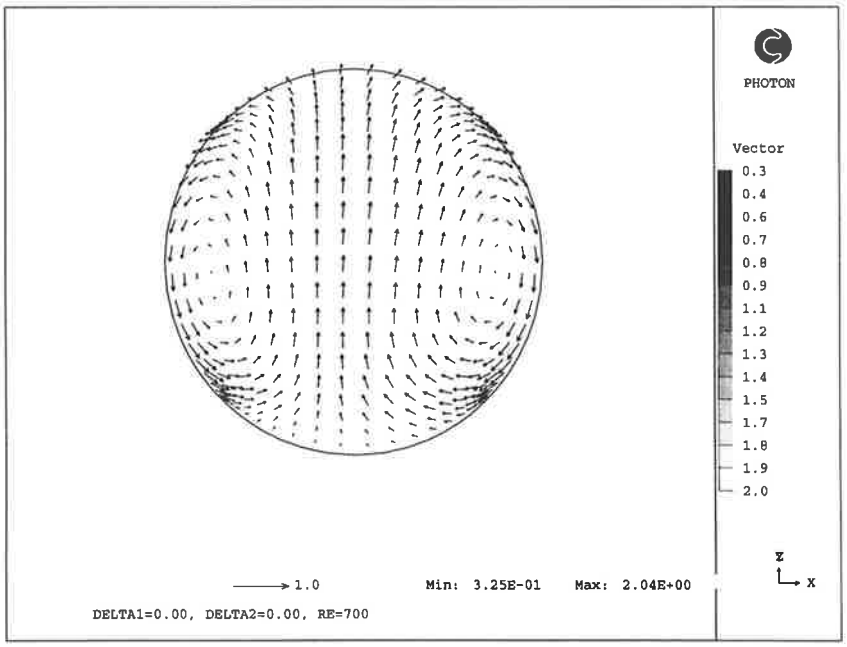

(b) $s = 17.33$

Figure 6.18: Secondary velocity vector field for Model A (curved artery with no constriction) at s=15.24 and 17.33 and for $Re = 700$

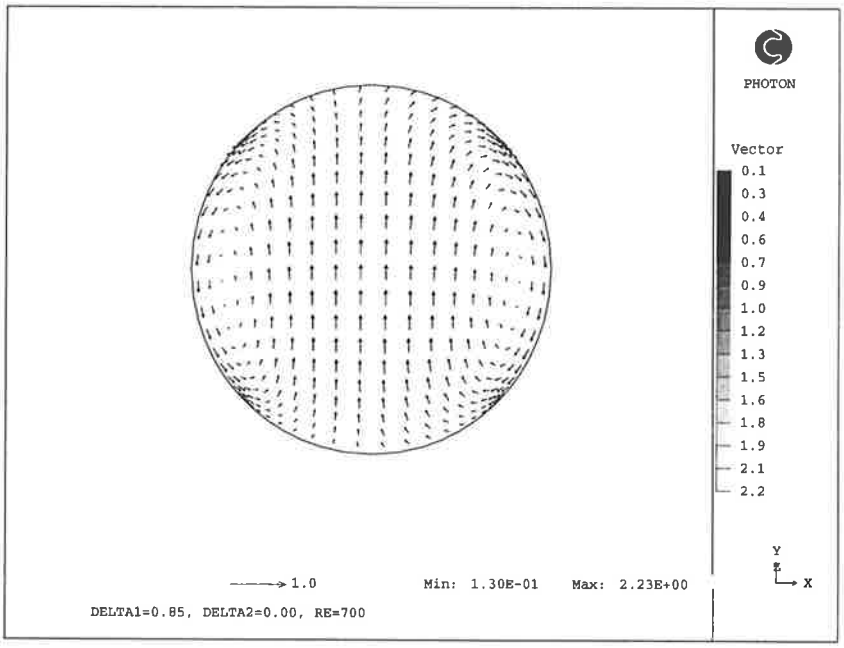

(a) $s = 12.09$

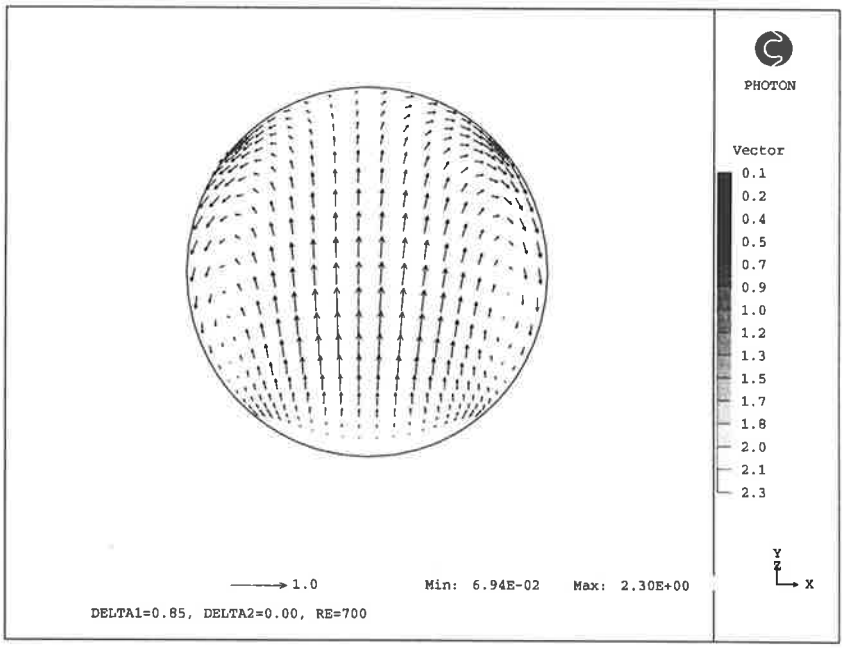

(b) $s = 13.84$

Figure 6.19: Secondary velocity vector field for Model B1 (curved artery with stenosis on inner wall at 40.49% stenosis) at s=12.09 and 13.84 and for $Re = 700$

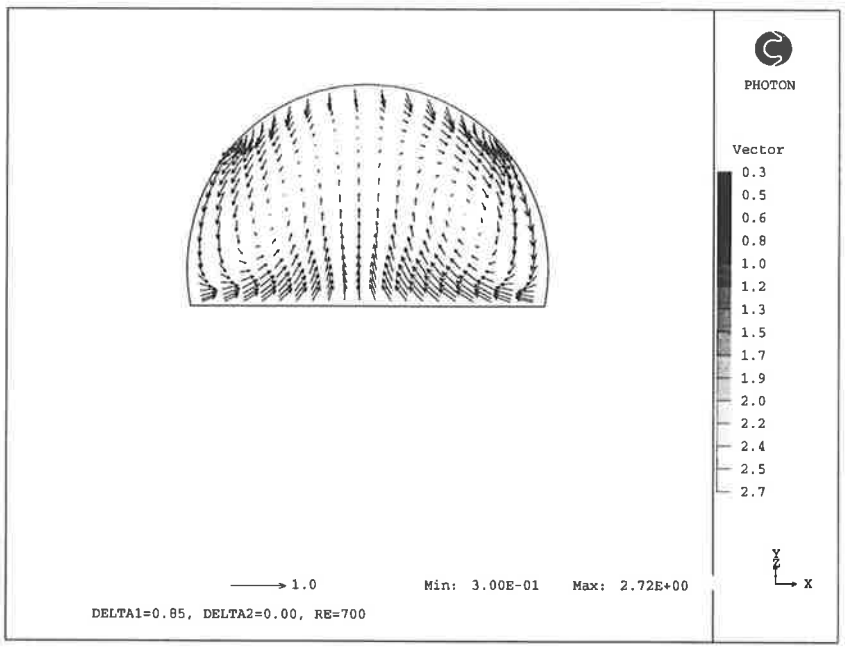

(a) $s = 15.24$

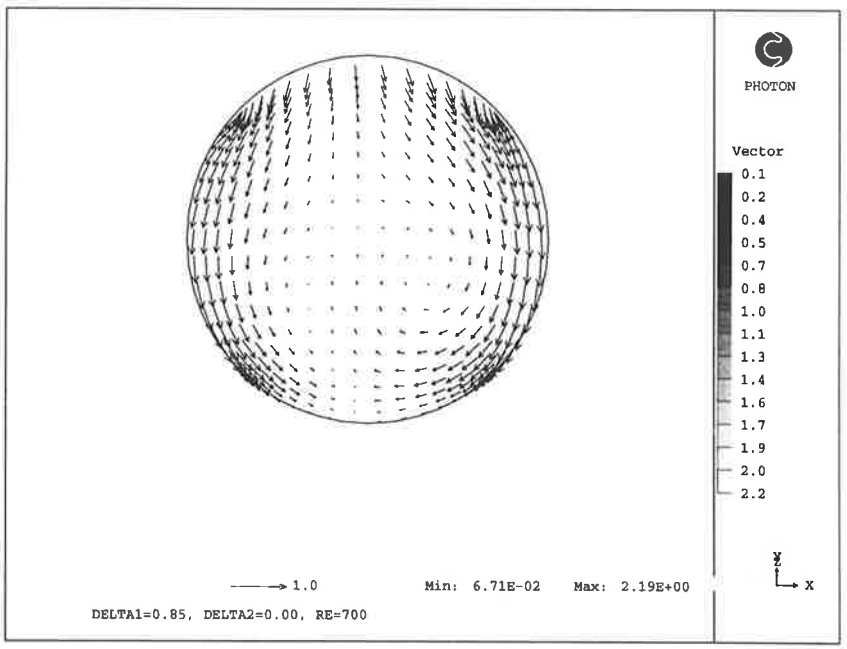

(b) $s = 17.33$

Figure 6.20: Secondary velocity vector field for Model B1 (curved artery with stenosis on inner wall at 40.49% stenosis) at s=15.24 and 17.33 and for $Re = 700$

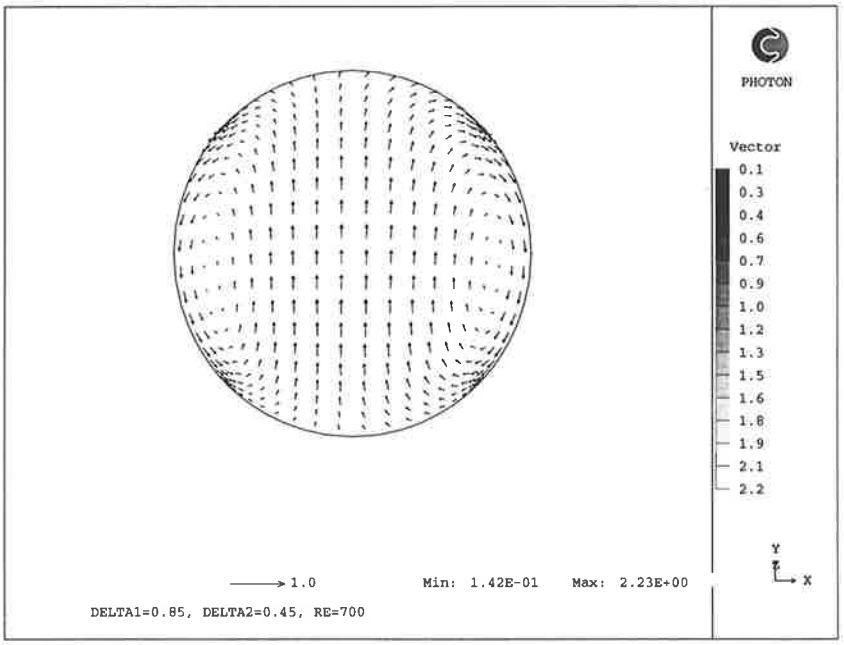

(a) $s = 12.09$

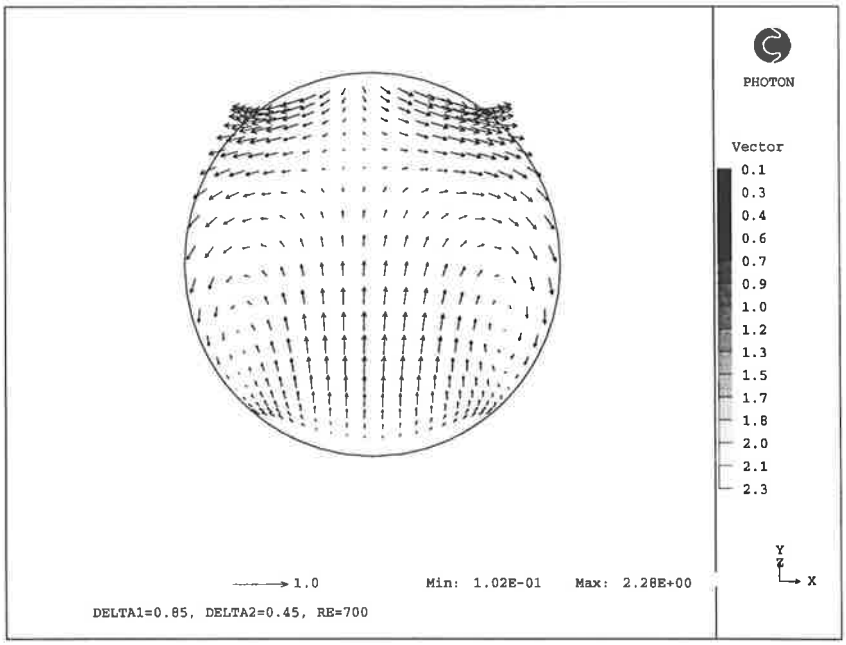

(b) $s = 13.84$

Figure 6.21: Secondary velocity vector field for Model C4 (curved artery with stenoses on inner and outer walls with 57.67% stenosis) at s=12.09 and 13.84 and for $Re = 700$

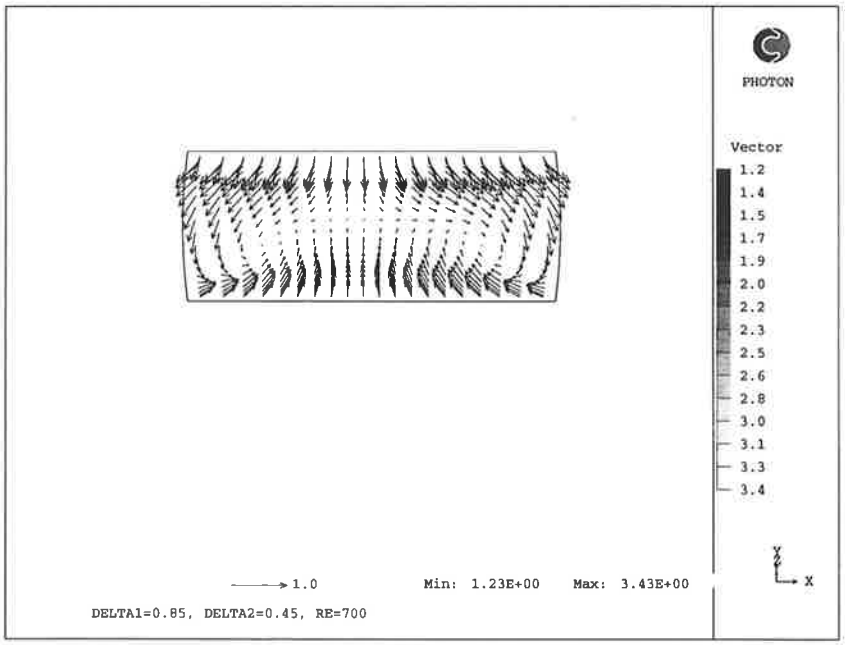

(a) $s = 15.24$

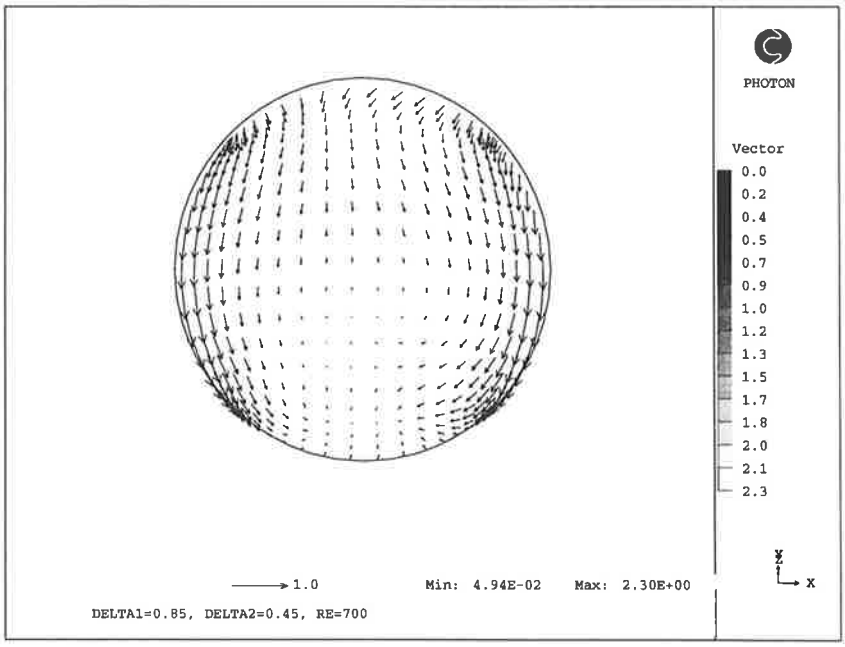

(b) $s = 17.33$

Figure 6.22: Secondary velocity vector field for Model C4 (curved artery with stenoses on inner and outer walls with 57.67% stenosis) at s=15.24 and 17.33 and for $Re = 700$

6.4.3 Wall Shear Stress

It has already been mentioned that for incompressible fluids with no slip condition at the rigid wall, the dimensional wall shear stress, τ_w, in the axial direction may be given by :

$$\tau_w = \mu \left. \frac{\partial \mathbf{w}}{\partial \mathbf{n}} \right|_{wall} \tag{6.6}$$

where $\frac{\partial \mathbf{w}}{\partial \mathbf{n}}$ is the partial derivative of the tangential velocity with respect to the unit normal vector at the wall in physical units and μ is the viscosity of the fluid. The manner in which the axial wall shear stress may be estimated from the velocity components has already been discussed in Section 5.4.3 and will not be repeated since the same procedure has been used here in the estimation of wall shear stress.

Axial Wall Shear Stress

Morgan and Young (1974) obtained an equation for the shearing stresses along the arterial wall using an integral method. Although the equation is for a straight tube with an axisymmetric obstruction, it would be interesting to compare our results with that obtained from the equation. Figures 6.23 and 6.24 show the graphs of the distribution of shearing stress on the walls along the axial position for Models B1 and C4 at $Re = 100$.

In Figure 6.23, the graphs for the wall shear stress on both sides of the walls are quite different in magnitude at the curvature and stenotic region. This is to be expected as in this case, only the inner wall has a protrusion. The shearing stresses on this side hence increases quite rapidly, reaching a maximum value of more than twice that on the outer unstenosed wall. However, on both the inner and outer walls, the maximum shear stress is achieved just before the throat of the stenosis, and this is consistent with the model proposed by Morgan and Young.

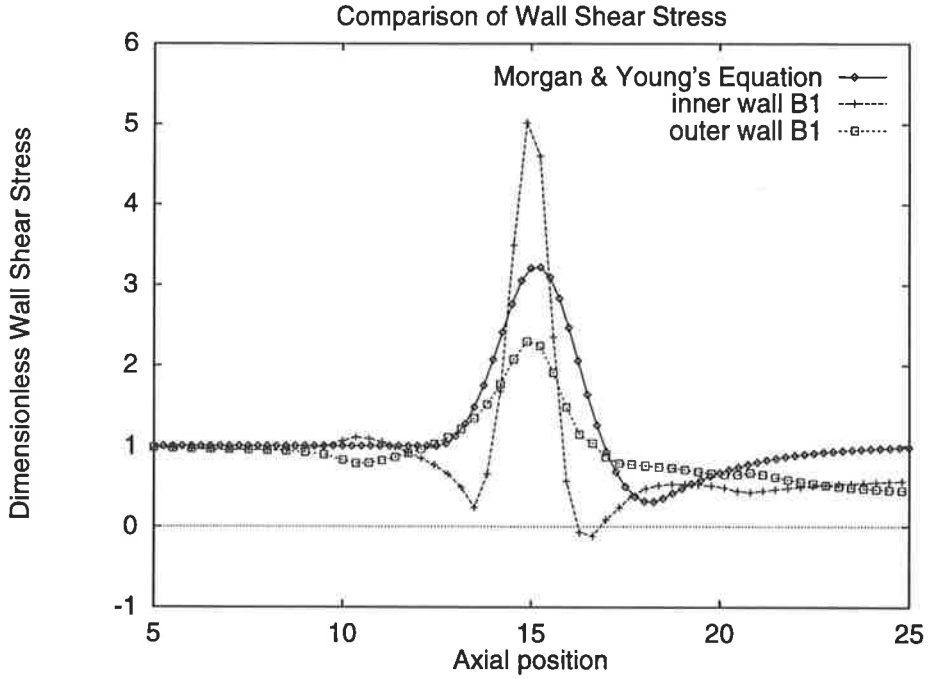

Figure 6.23: Comparison of axial wall shear stress between Model B1 and equation from Morgan and Young at $Re = 100$

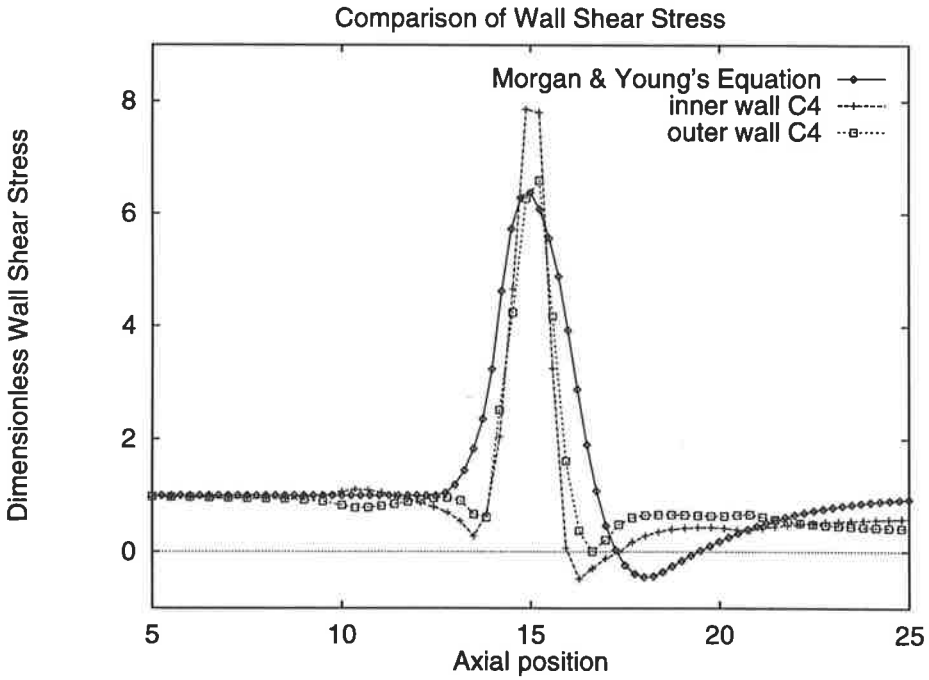

Figure 6.24: Comparison of axial wall shear stress between Model B1 and equation from Morgan and Young at $Re = 100$

In Figure 6.24, the shearing stresses on both walls are more or less similar in behaviour and magnitude. This is also to be expected as in this case, stenotic plaques are present in both walls. Also, the results are more consistent with the axisymmetric model of Morgan and Young although there are some differences in the pre-stenotic and post-stenotic regions. This is largely due to the effects of curvature of the present model at these locations.

The shearing stresses along the wall in the axial direction for Models B1 and C4 for Reynolds numbers 100, 400, 700 and 1000 are shown graphically in Figures 6.25 and 6.26. In each of these graphs, the shearing stresses along both the inner and outer walls (i.e. at $\alpha = \pi$ and 0 respectively) are plotted along the dimensionless axial distance from the inlet.

From the graphs, we observe that at low Reynolds numbers (e.g. $Re = 100$), the axial wall shear stresses on both walls for B1 and C4 are essentially positive. Backflow at both walls is hence not present at low Reynolds numbers. However, at moderate and high Reynolds numbers, the inner wall for Model B1 experiences a substantial magnitude of negative shear stress. Therefore, for a curved artery with a protrusion from the inner wall, we can expect backflow on the inner wall but not on the outer wall for moderate to high Reynolds numbers. The peak shear stresses along the inner wall are significantly higher than on the outer wall for the range of Reynolds number considered.

For Model C4, the graphs in Figure 6.26 show that for $Re = 400$, 700 and 1000, backflow is detected at both the inner and outer walls. This may be deduced from the negative shear stress on the walls. The flow separation region ranges from $s = 15.59$ to $s = 18.37$ on the inner wall, and from $s = 15.93$ to $s = 16.63$ on the outer wall. On the average, for $Re = 400$ to $Re = 1000$, the flow separation on the inner wall is about four times longer on the inner wall than on the outer wall for Model C4, in which the ratio of the stenotic heights, $\frac{\delta_2}{\delta_1}$ is around 1.89. However,

the peak shear stresses on both walls in this case are essentially equal.

A comparison of the ratios of peak shear stresses on the inner wall to the outer wall for Reynolds number ranging from 100 to 1200 is shown in Figure 6.27. As can be seen from the graph, the outer wall of a curved artery without any stenosis experiences a higher peak shear stress. This difference in shear stress could be an important factor in the genesis of atherosclerotic plaques.

It is common to find plaques growing first from the inner wall of the curvature and our Model B1 shows a significant rise in the relative shear stress on the inner wall at 40.5 % stenosis. A growth of plaque on the outer wall to about half the height of that in the inner wall, as in Model C4, would cause the shear stress on the outer wall to rise to a level almost equal to that on the inner wall. This is not so in a straight tube or axisymmetric case.

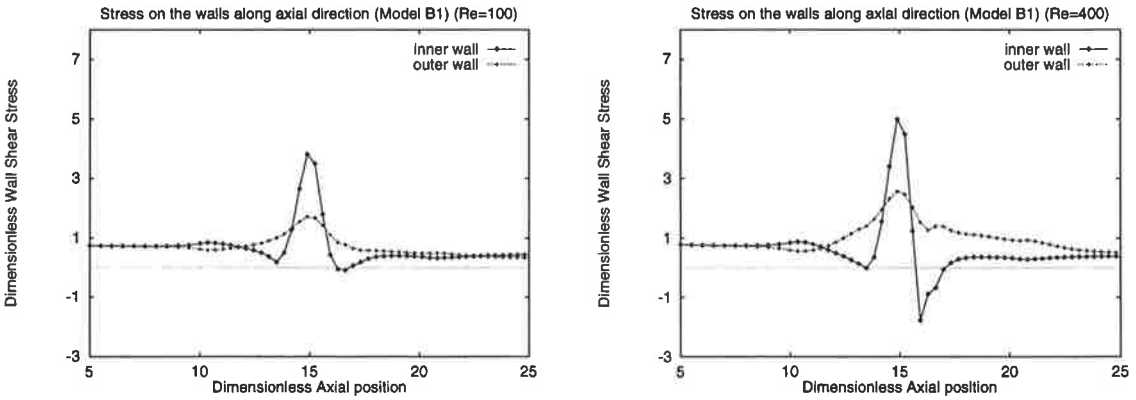

(a) $Re = 100$

(b) $Re = 400$

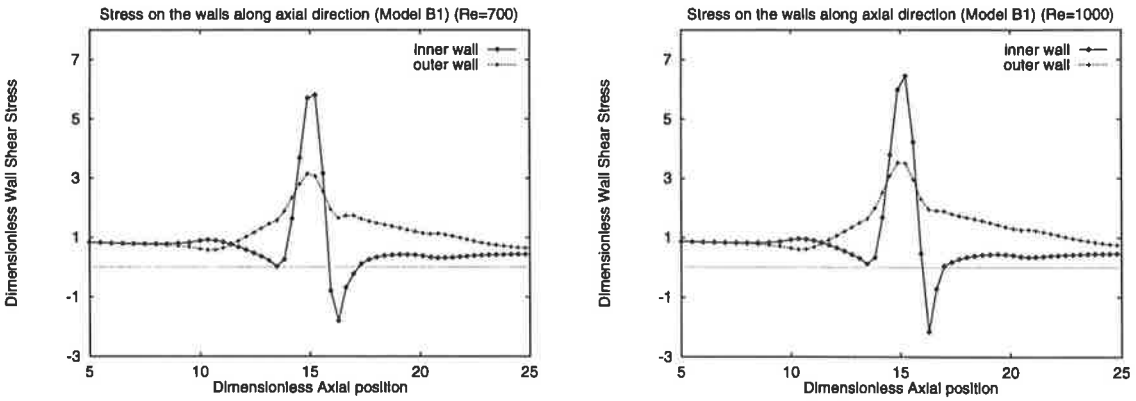

(a) $Re = 700$

(b) $Re = 1000$

Figure 6.25: Graphs of Dimensionless Wall Shear Stress along the axis of a curved artery with protrusion from one side of inner wall at 40.49% stenosis (Model B1) for various Reynolds numbers

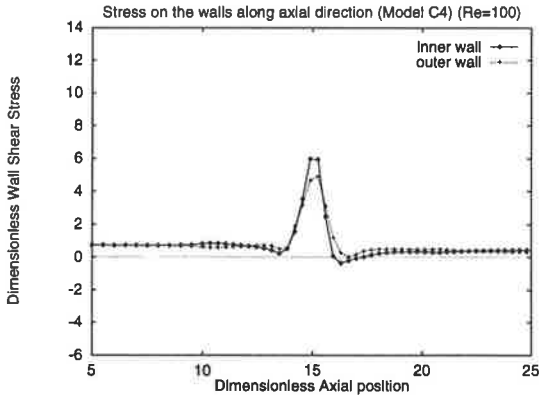

(a) $Re = 100$

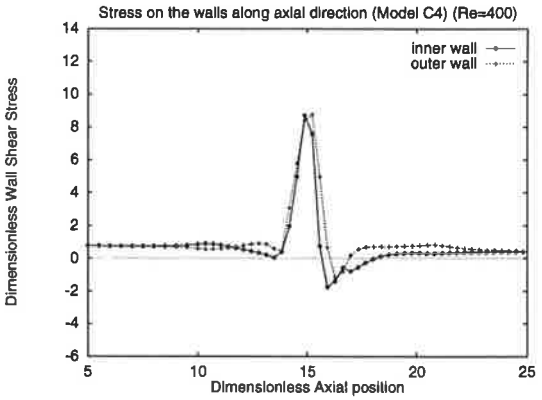

(b) $Re = 400$

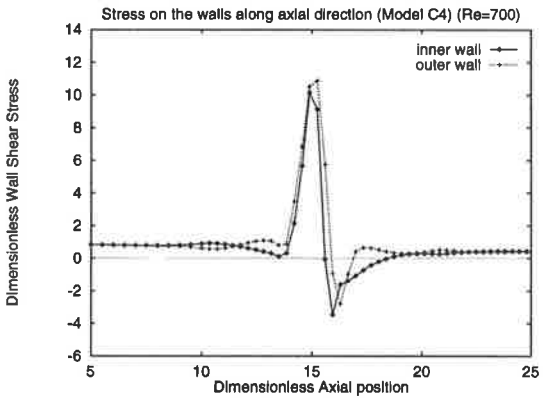

(a) $Re = 700$

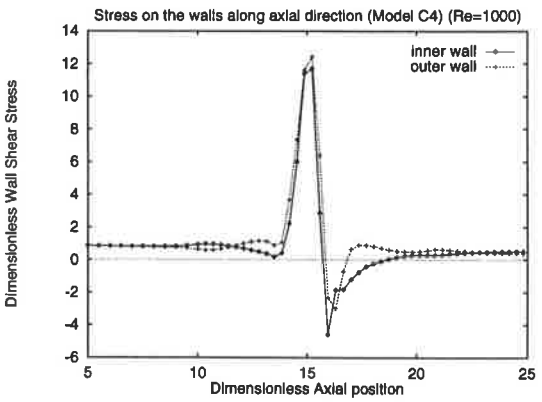

(b) $Re = 1000$

Figure 6.26: Graphs of Dimensionless Wall Shear Stress along the axis of a curved artery with protrusions from both inner and outer walls at 57.67% stenosis (Model C4) for various Reynolds numbers

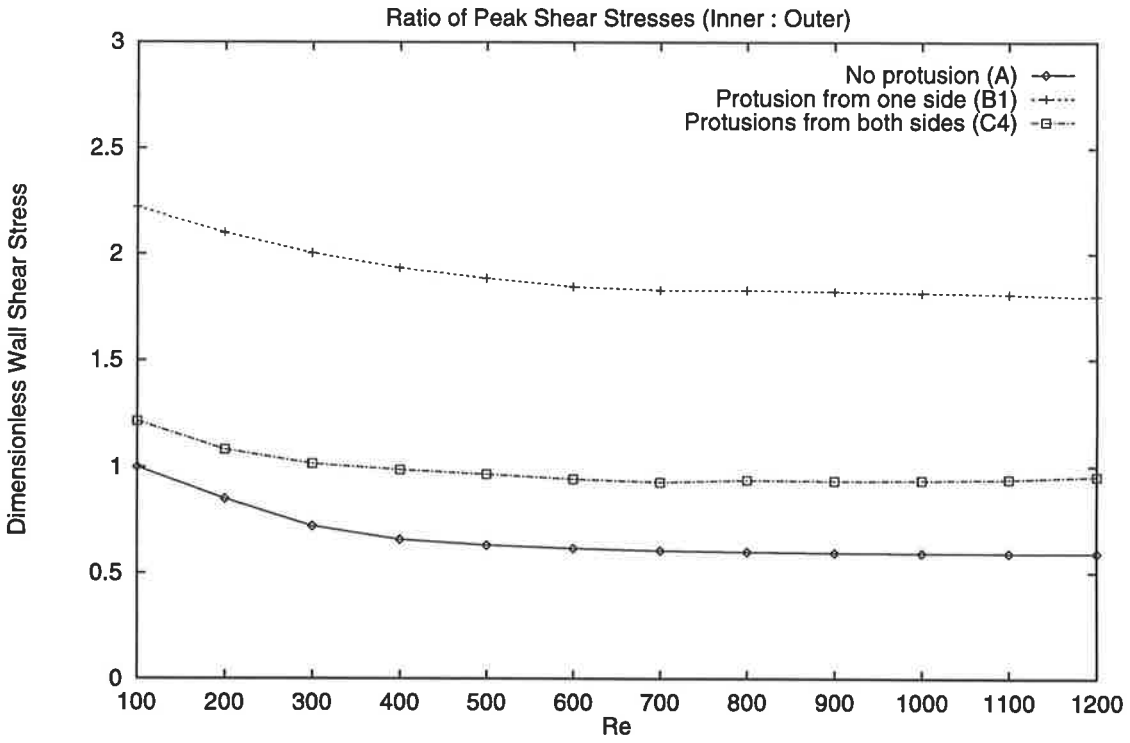

Figure 6.27: Graphs showing the ratio of peak wall shear stresses on inner to outer wall for Models A, B1 and C4 for a range of Reynolds numbers

Secondary Wall Shear Stress

It has already been shown in Section 6.4.2 that significant secondary flow motion has been detected in the models considered here. The shear stress along the walls in the circumferential direction due to secondary flow motion is defined in a similar way as the axial wall shear stress and may be calculated or estimated in a similar way as discussed before. However, it should be mentioned that for the calculation of secondary wall shear stress, instead of the axial velocity components, the velocity components used for quadratic curve fitting procedure are the components tangent to both the primary axis of flow and the wall. Like before, the two values closest to the wall and the no-slip condition form the three points necessary for the quadratic curve fitting.

The shearing stresses are also non-dimensionalised in the same manner as before. A typical set of graphs showing the secondary wall shear stress along the transverse position (i.e. along the walls and perpendicular to the z axis) at $Re = 700$ at various positions along the curved artery is presented in Figures 6.28 through 6.32. In these figures, the horizontal axes are the dimensionless distance from the centreline, measured along the wall (either the inner or outer) in a direction perpendicular to the z axis. Although only results from Models A, B1 and C4 are shown, the same pattern is observed in the other models.

Figure 6.28 shows that at the entrance of the curvature, i.e. at $s = 10.00$, the shear stresses on both the inner and outer walls due to secondary flow motion, though still insignificant, are beginning to be detected. There is virtually no difference at this point between Models A, B1 and C4, as would be expected. The secondary wall shear stresses on the inner wall and outer wall are of opposite signs in all the graphs, showing distinct secondary motion in the velocity field.

Figure 6.29 shows that at $s = 13.49$, i.e. at the portion of the bend before

the stenotic region, shearing stresses on the walls start to become more significant. However, for both Models B1 and C4, the presence of the stenosis on the inner wall of the bend results in a lower shear stress relative to that in Model A, which has no stenosis as can be seen in Figure 6.29(a). On the outer wall (Figure 6.29(b)), the presence of a stenosis in C4 elevates the secondary wall shear stress slightly, whereas there is no difference in Models A and B1 as would be expected.

At $s = 15.24$, the narrowest portion of the artery for Models B1 and C4, the shearing stresses on both the inner and outer walls for B1 and C4 become significantly higher than in Model A as can be seen in Figures 6.30 (a) and (b). The stenosis had begun to play an important role in creating significant secondary motion and causing the wall shear stress to rise up to five times that in an unstenosed bend.

From Figure 6.31, we observe even more significant rise in the secondary wall shear stress at $s = 16.98$, a position on the stenosed artery immediately after the stenosis. On the inner wall of Model B1, we observe a ten-fold increase in the secondary wall shear stress. This could be due to the asymmetry of the stenosis that is present in B1. On the other hand, Model C4 shows that the presence of a stenosis on the outer wall increases the secondary wall shear stress more significantly than on the inner wall despite the fact that the outer wall stenotic height is only about half that on the inner wall for Model C4.

Figures 6.32 (a) and (b) shows the situation at $s = 20.47$, at the exit of the curvature. We observe a drop in the secondary flow motion compared to at the bend. The secondary wall shear stresses on both walls begin to diminish.

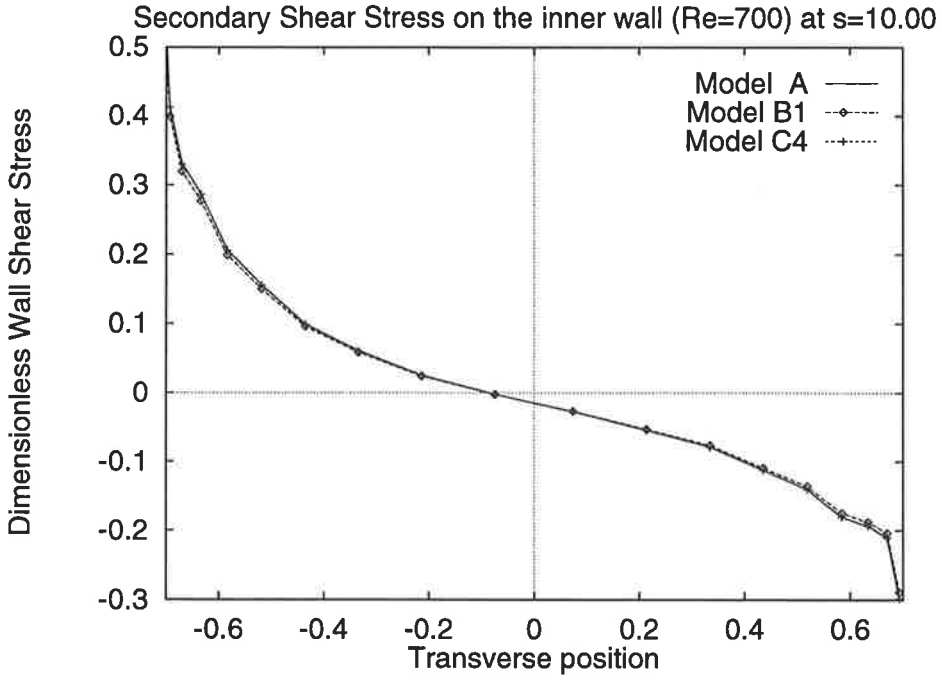

(a)

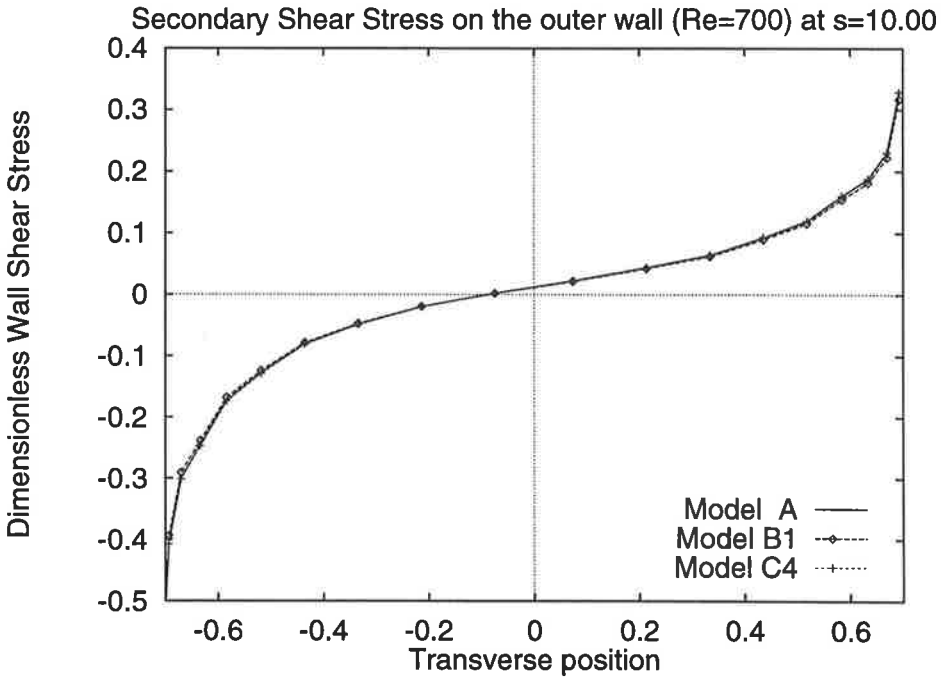

(b)

Figure 6.28: Graphs showing dimensionless wall shear stress at $Re = 700$ along the (a) inner wall and (b) outer wall, at $s = 10.00$

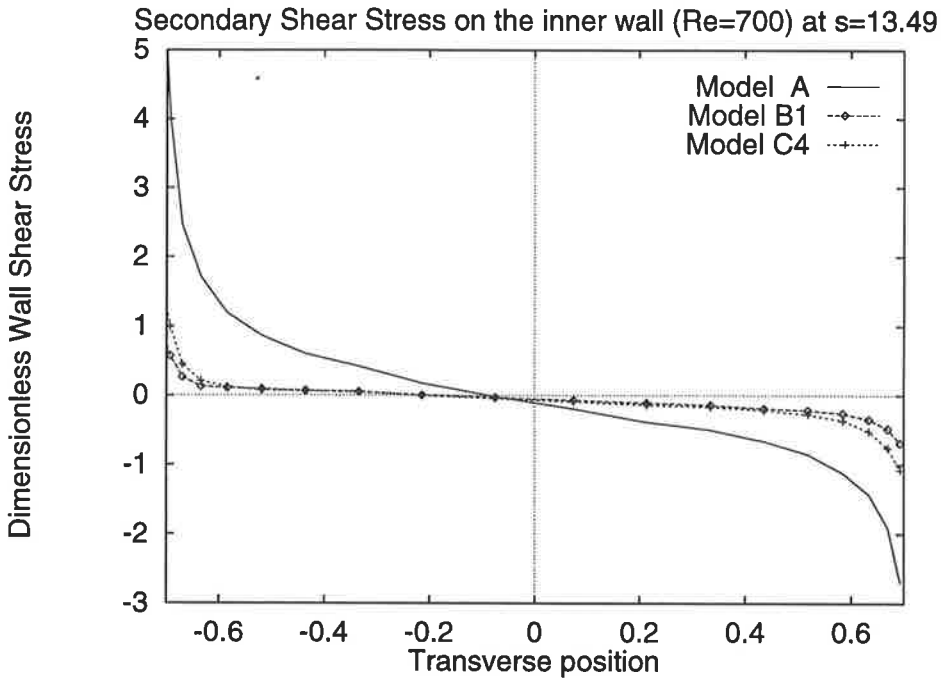

(a)

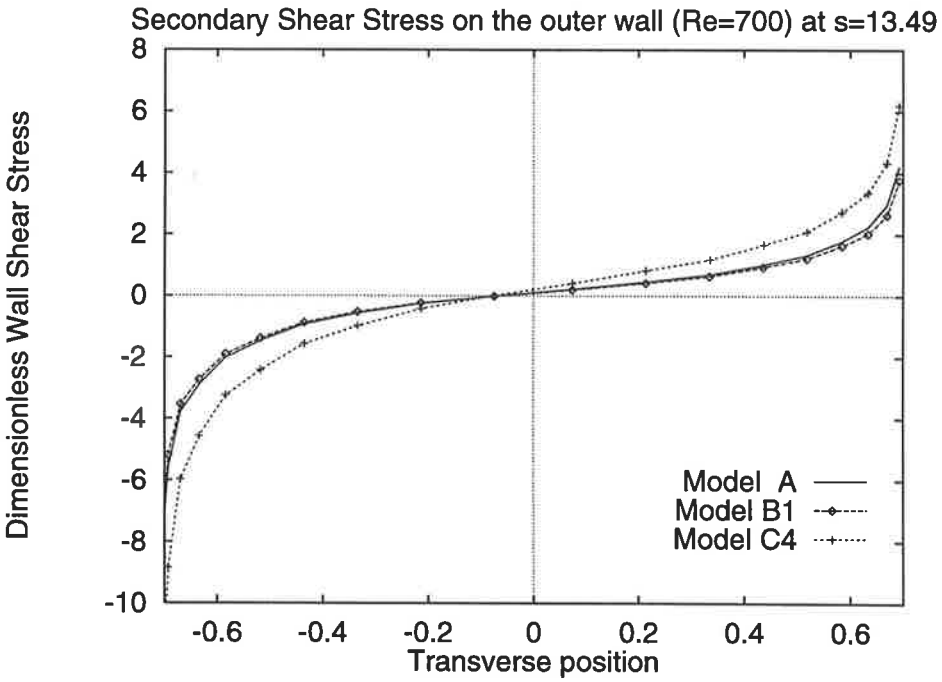

(b)

Figure 6.29: Graphs showing dimensionless wall shear stress at $Re = 700$ along the (a) inner wall and (b) outer wall, at $s = 13.49$

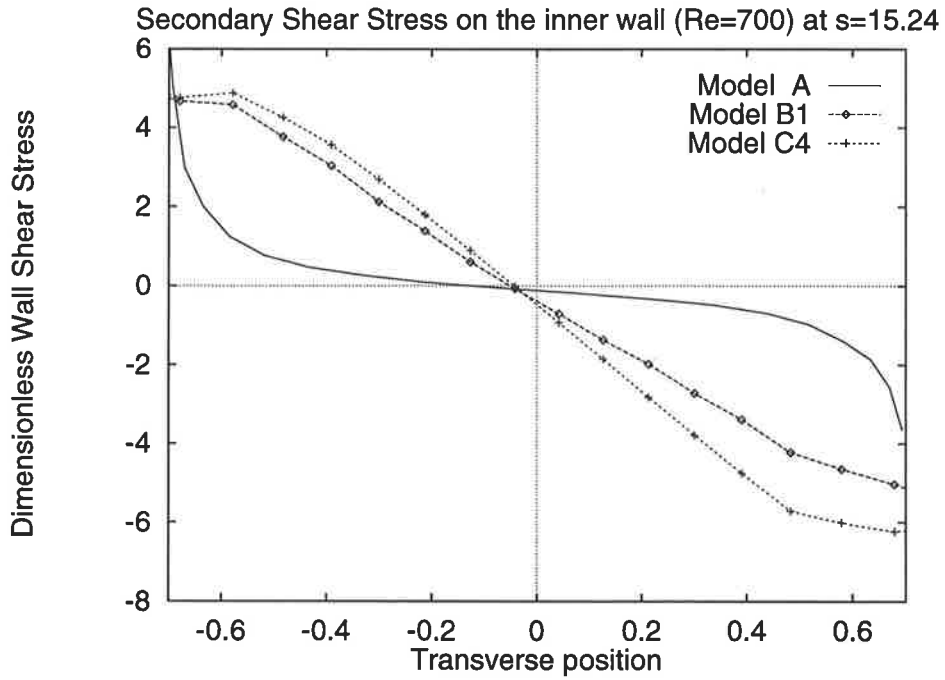

(a)

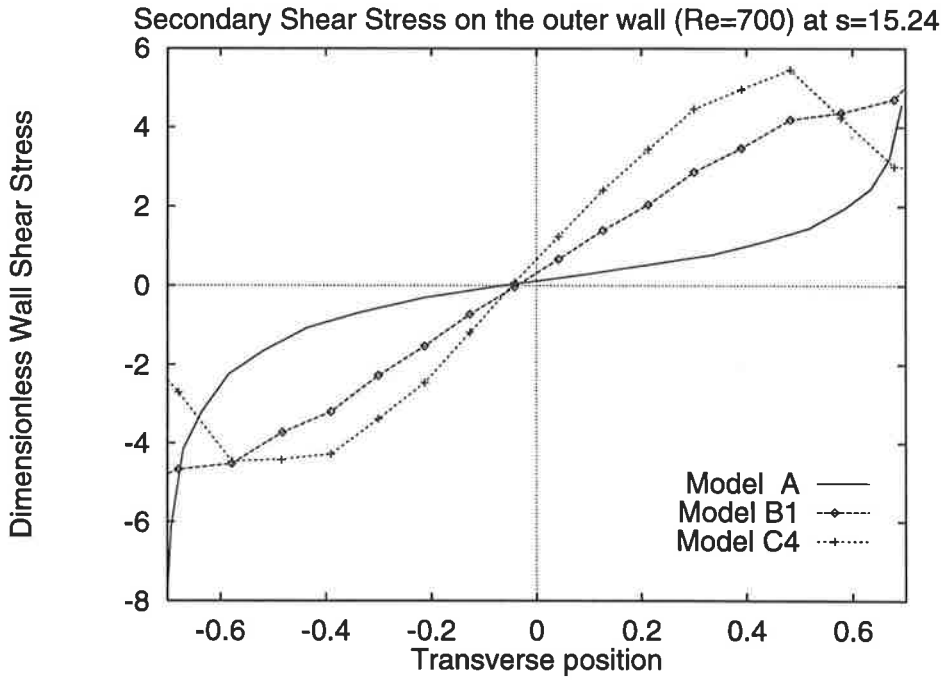

(b)

Figure 6.30: Graphs showing dimensionless wall shear stress at $Re = 700$ along the (a) inner wall and (b) outer wall, at $s = 15.24$

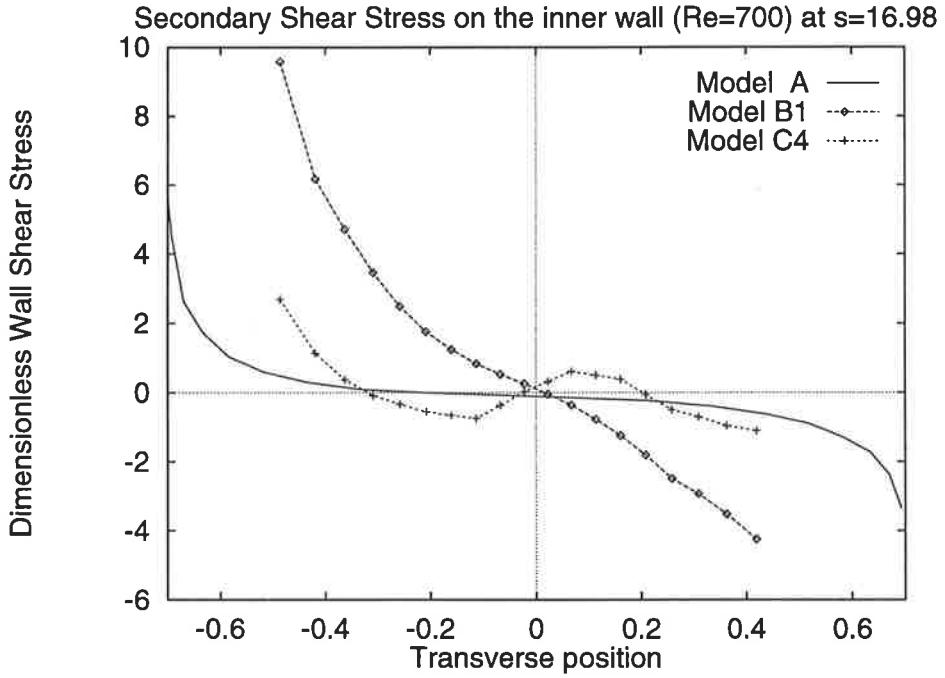

(a)

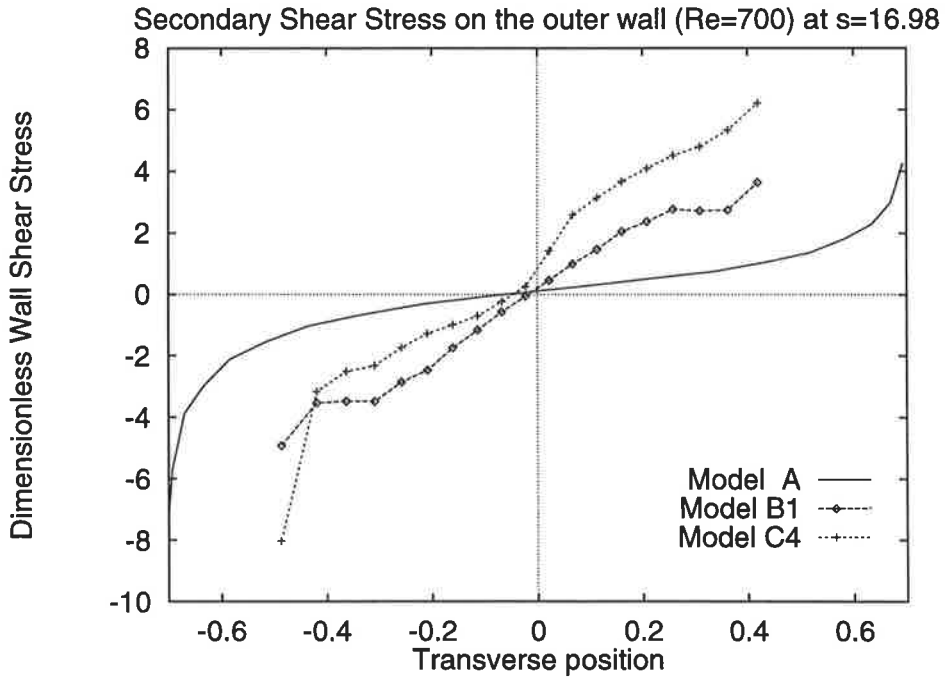

(b)

Figure 6.31: Graphs showing dimensionless wall shear stress at $Re = 700$ along the (a) inner wall and (b) outer wall, at $s = 16.98$

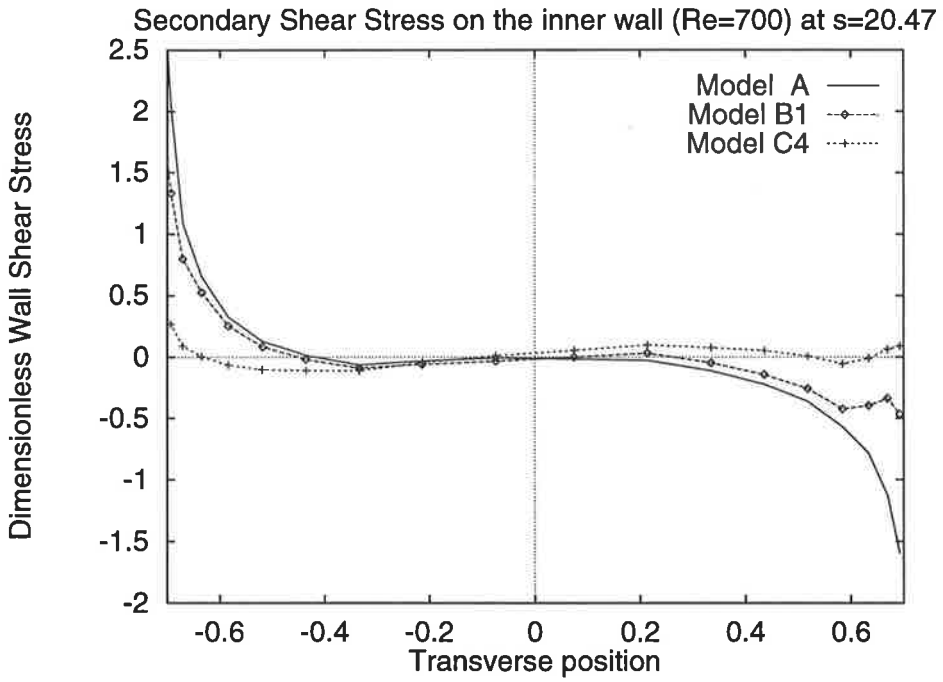

(a)

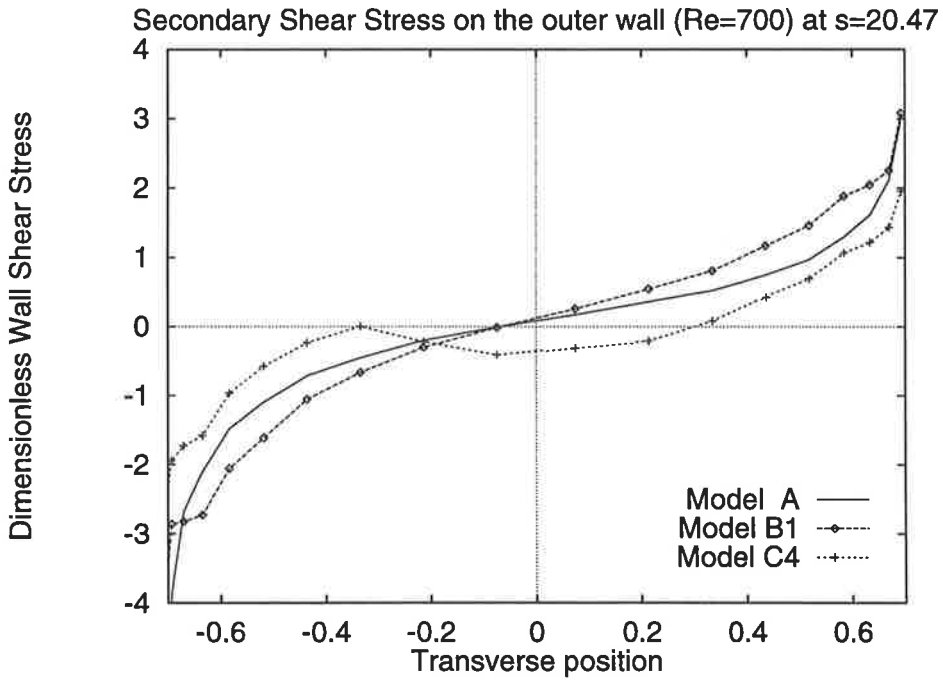

(b)

Figure 6.32: Graphs showing dimensionless wall shear stress at $Re = 700$ along the (a) inner wall and (b) outer wall, at $s = 20.47$

6.5 Conclusion

In this chapter, we have developed a model simulating blood flow in a curved artery with different conditions of stenosis at the bend. Some fluid mechanical phenomena have been discussed. In particular, we have examined the effects of curvature on the pressure drop, velocity profiles and shearing stresses on the walls, as well as secondary flow phenomena.

In terms of pressure drops, our models have shown that the curvature of an artery and the presence of stenoses in an artery will give rise to an increase in the pressure drop. This translates to a rise in relative flow resistance. Hence, one expects a higher resistance to blood flow in a curved stenosed artery than in a straight artery suffering from the same degree of stenosis.

The models include stenoses with percent stenosis ranging from about 40 to about 70%. As blood is assumed to be Newtonian in our models, we have not considered percent stenosis beyond 70%, since this would have reduced the lumen size and brought about non-Newtonian effects. Nonetheless, with the range of percent stenosis considered, the models examined in this chapter have been able to demonstrate the effects on the various flow characteristics due to the presence of asymmetric stenoses in a curved artery.

The elevated axial velocities and presence of significant secondary flow velocities found in the models due to the presence of stenoses in the curvature are also important factors for cardiologists to consider as these may lead to complications such as thrombosis or rupture of the plaques. The models also show that the geometry of the artery and the location (whether on the inner wall only or on both walls) of the stenoses are also possible contributing factors to these problems.

It is believed that high shear stress on the arterial walls may cause endothelial

damage (Fry 1968). Although the actual contribution of this factor in atherogenesis is still debatable, the relatively high shear stress on the stenotic side could be an important contributing factor to the overall progressive growth of the stenotic plaque. Nerem (1992) pointed out the importance of secondary wall shear stress in the atherosclerotic process. The models in this chapter have demonstrated the significant presence of secondary flow motion in curved arteries, particularly in the region between the throat of the stenosis and the downstream end of the stenosis. They have also shown that the presence of the stenosis and the asymmetry of it may cause the secondary wall shear stresses to rise very significantly.

As stresses are difficult to measure experimentally, it is thus useful to be able to examine them in a mathematical model and in this chapter, we have developed models of curved arteries which will help us gain further insight into this important aspect of hemodynamics.

CHAPTER 7

CONCLUSION

7.1 A Brief Summary

The three CFD models reported in this thesis provide detailed quantitative descriptions for the steady flow of blood through stenosed arteries. Flow characteristics such as pressure drops, flow velocities and shearing stresses on the arterial walls have been examined in detail.

The first model, Model I, compared to Model II and Model III, is fairly simple. It considers blood flow through an axisymmetric vessel with three stenoses in series, modelling a multiply stenosed artery. The equations are solved using the FIDAP code at a fixed Reynolds number. The results indicate the potential effectiveness of using commercial CFD codes in blood flow models. Moreover, Model I is an extension of a previously published work on paired stenoses.

Model II is constructed in three dimensions and it consists of an asymmetric stenosis, making the model physiologically more realistic in terms of geometry. The CFD code, PHOENICS, is employed to solve the system of equations for a range of Reynolds numbers and for three degrees of stenosis. The results from Model II include details of how stresses on the arterial walls may be estimated and analysed.

Model III is the most realistic of all three models. Like Model II, it also utilises

the PHOENICS code in the solution of the equations. Model III consists of three groups of models, namely, curved artery without constriction (Group A), curved artery with one protrusion from the inner wall of the bend (Group B) and curved artery with protrusions from both inner and outer walls of the bend (Group C). The numerical solutions from these groups of models provide information on pressure drops, flow velocities and wall shearing stresses for flow through a curved artery for various degrees of stenosis and for a range of Reynolds numbers. Secondary flow phenomena have also been examined in some detail and it has been shown that these have a significant effect on the overall flow pattern.

Where possible, comparisons between results obtained and available published results are made. The behaviour of the models is generally consistent with published reports, although in some cases, only qualitative comparisons are possible. Nevertheless, this study has achieved its objective of obtaining quantitative descriptions of blood flow through stenosed vessels through the use of CFD techniques, thus providing further insight into how the dynamics of blood flow may be related to some arterial disorders.

7.2 Clinical Significance of Present Study

The present study yields solutions to a number of mathematical models for blood flow through stenosed arteries. In particular, mathematical models of asymmetric arteries and curved arteries in three dimensions have been lacking in the literature even though such models may be more physiologically realistic. The present study has provided an analysis of such models using a powerful tool in CFD.

Results obtained in this study are particularly relevant to cardiologists who perform angioplasty procedures for coronary lesions. Model I provides information on the effects of multiple stenoses in arteries. One of the important conclusions drawn

from this model is that the effects of milder stenoses are diminished in the presence of more severe stenoses. However, the severity of the stenoses are relative, i.e. the mild stenoses are only mild when compared to the more severe stenoses. When treating an artery with a series of stenoses, the common practice among cardiologists is to deal with only the most severe lesion. The conclusion from Model I, however, shows that even though their effects may have been diminished, the other less severe stenoses should not be disregarded.

Model II examines asymmetrical stenoses and their effects on shearing stresses on the walls, providing some insight into the possible role of wall shear stress in atherogenesis. Model III concludes that the presence of curvature augments the increased resistance due to stenotic lesions. In practice, application of balloon angioplasty treatment on stenoses in a straight segment of the artery is far less complicated than that in a curved segment. Hence, if there are more than one stenosis of similar severity to treat, the usual practice is to give prior attention to the one on the less tortuous artery. However, the results from our study indicate that curved arteries with a stenosis generally experience a significantly higher flow resistance. In addition, the presence of secondary flow phenomena in curved arteries, bringing about elevated shear stress on the vessel walls, further suggests that both curvature and stenosis should be considered when interpreting coronary angiograms.

CFD codes have been used to solve the complex mathematical models and have provided valuable and detailed quantitative data for various flow characteristics in the models. Such detailed information may be difficult, if not impossible, to be attained through experiments. This study has successfully employed commercial CFD codes to construct and solve models, providing useful insight into the hemodynamics of blood flow in stenosed arteries. Accordingly, the long term application of this form of research promises to be an effective tool for gaining further insight into the pathology of arterial diseases. Consequently, in addition to angiographic procedures

and other experimental research, cardiologists may be provided with more information on the characteristics of flow in diseased vessels, thus assisting them in making certain practical decisions.

7.3 Recommendations for Future Study

While the present study has provided a comprehensive set of models on blood flow through arteries, there are still avenues where more research could be carried out in the continued search for more realistic and complete models.

The complete understanding of the complex fluid dynamics of flow through stenosed arteries and the associated pathological complications requires more than a steady flow and rigid tube analysis. Indeed, the effects of pulsatile flow and elastic wall boundaries have received much attention in modelling studies. Thus, incorporating these conditions in a curved artery model such as the one described in this study would result in an even more realistic model.

Although for reasons already discussed in preceding chapters, non-Newtonian effects have not been considered in the present study, it is possible to construct models of non-Newtonian flow in vessels where these effects become important. Many CFD codes nowadays have provisions for modelling of non-Newtonian flows (for example, PHOENICS uses the power-law model), making it possible to incorporate these features in the model.

The focus of the present study has been on coronary arteries, the main reason being the fact that coronary heart diseases are the main cause of death in the Western world. However, stenoses can also occur in other vessels in the arterial system. Modelling flows in other arteries may take a similar form. However, differences in vessel dimensions and flow characteristics may yield different results and implications, and this could be an interesting area for future study.

Experiments can be set up to verify and validate the models described in this study. This would usually involve the use of sophisticated equipment in a specialised biofluids laboratory. However, due to the constraints of time and other factors, the present study has not included an experimental study.

Nevertheless, the present study has produced results which are clinically significant, through the use of an increasingly popular CFD technique. The application of mathematical modelling and computational fluid dynamic techniques for the evaluation of the flow characteristics of blood in stenosed arteries has been and will continue to be a powerful and efficient way of providing valuable information.

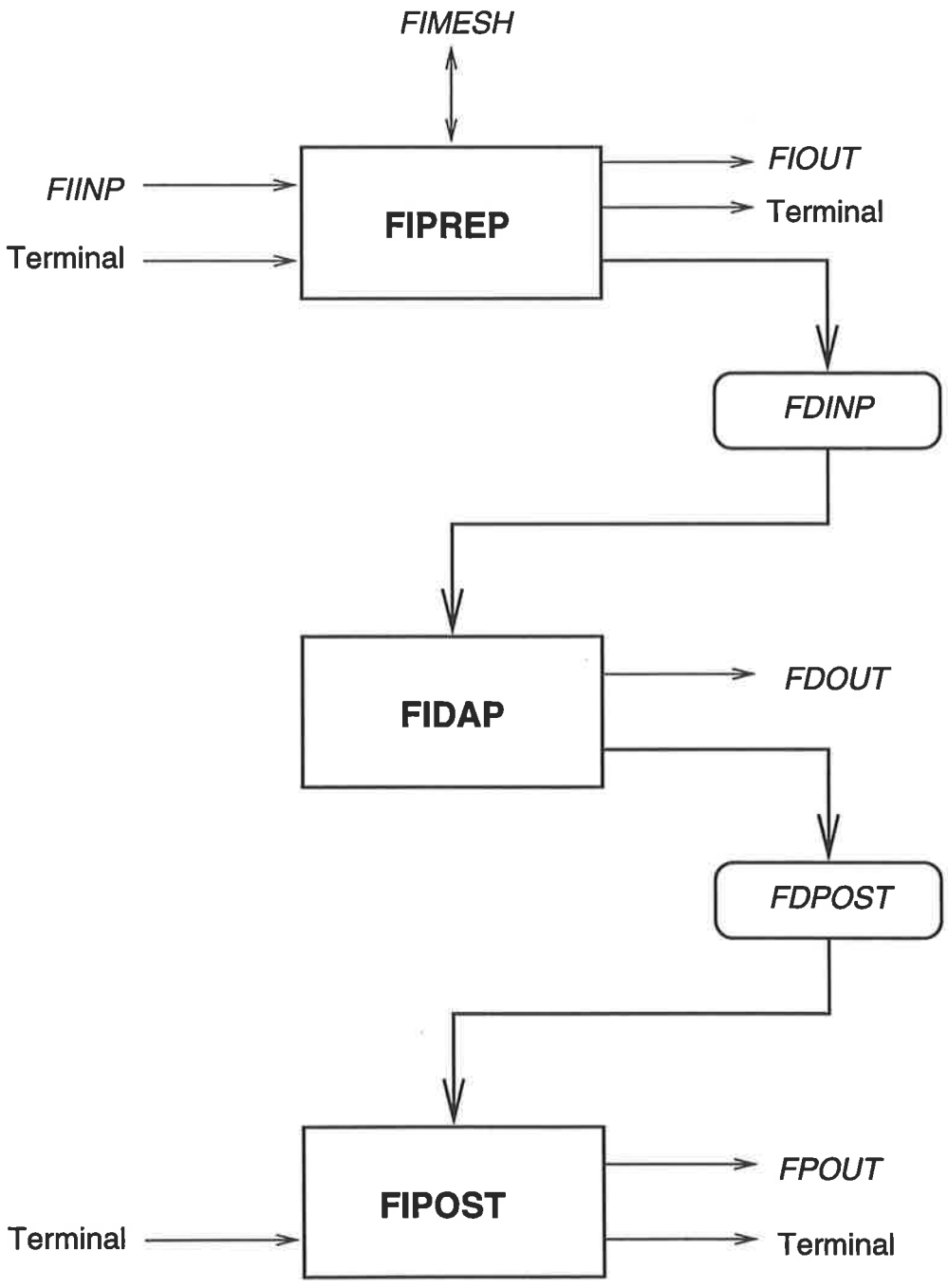

FIDAP file system and information flow

The basic flow of information is from FIPREP to FIDAP to FIPOST. An input file (called FIINP) describing the geometry of the model and the grid definition is fed to the FIPREP module. This is a pre-processing run where the grid information is checked and the grid generated. The process may also take place interactively at the computer terminal. The essential output of this module are the files FIMESH, FIOUT and FDINP. FIMESH contains information on the grid or mesh generation. FIOUT contains a listing of the valid commands entered and FDINP is used as an input for the next phase, FIDAP.

FIDAP accepts the input file FDINP, performs the numerical simulation and solves the equations, and writes the results to output files, FDOUT and FDPOST. FDOUT is a readable output file containing a summary of the information specified in the problem definition like node and element information, boundary condition data. It also contains information on values of the solved variables like velocity components, pressures and so on. Solution data is also available in a post-processing file FDPOST.

FDPOST is used by the next module, FIPOST, which performs post-processing tasks like graph-plotting and so on. FIPOST may also be used interactively, in which case terminal keyboard supplies the input and the terminal screen displays the output. FIPOST creates an output file FPOUT which summarises the input and the program response.

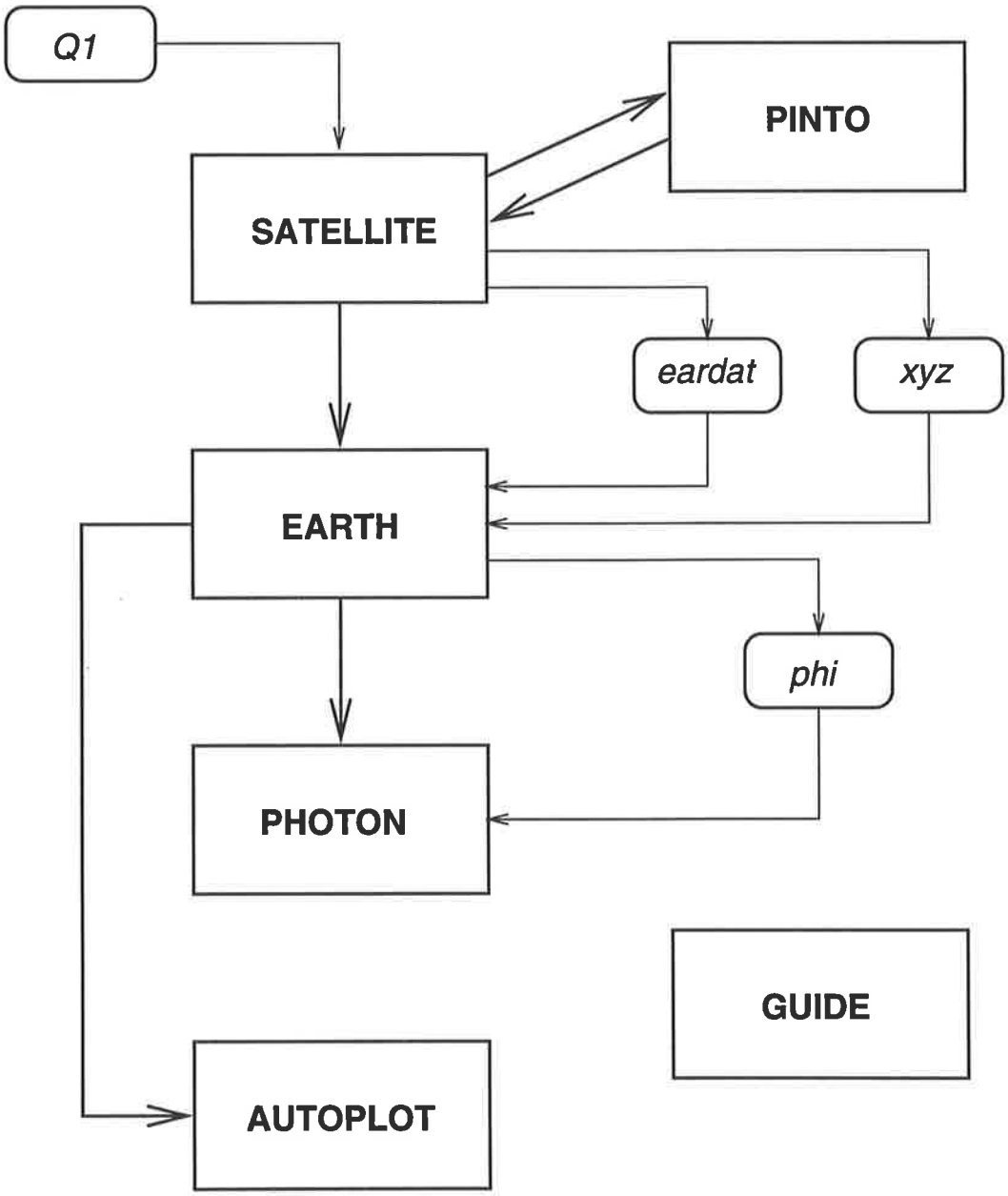

PHOENICS program relationships and file system

The input file in PHOENICS is known as the Q1 file which can either be created using an editor or through the interactive use of the SATELLITE module. Q1 contains information on the geometry of the model, the grid composition, fluid properties, boundary conditions of the flow and various solution options. The language used in the Q1 file is the PHOENICS Input Language, or PIL.

In the pre-processing phase, the Q1 file serves as the input for SATELLITE which checks the various parameters. SATELLITE is run interactively and can be used to display the geometry of the model, the boundary conditions and so on. Upon exiting SATELLITE, two files "eardat" and "xyz" are created. eardat contains relevant data to be used in EARTH, the next module. EARTH also uses xyz, a file containing information on the geometry of the model.

EARTH is the actual processing or "number-crunching" program, which utilises the finite volume CFD code and the SIMPLER algorithm to solve the governing equations. During the execution, the user is able monitor the values of the primitive variables at any chosen cell in the grid as well as the convergence patterns. EARTH allows the user to alter the relaxation factor for any one of the variables to be solved to aid the convergence. When either convergence is achieved or the maximum number of iterations is reached, the execution is halted and the output file, "phi" containing the values of the solved variables is created.

A post-processor, PHOTON, is another interactive program which first reads in the phi and xyz files, and performs various post-processing tasks. PHOTON may be used to plot velocity fields, pressure and temperature distributions and streamline plots of flow.

AUTOPLOT is a graph plotting program which accepts command on-line and produce various graphs using the data obtained by EARTH and stored in phi and xyz. PINTO is an interpolation program used for grid refinement. GUIDE is a "standalone" on-line user guide.

The following page shows a typical output on the screen at the end of an interactive EARTH run when convergence is achieved.

DELTA1=1.05, DELTA2=0.00, RE=1000 7

Spot Values at (10, 10, 35)

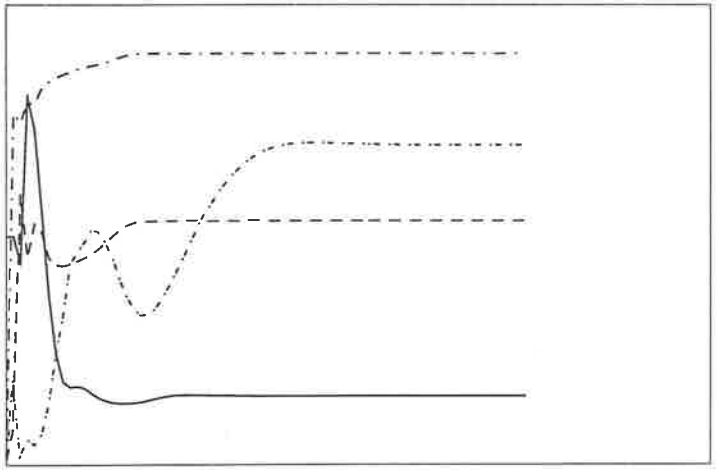

% Error - Cut off 1.000E+00 %

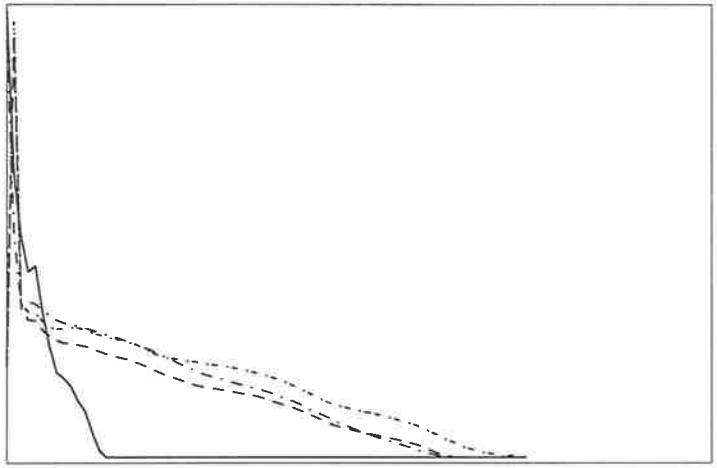

Min	Max	Spot Value	Change	Variable	Max	% Error	Change
-2.00E+03	2.00E+03	-1.44E+03	-1.10E-03	P1	1.00E+02	4.04E-05	-6.06E-06
0.00E+00	2.00E-02	1.40E-02	9.13E-08	U1	1.00E+16	9.85E-01	-1.35E-01
0.00E+00	2.00E+00	1.07E+00	0.00E+00	V1	1.00E+17	8.25E-01	2.46E-02
0.00E+00	5.00E+00	4.52E+00	0.00E+00	W1	1.00E+13	8.57E-01	3.14E-04

NX	NY	NZ		ISWEEP	489	Time now	1:02
20	20	80		IZSTEP	1	(h:m) est	6:24

Press a character key
to interrupt.

Appendix C : Sample FIDAP input file

```
*TITLE
FLOW THROUGH TRIPLE STENOSES   Re = 100   (96  96  91)
*FIMESH(2-D,IMAX=27,JMAX=3)
EXPI(DELTAS)
1 0 8 0 8 0 14 0 8 0 12 0 14 0 16 0 14 0 16 0 16 0 18 0 16 0 14
EXPJ(DELTAS)
/1  2  3
 1  0 18
PARAMETER
VGRAD  4.0
HGRAD  0.9
/
POINT(SYSTEM=1)
/Pt#  I  J  K  x     y  z
  1   1  1  1  0     0
  2   3  1  1  1.5   0
  3   5  1  1  2.25  0
  4   7  1  1  3.75  0
  5   9  1  1  4.25  0
  6  11  1  1  4.75  0
  7  13  1  1  5.25  0
  8  15  1  1  6.75  0
  9  17  1  1  7.25  0
 10  19  1  1  7.75  0
 11  21  1  1  8.25  0
 12  23  1  1  9.75  0
 13  25  1  1  10.25 0
 14  27  1  1  20    0
 15  27  3  1  20    1
 16  25  3  1  10    1
 17  23  3  1  9.5   0.505
 18  21  3  1  8.5   0.505
 19  19  3  1  8     1
 20  17  3  1  7     1
 21  15  3  1  6.5   0.434
 22  13  3  1  5.5   0.434
 23  11  3  1  5     1
 24   9  3  1  4     1
 25   7  3  1  3.5   0.434
 26   5  3  1  2.5   0.434
 27   3  3  1  2     1
 28   1  3  1  0     1
LINE
/ Start Pt.  End Pt.  Ratio IRAT  Flag
  1  28   VGRAD  4
  2  27   VGRAD  4
  3  26   VGRAD  4
  4  25   VGRAD  4
  5  24   VGRAD  4
  6  23   VGRAD  4
```

```
  7  22   VGRAD  4
  8  21   VGRAD  4
  9  20   VGRAD  4
 10  19   VGRAD  4
 11  18   VGRAD  4
 12  17   VGRAD  4
 13  16   VGRAD  4
 14  15   VGRAD  4
  1   2
 28  27
  2   3
  3   4
  4   5
  5   6
 24  23
  6   7
  7   8
  8   9
  9  10
 20  19
 10  11
 11  12
 12  13
 13  14
 16  15
/Define curved edge
CURVE
/Startpt  Endpt  #Datapt  Ratio  IRAT  Flag
  27   26   4
  2.1   0.875
  2.2   0.753
  2.3   0.637
  2.4   0.530
CURVE
  26   25   9
  2.6   0.353
  2.7   0.287
  2.8   0.239
  2.9   0.210
  3.0   0.200
  3.1   0.210
  3.2   0.239
  3.3   0.287
  3.4   0.353
CURVE
  25   24   4
  3.6   0.530
  3.7   0.637
  3.8   0.753
  3.9   0.875
CURVE
  23   22   4
```

```
  5.1   0.875
  5.2   0.753
  5.3   0.637
  5.4   0.530
CURVE
  22   21   9
  5.6   0.353
  5.7   0.287
  5.8   0.239
  5.9   0.210
  6.0   0.200
  6.1   0.210
  6.2   0.239
  6.3   0.287
  6.4   0.353
CURVE
  21   20   4
  6.6   0.530
  6.7   0.637
  6.8   0.753
  6.9   0.875
CURVE
  19   18   4
  8.1   0.890
  8.2   0.784
  8.3   0.682
  8.4   0.589
CURVE
  18   17   9
  8.6   0.434
  8.7   0.376
  8.8   0.334
  8.9   0.309
  9.0   0.300
  9.1   0.309
  9.2   0.334
  9.3   0.376
  9.4   0.434
CURVE
  17   16   4
  9.6   0.589
  9.7   0.682
  9.8   0.784
  9.9   0.890
SURFACE
1  15
ELEMENTS(QUADRILATERAL,NODES=9,ALL)
BCNODE(UX)
28 15 0.
BCNODE(UY)
1  14 0.
28 15 0.
```

```
1  28 0.
BCNODE(UX,PARABOLIC=1)
1  28 1.0
END
*FIPREP
PROBLEM(AXI-SYMMETRIC,NONLINEAR)
EXECUTION(NEWJOB)
DENSITY(CONSTANT=1.)
VISCOSITY(CONSTANT=.01)
PRESSURE(PENALTY=1.E-6)
ICNODE(STOKES)
SOLUTION(Q.N.=6)
STRATEGY(S.S.=3)
DATAPRINT(NORMAL)
PRINTOUT(ALL)
NODES(FIMESH)
ELEMENTS(NODES=9,QUADRILATERAL,FIMESH)
RENUMBER
END
*END
```

```
TALK=T;RUN( 1, 1);VDU=X11-TERM
IRUNN    =       1 ;LIBREF =       0
************************************************************
 Group 1. Run Title
TEXT(STENOSIS in 3-D, D=1.45, RE=245.33 )
************************************************************
 Group 2. Transience
STEADY  =    T
************************************************************
 Groups 3, 4, 5  Grid Information
   * Overall number of cells, RSET(M,NX,NY,NZ,tolerance)
RSET(M,10,10,70)
   * Overall domain extent, RSET(D,name,XULAST,YVLAST,ZWLAST)
RSET(D,CHAM,1.000E+00,1.000E+00,2.800E+01)
************************************************************
 Group 6. Body-Fitted coordinates
BFC=T
   * Set points
GSET(P,P1,-7.0700E-01,-7.0700E-01,0.0000E+00)
GSET(P,P2,0.0000E+00,-1.0000E+00,0.0000E+00)
GSET(P,P3,7.0700E-01,-7.0700E-01,0.0000E+00)
GSET(P,P4,1.0000E+00,0.0000E+00,0.0000E+00)
GSET(P,P5,7.0700E-01,7.0700E-01,0.0000E+00)
GSET(P,P6,0.0000E+00,1.0000E+00,0.0000E+00)
GSET(P,P7,-7.0700E-01,7.0700E-01,0.0000E+00)
GSET(P,P8,-1.0000E+00,0.0000E+00,0.0000E+00)
  ** points for K32  **
GSET(P,P11,-0.66346,-0.74821,10.30000)
GSET(P,P12,-0.70710, 0.70710,10.30000)
GSET(P,P13,-0.50000, 0.86600,10.30000)
GSET(P,P14, 0.00000, 1.00000,10.30000)
GSET(P,P15, 0.50000, 0.86600,10.30000)
GSET(P,P16, 0.70710, 0.70710,10.30000)
GSET(P,P17, 0.66346,-0.74821,10.30000)
  ** points for K33  **
GSET(P,P21,-0.96144,-0.27500,10.60000)
GSET(P,P22,-0.70710, 0.70710,10.60000)
GSET(P,P23,-0.50000, 0.86600,10.60000)
GSET(P,P24, 0.00000, 1.00000,10.60000)
GSET(P,P25, 0.50000, 0.86600,10.60000)
GSET(P,P26, 0.70710, 0.70710,10.60000)
GSET(P,P27, 0.96144,-0.27500,10.60000)
  ** points for K34  **
GSET(P,P31,-0.99385, 0.11076,10.90000)
GSET(P,P32,-0.70710, 0.70710,10.90000)
GSET(P,P33,-0.50000, 0.86600,10.90000)
GSET(P,P34, 0.00000, 1.00000,10.90000)
GSET(P,P35, 0.50000, 0.86600,10.90000)
GSET(P,P36, 0.70710, 0.70710,10.90000)
GSET(P,P37, 0.99385, 0.11076,10.90000)
```

```
  ** points for K35  **
GSET(P,P41,-0.93196, 0.36255,11.20000)
GSET(P,P42,-0.70710, 0.70710,11.20000)
GSET(P,P43,-0.50000, 0.86600,11.20000)
GSET(P,P44, 0.00000, 1.00000,11.20000)
GSET(P,P45, 0.50000, 0.86600,11.20000)
GSET(P,P46, 0.70710, 0.70710,11.20000)
GSET(P,P47, 0.93196, 0.36255,11.20000)
  ** points for K36  **
GSET(P,P51,-0.89303, 0.45000,11.50000)
GSET(P,P52,-0.70710, 0.70710,11.50000)
GSET(P,P53,-0.50000, 0.86600,11.50000)
GSET(P,P54, 0.00000, 1.00000,11.50000)
GSET(P,P55, 0.50000, 0.86600,11.50000)
GSET(P,P56, 0.70710, 0.70710,11.50000)
GSET(P,P57, 0.89303, 0.45000,11.50000)
  ** points for K37  **
GSET(P,P61,-0.93196, 0.36255,11.80000)
GSET(P,P62,-0.70710, 0.70710,11.80000)
GSET(P,P63,-0.50000, 0.86600,11.80000)
GSET(P,P64, 0.00000, 1.00000,11.80000)
GSET(P,P65, 0.50000, 0.86600,11.80000)
GSET(P,P66, 0.70710, 0.70710,11.80000)
GSET(P,P67, 0.93196, 0.36255,11.80000)
  ** points for K38  **
GSET(P,P71,-0.99385, 0.11076,12.10000)
GSET(P,P72,-0.70710, 0.70710,12.10000)
GSET(P,P73,-0.50000, 0.86600,12.10000)
GSET(P,P74, 0.00000, 1.00000,12.10000)
GSET(P,P75, 0.50000, 0.86600,12.10000)
GSET(P,P76, 0.70710, 0.70710,12.10000)
GSET(P,P77, 0.99385, 0.11076,12.10000)
  ** points for K39  **
GSET(P,P81,-0.96144,-0.27500,12.40000)
GSET(P,P82,-0.70710, 0.70710,12.40000)
GSET(P,P83,-0.50000, 0.86600,12.40000)
GSET(P,P84, 0.00000, 1.00000,12.40000)
GSET(P,P85, 0.50000, 0.86600,12.40000)
GSET(P,P86, 0.70710, 0.70710,12.40000)
GSET(P,P87, 0.96144,-0.27500,12.40000)
  ** points for K40  **
GSET(P,P91,-0.66346,-0.74821,12.70000)
GSET(P,P92,-0.70710, 0.70710,12.70000)
GSET(P,P93,-0.50000, 0.86600,12.70000)
GSET(P,P94, 0.00000, 1.00000,12.70000)
GSET(P,P95, 0.50000, 0.86600,12.70000)
GSET(P,P96, 0.70710, 0.70710,12.70000)
GSET(P,P97, 0.66346,-0.74821,12.70000)
  ** points for K41  **
GSET(P,P101,-7.0700E-01,-7.0700E-01,1.3E+01)
GSET(P,P102,0.0000E+00,-1.0000E+00,1.3E+01)
GSET(P,P103,7.0700E-01,-7.0700E-01,1.3E+01)
```

```
GSET(P,P104,1.0000E+00,0.0000E+00,1.3E+01)
GSET(P,P105,7.0700E-01,7.0700E-01,1.3E+01)
GSET(P,P106,0.0000E+00,1.0000E+00,1.3E+01)
GSET(P,P107,-7.0700E-01,7.0700E-01,1.3E+01)
GSET(P,P108,-1.0000E+00,0.0000E+00,1.3E+01)
   * Set lines/arcs
GSET(L,A1,P1,P3,10,S2,ARC,P2)
GSET(L,A2,P1,P7,10,S2,ARC,P8)
GSET(L,A3,P3,P5,10,S2,ARC,P4)
GSET(L,A4,P7,P5,10,S2,ARC,P6)
   * lines/arcs for K32
GSET(L,LA1,P11,P17,10,S.85)
GSET(L,LA2,P11,P13,10,S2,ARC,P12)
GSET(L,LA3,P17,P15,10,S2,ARC,P16)
GSET(L,LA4,P13,P15,10,S2,ARC,P14)
   * lines/arcs for K33
GSET(L,LB1,P21,P27,10,S.85)
GSET(L,LB2,P21,P23,10,S2,ARC,P22)
GSET(L,LB3,P27,P25,10,S2,ARC,P26)
GSET(L,LB4,P23,P25,10,S2,ARC,P24)
   * lines/arcs for K34
GSET(L,LC1,P31,P37,10,S.85)
GSET(L,LC2,P31,P33,10,S2,ARC,P32)
GSET(L,LC3,P37,P35,10,S2,ARC,P36)
GSET(L,LC4,P33,P35,10,S2,ARC,P34)
   * lines/arcs for K35
GSET(L,LD1,P41,P47,10,S.85)
GSET(L,LD2,P41,P43,10,S2,ARC,P42)
GSET(L,LD3,P47,P45,10,S2,ARC,P46)
GSET(L,LD4,P43,P45,10,S2,ARC,P44)
   * lines/arcs for K36
GSET(L,LE1,P51,P57,10,S.85)
GSET(L,LE2,P51,P53,10,S2,ARC,P52)
GSET(L,LE3,P57,P55,10,S2,ARC,P56)
GSET(L,LE4,P53,P55,10,S2,ARC,P54)
   * lines/arcs for K37
GSET(L,LF1,P61,P67,10,S.85)
GSET(L,LF2,P61,P63,10,S2,ARC,P62)
GSET(L,LF3,P67,P65,10,S2,ARC,P66)
GSET(L,LF4,P63,P65,10,S2,ARC,P64)
   * lines/arcs for K38
GSET(L,LG1,P71,P77,10,S.85)
GSET(L,LG2,P71,P73,10,S2,ARC,P72)
GSET(L,LG3,P77,P75,10,S2,ARC,P76)
GSET(L,LG4,P73,P75,10,S2,ARC,P74)
   * lines/arcs for K39
GSET(L,LH1,P81,P87,10,S.85)
GSET(L,LH2,P81,P83,10,S2,ARC,P82)
GSET(L,LH3,P87,P85,10,S2,ARC,P86)
GSET(L,LH4,P83,P85,10,S2,ARC,P84)
   * lines/arcs for K40
GSET(L,LI1,P91,P97,10,S.85)
```

```
GSET(L,LI2,P91,P93,10,S2,ARC,P92)
GSET(L,LI3,P97,P95,10,S2,ARC,P96)
GSET(L,LI4,P93,P95,10,S2,ARC,P94)
   * lines/arcs for K41
GSET(L,AA1,P101,P103,10,S2,ARC,P102)
GSET(L,AA2,P101,P107,10,S2,ARC,P108)
GSET(L,AA3,P103,P105,10,S2,ARC,P104)
GSET(L,AA4,P107,P105,10,S2,ARC,P106)
   * Set frames
GSET(F,F1,P1,-,P3,-,P5,-,P7,-)
GSET(F,F32,P11,-,P17,-,P15,-,P13,-)
GSET(F,F33,P21,-,P27,-,P25,-,P23,-)
GSET(F,F34,P31,-,P37,-,P35,-,P33,-)
GSET(F,F35,P41,-,P47,-,P45,-,P43,-)
GSET(F,F36,P51,-,P57,-,P55,-,P53,-)
GSET(F,F37,P61,-,P67,-,P65,-,P63,-)
GSET(F,F38,P71,-,P77,-,P75,-,P73,-)
GSET(F,F39,P81,-,P87,-,P85,-,P83,-)
GSET(F,F40,P91,-,P97,-,P95,-,P93,-)
GSET(F,F41,P101,-,P103,-,P105,-,P107,-)
   * Match a grid mesh
GSET(M,F1,+I+J,1,1,1,LAP5)
GSET(M,F32,+I+J,1,1,32,LAP5)
GSET(M,F33,+I+J,1,1,33,LAP5)
GSET(M,F34,+I+J,1,1,34,LAP5)
GSET(M,F35,+I+J,1,1,35,LAP5)
GSET(M,F36,+I+J,1,1,36,LAP5)
GSET(M,F37,+I+J,1,1,37,LAP5)
GSET(M,F38,+I+J,1,1,38,LAP5)
GSET(M,F39,+I+J,1,1,39,LAP5)
GSET(M,F40,+I+J,1,1,40,LAP5)
GSET(M,F41,+I+J,1,1,41,LAP5)
   * Copy/Transfer/Block grid planes
GSET(C,K31,F,K1,1,10,1,10,+,0,0,10,INC,1)
GSET(T,K32,F,K31,1,10,1,10,1)
GSET(T,K33,F,K32,1,10,1,10,1)
GSET(T,K34,F,K33,1,10,1,10,1)
GSET(T,K35,F,K34,1,10,1,10,1)
GSET(T,K36,F,K35,1,10,1,10,1)
GSET(T,K37,F,K36,1,10,1,10,1)
GSET(T,K38,F,K37,1,10,1,10,1)
GSET(T,K39,F,K38,1,10,1,10,1)
GSET(T,K40,F,K39,1,10,1,10,1)
GSET(T,K41,F,K40,1,10,1,10,1)
GSET(C,K71,F,K41,1,10,1,10,+,0,0,15,INC,1)
   **********
NONORT  =    T
   * X-cyclic boundaries switched
************************************************************
 Group 7. Variables: STOREd,SOLVEd,NAMEd
ONEPHS  =    T
   * Non-default variable names
```

```
NAME(43) =HPOR ; NAME(44) =NPOR
NAME(45) =EPOR ; NAME(46) =VPOR
NAME(47) =WCRT ; NAME(48) =VCRT
NAME(49) =DEN1 ; NAME(50) =UCRT
   * Solved variables list
SOLVE(P1  ,U1  ,V1  ,W1  )
   * Stored variables list
STORE(UCRT,DEN1,VCRT,WCRT,VPOR,EPOR,NPOR,HPOR)
   * Additional solver options
SOLUTN(P1  ,Y,Y,Y,N,N,N)
************************************************************
 Group 8. Terms & Devices
************************************************************
 Group 9. Properties
RHO1    = 1.000E+03
ENUL    = 3.8E-3 ;ENUT   = 0.000E+00
************************************************************
 Group 10.Inter-Phase Transfer Processes
************************************************************
 Group 11.Initialise Var/Porosity Fields
FIINIT(HPOR) =  1.000E+00 ;FIINIT(NPOR) =  1.000E+00
FIINIT(EPOR) =  1.000E+00 ;FIINIT(VPOR) =  1.000E+00
FIINIT(UCRT) =  0.000E+00
  No PATCHes used for this Group

RSTGRD  =    F

INIADD  =    F
************************************************************
 Group 12. Convection and diffusion adjustments
************************************************************
 Group 13. Boundary & Special Sources

PATCH (KESOURCE,PHASEM,1,10,1,10,1,70,1,1)

**  inlet definitions  **

INLET (BFCIN11 ,LOW   ,1,10,1,1,#1,#1,1,1)
VALUE (BFCIN11 ,P1  , GRND1    )
VALUE (BFCIN11 ,U1  , GRND1    )
VALUE (BFCIN11 ,V1  , GRND1    )
VALUE (BFCIN11 ,W1  , GRND1    )
VALUE (BFCIN11 ,WCRT, 2.520E-01)

INLET (BFCIN12 ,LOW   ,1,10,10,10,#1,#1,1,1)
VALUE (BFCIN12 ,P1  , GRND1    )
VALUE (BFCIN12 ,U1  , GRND1    )
VALUE (BFCIN12 ,V1  , GRND1    )
VALUE (BFCIN12 ,W1  , GRND1    )
VALUE (BFCIN12 ,WCRT, 2.520E-01)

INLET (BFCIN13 ,LOW   ,1,1,2,9,#1,#1,1,1)
```

```
VALUE (BFCIN13 ,P1  , GRND1    )
VALUE (BFCIN13 ,U1  , GRND1    )
VALUE (BFCIN13 ,V1  , GRND1    )
VALUE (BFCIN13 ,W1  , GRND1    )
VALUE (BFCIN13 ,WCRT, 2.520E-01)

INLET (BFCIN14 ,LOW ,10,10,2,9,#1,#1,1,1)
VALUE (BFCIN14 ,P1  , GRND1    )
VALUE (BFCIN14 ,U1  , GRND1    )
VALUE (BFCIN14 ,V1  , GRND1    )
VALUE (BFCIN14 ,W1  , GRND1    )
VALUE (BFCIN14 ,WCRT, 2.520E-01)

INLET (BFCIN21 ,LOW ,2,9,2,2,#1,#1,1,1)
VALUE (BFCIN21 ,P1  , GRND1    )
VALUE (BFCIN21 ,U1  , GRND1    )
VALUE (BFCIN21 ,V1  , GRND1    )
VALUE (BFCIN21 ,W1  , GRND1    )
VALUE (BFCIN21 ,WCRT, 4.480E-01)

INLET (BFCIN22 ,LOW ,2,9,9,9,#1,#1,1,1)
VALUE (BFCIN22 ,P1  , GRND1    )
VALUE (BFCIN22 ,U1  , GRND1    )
VALUE (BFCIN22 ,V1  , GRND1    )
VALUE (BFCIN22 ,W1  , GRND1    )
VALUE (BFCIN22 ,WCRT, 4.480E-01)

INLET (BFCIN23 ,LOW ,2,2,3,8,#1,#1,1,1)
VALUE (BFCIN23 ,P1  , GRND1    )
VALUE (BFCIN23 ,U1  , GRND1    )
VALUE (BFCIN23 ,V1  , GRND1    )
VALUE (BFCIN23 ,W1  , GRND1    )
VALUE (BFCIN23 ,WCRT, 4.480E-01)

INLET (BFCIN24 ,LOW ,9,9,3,8,#1,#1,1,1)
VALUE (BFCIN24 ,P1  , GRND1    )
VALUE (BFCIN24 ,U1  , GRND1    )
VALUE (BFCIN24 ,V1  , GRND1    )
VALUE (BFCIN24 ,W1  , GRND1    )
VALUE (BFCIN24 ,WCRT, 4.480E-01)

INLET (BFCIN31 ,LOW ,3,8,3,3,#1,#1,1,1)
VALUE (BFCIN31 ,P1  , GRND1    )
VALUE (BFCIN31 ,U1  , GRND1    )
VALUE (BFCIN31 ,V1  , GRND1    )
VALUE (BFCIN31 ,W1  , GRND1    )
VALUE (BFCIN31 ,WCRT, 5.880E-01)

INLET (BFCIN32 ,LOW ,3,8,8,8,#1,#1,1,1)
VALUE (BFCIN32 ,P1  , GRND1    )
VALUE (BFCIN32 ,U1  , GRND1    )
VALUE (BFCIN32 ,V1  , GRND1    )
```

```
VALUE (BFCIN32 ,W1   , GRND1    )
VALUE (BFCIN32 ,WCRT, 5.880E-01)

INLET (BFCIN33 ,LOW ,3,3,4,7,#1,#1,1,1)
VALUE (BFCIN33 ,P1   , GRND1    )
VALUE (BFCIN33 ,U1   , GRND1    )
VALUE (BFCIN33 ,V1   , GRND1    )
VALUE (BFCIN33 ,W1   , GRND1    )
VALUE (BFCIN33 ,WCRT, 5.880E-01)

INLET (BFCIN34 ,LOW ,8,8,4,7,#1,#1,1,1)
VALUE (BFCIN34 ,P1   , GRND1    )
VALUE (BFCIN34 ,U1   , GRND1    )
VALUE (BFCIN34 ,V1   , GRND1    )
VALUE (BFCIN34 ,W1   , GRND1    )
VALUE (BFCIN34 ,WCRT, 5.880E-01)

INLET (BFCIN41 ,LOW ,4,7,4,4,#1,#1,1,1)
VALUE (BFCIN41 ,P1   , GRND1    )
VALUE (BFCIN41 ,U1   , GRND1    )
VALUE (BFCIN41 ,V1   , GRND1    )
VALUE (BFCIN41 ,W1   , GRND1    )
VALUE (BFCIN41 ,WCRT, 6.720E-01)

INLET (BFCIN42 ,LOW ,4,7,7,7,#1,#1,1,1)
VALUE (BFCIN42 ,P1   , GRND1    )
VALUE (BFCIN42 ,U1   , GRND1    )
VALUE (BFCIN42 ,V1   , GRND1    )
VALUE (BFCIN42 ,W1   , GRND1    )
VALUE (BFCIN42 ,WCRT, 6.720E-01)

INLET (BFCIN43 ,LOW ,4,4,5,6,#1,#1,1,1)
VALUE (BFCIN43 ,P1   , GRND1    )
VALUE (BFCIN43 ,U1   , GRND1    )
VALUE (BFCIN43 ,V1   , GRND1    )
VALUE (BFCIN43 ,W1   , GRND1    )
VALUE (BFCIN43 ,WCRT, 6.720E-01)

INLET (BFCIN44 ,LOW ,7,7,5,6,#1,#1,1,1)
VALUE (BFCIN44 ,P1   , GRND1    )
VALUE (BFCIN44 ,U1   , GRND1    )
VALUE (BFCIN44 ,V1   , GRND1    )
VALUE (BFCIN44 ,W1   , GRND1    )
VALUE (BFCIN44 ,WCRT, 6.720E-01)

INLET (BFCIN5 ,LOW ,5,6,5,6,#1,#1,1,1)
VALUE (BFCIN5 ,P1   , GRND1    )
VALUE (BFCIN5 ,U1   , GRND1    )
VALUE (BFCIN5 ,V1   , GRND1    )
VALUE (BFCIN5 ,W1   , GRND1    )
VALUE (BFCIN5 ,WCRT, 7.000E-01)
```

```
PATCH (OUT      ,HIGH  ,#1,#1,#1,#1,#12,#12,1,1)
COVAL (OUT      ,P1   , FIXVAL    , 0.000E+00)

PATCH (W1       ,WWALL ,#1,#1,#1,#1,#1,#12,1,1)
COVAL (W1       ,V1   , GRND2     , 0.000E+00)
COVAL (W1       ,W1   , GRND2     , 0.000E+00)

PATCH (W2       ,EWALL ,#1,#1,#1,#1,#1,#12,1,1)
COVAL (W2       ,V1   , GRND2     , 0.000E+00)
COVAL (W2       ,W1   , GRND2     , 0.000E+00)

PATCH (W3       ,SWALL ,#1,#1,#1,#1,#1,#12,1,1)
COVAL (W3       ,U1   , GRND2     , 0.000E+00)
COVAL (W3       ,W1   , GRND2     , 0.000E+00)

PATCH (W4       ,NWALL ,#1,#1,#1,#1,#1,#12,1,1)
COVAL (W4       ,U1   , GRND2     , 0.000E+00)
COVAL (W4       ,W1   , GRND2     , 0.000E+00)

BFCA     = 1.000E+03
************************************************************
 Group 14. Downstream Pressure For PARAB
************************************************************
 Group 15. Terminate Sweeps
LSWEEP   =   3000
SELREF   =    T
RESFAC   = 1.000E-02
************************************************************
 Group 16. Terminate Iterations
************************************************************
 Group 17. Relaxation
RELAX(P1   ,LINRLX, 1.000E-01)
RELAX(U1   ,FALSDT, 5.000E-01)
RELAX(V1   ,FALSDT, 5.000E-01)
RELAX(W1   ,FALSDT, 5.000E-01)
************************************************************
 Group 18. Limits
************************************************************
 Group 19. EARTH Calls To GROUND Station
GENK     =    T
************************************************************
 Group 20. Preliminary Printout
ECHO     =    T
************************************************************
 Group 21. Print-out of Variables
OUTPUT(HPOR,N,N,N,Y,N,N)
OUTPUT(NPOR,N,N,N,Y,N,N)
OUTPUT(EPOR,N,N,N,Y,N,N)
OUTPUT(VPOR,N,N,N,Y,N,N)
************************************************************
 Group 22. Monitor Print-Out
IXMON    =       5 ;IYMON  =       5 ;IZMON  =      35
```

```
 TSTSWP  =      1
 ************************************************************
  Group 23.Field Print-Out & Plot Control
   No PATCHes used for this Group
 ************************************************************
  Group 24. Dumps For Restarts
 ************************************************************
 MENSAV(S,RELX,DEF,1.0000E-01,5.0000E-02,0)
 MENSAV(S,PHSPROP,DEF,200,0,1.0005E+03,1.7880E-06)
 MENSAV(S,FLPRP,DEF,LAMINAR,CONSTANT,AIR-CONSTANT)
STOP
```

Appendix E

Ang, K.C. and Mazumdar, J. (1995) Mathematical modelling of Triple Arterial Stenoses.
Australasian Physical & Engineering Sciences in Medicine, v. l8 (2), pp.89-94, 1995

NOTE: This publication is included on pages 174-179 in the print copy of the thesis held in the University of Adelaide Library.

Bibliography

Altobelli, S.A. and Nerem, R.M. 1985, An experimental study of coronary artery fluid mechanics. *Journal of Biomechanical Engineering*, Vol. 107, pp. 16-23.

Ang, K.C. and Mazumdar, J.N. 1995, Mathematical modelling of triple arterial stenoses. *Australasian Physical and Engineering Sciences in Medicine*, Vol. 18, pp. 89-94.

Ang, K.C. and Mazumdar, J.N. 1996, Mathematical modelling of three dimensional flow through an asymmetric stenosis. *Mathematical and Computer Modelling* (to appear).

Asakura, T. and Karino, T. 1990, Flow patterns and spatial distribution of atherosclerotic lesions in human coronary arteries. *Circulation Research*, Vol. 66, pp. 1045-1066.

Back, L.H., Liem, T.K., Kwack, E.Y. and Crawford, D.W. 1992, Flow measurements in a highly curved atherosclerotic coronary artery cast of man. *Journal of Biomechanical Engineering*, Vol. 114, pp. 232-240.

Becker, A.E. and Anderson, R.H. 1983, *Cardiac Pathology - An integrated text and colour atlas*, Gower Medical Publishing, Edinburgh. pp. 3.4.

Berger, S.A., Talbort, L. and Yao, L.S. 1983, Flow in curved pipes. *Annual Review of Fluid Mechanics*, Vol. 15, pp. 461-512.

Bray, J.J., Cragg, P.A., Macknight, A.D.C., Mills, R.G. and Taylor, D.W. (eds) 1989, *Lecture Notes on Human Physiology, 2nd edition*, Blackwell Scientific Publications, Oxford. pp. 421.

Chakravarty, S. and Chowdhurry, A.G. 1988, Response of blood flow through an artery under stenotic conditions. *Rheologica Acta*, Vol. 27, pp. 418-427.

Chakravarty, S. and Datta, A. 1989, Effects of stenosis on arterial rheology through a mathematical model. *Mathematical and Computer Modelling*, Vol. 12, pp. 1601-1612.

Chakravarty, S. and Datta, A. 1990, Dynamic response of arterial blood flow in the presence of multi-stenoses. *Mathematical and Computer Modelling*, Vol.

13, pp. 37-55.

Chang, L.J. and Tarbell, J.M. 1988, A numerical study of flow in curved tubes simulating coronary arteries. *Journal of Biomechanics*, Vol. 21, pp. 927-937.

Chow, J.C.F. and Soda, K. 1972, Laminar flow in tubes with constriction. *The Physics of Fluids*, Vol. 15, pp. 1700-1708.

Desphande, M.D., Giddens, D.P. and Mabon, R.F. 1976, Steady laminar flow through modelled vascular stenoses. *Journal of Biomechanics*, Vol. 9, pp. 165-174.

Dinnar, U. 1981, *Cardiovascular Fluid Dynamics*, CRC Press, Florida.

Dvinsky, A.S. and Ojha, M. 1994, Simulation of three-dimensional pulsatile flow through an asymmetric stenosis. *Medical & Biological Engineering & Computing*, Vol. 32, pp. 138-142.

FIDAP User Manual, Revision 6.0 1991, Fluid Dynamics International,Inc.

Fiddian, R.V., Byar, D. and Edwards, E.A. 1964, Factors affecting flow through a stenosed vessel. *Archives of Surgery*, Vol. 88, pp. 83-90.

Flectcher, C.A.J. 1988, *Computational Techniques for Fluid Dynamics I : Fundamental and General Techniques*, Springer-Verlag, Berlin.

Forrester, J.H. and Young, D.F. 1970a, Flow through a converging-diverging tube and its implications in occlusive vascular disease - I. *Journal of Biomechanics*, Vol. 3, pp. 297-305.

Forrester, J.H. and Young, D.F. 1970b, Flow through a converging-diverging tube and its implications in occlusive vascular disease - II. *Journal of Biomechanics*, Vol. 3, pp. 307-316.

Friedman, M. 1969, *Pathogenesis of Coronary Artery Disease*, McGraw Hill, New York. pp. 75-135.

Fry, D.L. 1968, Acute vascular endothelial changes associated with increased blood velocity gradients. *Circulation Research*, Vol. 22, pp. 165-197.

Fung, Y.C. 1984, *Biodynamics : Circulation*, Springer-Verlag, New York.

Ganong, W.F. 1987, *Review of Medical Physiology*, Appleton & Lange, California.

Gessner, F.B. 1973, Hemodynamic theories of atherogenesis. *Circulation Research*, Vol. 33, pp. 259-266.

Glagov, S., Zarins, C., Giddens, D.P. and Ku, D.N. 1988, Hemodynamics and atherosclerosis. *Archives of Pathology & Laboratory Medicine*, Vol. 112, pp. 1018-1031.

Huang, H., Modi, V.J. and Seymour, B.R. 1993, A new finite difference scheme and its application to flows in stenosed arteries. *Contemporary Mathematics*, Vol. 141, pp. 337-350.

Jensen, D. 1980, *The Principles of Physiology, 2nd edition*, Appleton-Century-Crofts, New York. pp. 546.

Johnston, P.R. and Kilpatrick, D. 1991a, Mathematical modelling of paired stenosis. *Computers in Cardiology*, pp. 229-232.

Johnston, P.R. and Kilpatrick, D. 1991b , Mathematical modelling of flow through an irregular arterial stenosis. *Journal of Biomechanics*, Vol. 24, pp. 1069-1077.

Kannel, W.B., Brand, N., Skinner, J.J.Jr., Dawber, T.R. and McNamara, P.M. 1967a, The relation of adiposity to blood pressure and development of hypertension : The Framingham Study. *Annual International Medicine*, Vol. 67, pp. 48.

Kannel, W.B., Castelli, W.P. and McNamara, P.M. 1968, Cigarette smoking and risk of CHD - Epidemiologic clues to pathogenesis : The Framingham Study. *National Cancer Institute Monograph Number 28*, Vol. 28, pp. 9-20.

Kannel, W.B., Dawber, T.R., Friedman, G.D., Glennon, W.E. and McNamara, P.M. 1964, Risk factors in CHD - An evaluation of several serum lipids as predictors of CHD : The Framingham Study. *Annual International Medicine*, Vol. 61, pp. 888.

Kannel, W.B., Dawber, T.R., Kagan, A., Revotskie, N. and Stokes, J. 1961, III : Factors of risk in the development of coronary heart disease - six year follow-up experience : The Framingham Study. *Annual International Medicine*, Vol. 55, pp. 33.

Kannel, W.B., LeBaner, E.J., Dawber, T.R. and McNamara, P.M. 1967b, Relation of body weight to development of coronary heart disease : The Framingham Study. *Circulation*, Vol. 35, pp. 734-744.

Kindt, G.W. and Youmans, J.R. 1969, The effect of stricture length on critical arterial stenosis. *Surgery, Gynecology and Obstetrics*, Vol. 128, pp. 729-734.

Lannigan, R. 1966, *Cardiac Pathology*, Butterworth & Co., London. pp. 204-256.

Lee, J.S. and Fung, Y.C. 1970, Flow in locally constricted tubes at low Reynolds numbers. *Journal of Applied Mechanics*, Vol. 37, pp. 9-16.

Lee, T.S. 1994, Steady laminar fluid flow through variable constrictions in vascular tube. *Journal of Fluids Engineering*, Vol. 116, pp. 66-71.

Luo, X.Y. and Kuang, Z.B. 1992, Non-Newtonian flow patterns associated with an arterial stenosis. *Journal of Biomechanical Engineering, ASME*, Vol. 114, pp. 512-514.

Ma, X., Lee, G.C. and Wu, S.G. 1992, Numerical simulation for the propagation of non-linear pulsatile waves in arteries. *Journal of Biomechanical Engineering*, Vol. 114, pp. 490-496.

Mann, F.C., Herrick, J.F., Essex, H.E. and Baldes, E.J. 1963, The effect on blood flow of decreasing the lumen of a blood vessel. *Surgery*, Vol. 53, pp. 513-524.

Mates, R.E., Gupta, R.L., Bell, A.C. and Klocke, F.J. 1978, Fluid dynamics of coronary artery stenosis. *Circulation Research*, Vol. 42, pp. 152-162.

May, A.G., De Wesse, J.A. and Rob, C.G. 1963, Hemodynamic effects of arterial stenosis. *Surgery*, Vol. 53, pp. 513-524.

Mazumdar, J.N. 1992, *Biofluid Mechanics*, World Scientific Publishing, Singapore.

McDonald, D.A. 1960, *Blood Flow in Arteries, 2nd edition*, Edward Arnold, London.

Morgan, B.E. and Young, D.F. 1974, An integral method for the analysis of flow in arterial stenosis. *Bulletin of Mathematical Biology*, Vol. 36, pp. 39-53.

Nakamura, M. and Sawada, T. 1988, Numerical study on the flow of a non-Newtonian fluid through an axisymmetric stenosis. *Journal of Biomechanical Engineering, ASME*, Vol. 110, pp. 137-143.

National Heart Foundation of Australia 1993, *Annual Report*,

National Heart Foundation of Australia 1994, *Annual Report*,

Nerem, R.M. 1992, Vascular fluid mechanics, the arterial wall, and atherosclerosis. *Journal of Biomechanical Engineering, ASME*, Vol. 114, pp. 274-282.

Nerem, R.M. and Cornhill, J.F. 1980, The role of fluid mechanics in atherogenesis. *Journal of Biomechanical Engineering, ASME*, Vol. 102, pp. 181-189.

Padmanabhan, N. 1980, Mathematical model of arterial stenosis. *Medical & Biological Engineering & Computing*, Vol. 18, pp. 281-286.

Padmanabhan, N. and Devanathan, R. 1981, Mathematical model of an arterial stenosis, allowing for tethering. *Medical & Biological Engineering & Computing*, Vol. 19, pp. 386-390.

Padmanabhan, N. and Jayaraman, G. 1984, Flow in a curved tube with constriction - an application to the arterial system. *Medical & Biological Engineering & Computing*, Vol. 22, pp. 216-224.

Patankar, S.V. 1980, *Numerical Heat Transfer and Fluid Flow*, McGraw Hill, Washington.

Pedley, T.J. 1980, *The Fluid Mechanics of Large Blood Vessels*, Cambridge University Press, U.K..

Perić, M. 1994, Computation of engineering flows. *Ship Technology Research*, Vol. 41, pp. 204-214.

Perktold, K., Nerem, R.M. and Peter, R.O. 1991, A numerical calculation of flow in a curved tube model of the left main coronary artery. *Journal of Biomechanics*, Vol. 24, pp. 175-189.

Perktold, K., Thurner, E. and Kenner, T. 1994, Flow and stress characteristics in rigid walled and compliant carotid artery bifurcation models. *Medical & Biological Engineering & Computing*, Vol. 32, pp. 19-26.

PHOENICS Manual : The PHOENICS Reference Manual (CHAM/TR200a) 1991, CHANM, London.

PHOENICS Manual : The PHOTON User Guide (CHAM/TR140) 1991, CHAM, London.

PHOENICS Manual : A Guide to the PHOENICS Input Language (CHAM/TR100) 1992, CHAM, London.

PHOENICS Manual : The PHOENICS Menu User Guide (CHAM/TR217) 1993, CHAM, London.

Rathish Kumar, B.V. and Naidu, K.B. 1996, A pulsatile suspension flow simulation in a stenosed vessel. *Mathematical and Computer Modelling*, Vol. 23, No. 5, pp. 75-86.

Reul, H. 1984, Cardiovascular simulation models. *Life Support Systems*, No. 2, pp. 77-98.

Roache, P.J. 1976, *Computational Fluid Dynamics*, Hermosa Albuquerque, New Mexico.

Rodbard, S. 1966, Dynamics of blood flow in stenotic vascular lesions. *The American Heart Journal*, Vol. 72, pp. 698-704.

Rooz, E., Young, D.F. and Rogge, T.R. 1982, A finite element simulation of pulsatile flow in flexible obstructed tubes. *Journal of Biomechanical Engineering, ASME*, Vol. 104, pp. 119-124.

Sabbah, H.N., Walburn, F.J. and Stein, P.D. 1984, Patterns of flow in the left coronary artery. *Journal of Biomechanical Engineering, ASME*, Vol. 106, pp. 272-279.

Schlichting, H. 1968, *Boundary Layer Theory, 6th edition*, McGraw Hill, New York. pp. 122.

Schmidt, R.F. and Thews, G. (eds) 1987, *Human Physiology, 2nd edition*, Springer-Verlag, Berlin.

Shipley, R.E. and Gregg, D.E. 1944, The effect of external constriction on a blood vessel on blood flow. *American Journal of Physiology*, Vol. 141, pp. 289-296.

Sidik, W.A. and Mazumdar, J.N. 1994, A mathematical study of turbulent blood flow through arterial bifurcation. *Australasian Physical and Engineering Sciences in Medicine*, Vol. 17, pp. 1-13.

Strong, J.P. and McGill, H.C.Jr. 1962, The history of coronary atherosclerosis. *American Journal of Pathology*, Vol. 40, pp. 37.

Talbort, L. and Gong, K.O. 1983, Pulsatile entrance flow in a curved pipe. *Journal of Fluid Mechanics*, Vol. 127, pp. 1-25.

Tandon, P.N., Rana, U.V.S., Kawahara, M. and Katiyar, V.K. 1993, A model for blood flow through a stenotic tube. *International Journal of Biomedical Computing*, Vol. 32, pp. 61-78.

Texon, M. 1963, The role of vascular dynamics in the development of atherosclerosis. *Atherosclerosis and its origins*, pp. 167-195.

Tu, C., Deville, M., Dheur, L. and Vanderschuren, L. 1992, Finite element simulation of pulsatile flow through arterial stenosis. *Journal of Biomechanics*, Vol. 25, pp. 1141-1152.

Umezu, M., Murayama, Y., Nogawa, A. and Kijima, T. 1992, The effects of inner shapes of plastic connectors on blood in an extracorporeal circulation. *7th International Conference on Biomedical Engineering, Singapore.*

Vlodaver, Z. *et al* 1976, *Coronary Heart Disease*, Springer-Verlag, New York.

Young, D.F. 1968, Effect of a time-dependent stenosis on flow through a tube. *Journal of Engineering for Industry, ASME*, Vol. 90, pp. 248-254.

Young, D.F. 1979, Fluid mechanics of arterial stenoses. *Journal of Biomechanical Engineering, ASME*, Vol. 101, pp. 157-175.

Young, D.F. and Tsai, F.Y. 1973, Flow characteristics in models of arterial stenoses - I. Steady Flow. *Journal of Biomechanics*, Vol. 6, pp. 395-410.

ERRATA

1. On page 35, the following paragraph should appear before the beginning of the section on Poiseuille Flow Formula :

   Typical values of Reynolds number for blood flow range from very low values of about 10 to as high as 2000 (McDonald 1960), and entering into regions of turbulent flow, depending on various factors such as size and nature of the artery. However, in numerical modelling of blood flow, the range of Reynolds number that can be used without causing instabilities is usually limited by factors such as the method of solution, the computational grid size and the geometry of the model. In the present study, the computational analysis had permitted a range of Reynolds number up to around 1000.

2. On page 60, the following paragraph should appear after the last line of text :

   It should be noted that in each of these graphs, the outlet pressure is only approximately zero and not exactly zero. The slight discrepancy is due to accumulated computational errors, which may be neglected since our principal interest is in the qualitative comparison between the cases here.

3. On page 82, the following line should be added to the caption of Figure 5.4 :

   (Note that more simulations have been carried out in this case to generate more data points so as to give a better illustration of the general trend)

4. On page 85, the following line should be added to the caption of Figure 5.5 :

   Note that additional data points were generated from simulations (not reported in the main text) in order to provide values so that a smoother curve may be plotted.

5. On page 161, the following line should appear below the title for Appendix C :

   (Note : the quantities in the input file are dimensionless)

6. On page 165, the following line should appear below the title for Appendix D :

   (Note : the quantities in the input file are dimensionless)